



Micro and Nanoelectrochemical Modification of Self-assembled Monolayers

(Mikro- und Nanoelektrochemische Modifikation von selbstassemblierten
Monolagen)

Von der Fakultät für Mathematik und Naturwissenschaften
der Carl von Ossietzky Universität Oldenburg
zur Erlangung des Grades eines
Doktors der Naturwissenschaften (Dr. rer. nat.)
angenommene Dissertation

von

Jatin Kumar Sinha

Geboren am 07. Juli 1978 in Puri, Orissa, India

Oldenburg, September 2007

1. Gutachter: Prof. Dr. Gunther Wittstock
2. Gutachter: Prof. Dr. Katharina Al-Shamery

Tag Der Disputation: 05. March 2008

to my wife
ANINDITA

Die vorliegende Arbeit wurde in der Zeit von März 2003 bis September 2007 unter der Anleitung von Herrn Prof. Dr. Gunther Wittstock am Institut für Reine und Angewandte Chemie, vormals Fachbereich Chemie, der Carl von Ossietzky Universität Oldenburg angefertigt

Zusammenfassung

Gelöste Metallionen können an fest/flüssig-Grenzflächen eine Reihe von Reaktionen eingehen. Während galvanische Abscheidungen bereits recht gründlich untersucht sind, gibt es eine ganze Reihe weiterer Reaktionen, die auf molekularem Niveau unzureichend aufgeklärt sind, obwohl sie sowohl technologisch (organische Additive in der Galvanik, molekulare Elektronik) als auch in der Natur (Retention und Mobilisierung von Metallionen an organischen Partikeln und halbleitenden Mineralien) eine bedeutende Rolle spielen.

In dieser Arbeit wurden definierte Modelloberflächen aus selbst-assemblierten Monolagen erzeugt und charakterisiert. Dabei kamen zwei sehr unterschiedliche Typen von Monolagen zum Einsatz. Monolagen aus Nonanthiol und 1,9-Nonandithiol auf Gold wurden bezüglich ihrer Bindungsfähigkeit für Silberionen untersucht. Dabei wurde die Reaktion über eine lokale Strommessung an einer Silberultramikroelektrode verfolgt. Zum Einsatz kamen chronoamperometrische Pulsprogramme, mit denen eine deutliche Unterscheidung zwischen Abscheidungen durch Überpotential- und Unterpotentialabscheidung möglich war. Präpariert wurden außerdem Cd-Ultramikroelektroden, mit denen die Anwendung des Konzeptes auch auf andere Metallionen möglich ist. Die Wechselwirkung von Metallionen mit Monolagen aus Nonanthiol und 1,9-Nonandithiol wurde auch über Cyclovoltammetrie an der Substratelektrode untersucht. Dabei konnte die Anreicherung von Cd^{2+} Ionen an der Oberfläche untersucht werden, was für analytische Bestimmungen interessant ist.

Der zweite Monolagentyp basiert auf Monoschichten aus β -Cyclodextrinen auf Siliziumdioxid. Diese Monolagen können redoxaktive Gastmoleküle nichtkovalent binden. Es wurden Schichten mit Ferrocen-terminierten Dendrimeren und gebundenem Cytochrom c untersucht. In diesen Fällen konnten sowohl eine Abbildung gemusterter Oberflächen mit der elektrochemischen Rastermikroskopie, eine lokale Modifizierung der Dendrimer-modifizierten Schichten als auch eine Bestimmung der Grenzflächenkonzentration der redoxaktiven Gastmoleküle durch chronoamperometrische Pulsverfahren an positionierbaren Ultramikroelektroden erreicht werden.

Abstract

Dissolved metal ions can undergo a number of reactions at the solid/liquid interface. While galvanic depositions are already quite well investigated, there are a number of reactions which are insufficiently elucidated although they play an important role in technology (organic additives in electroplating, molecular electronics) as well as in nature (retention and mobilization of metal ions at organic particles and semi-conducting minerals).

In this work self-assembled monolayers were produced and characterized as defined model surfaces. Two very different types of monolayers were used. Monolayers of nonanethiol and 1,9-nonanedithiol on gold were investigated with respect to their binding capacity for silver ions. The reaction was followed by measuring the current locally at a silver ultramicroelectrode. Chronoamperometric pulse programs were employed and enabled a clear distinction between underpotential and overpotential deposition. In addition, cadmium ultramicroelectrodes were prepared, demonstrating the possibility to extend the concept to other metal ions. The interaction of metal ions and monolayers of nonanethiol and 1,9-nonanethiol was also investigated by means of cyclic voltammetry at the substrate electrode. The accumulation of Cd^{2+} ions at the substrate surface could be investigated which is interesting for analytical detections.

The second type of monolayers is based on monolayers of β -cyclodextrines on silicon dioxide. These monolayers can bind redox-active guest molecules non-covalently. Layers of ferrocene-terminated dendrimers and attached cytochrome c were investigated. In these cases, imaging of patterned surfaces using scanning electrochemical microscopy, modification of dendrimer-modified layers, as well as the determination of the surface concentration of redox-active guest molecules by means of chronoamperometric pulse techniques at positionable ultramicroelectrodes could be achieved.

Acknowledgements

I would like to express my deepest gratitude to my supervisor and mentor, Prof. Dr. Gunther Wittstock for his generous guidance, support and encouragement throughout the course of my study in Oldenburg. His charming personality coupled with his ethos of sheer hard work has made it a privilege to work under him. His guidance has enabled me to broaden my scientific knowledge and new ways to motivate myself. I am certain, future postgraduate students would benefit from his vast pool of scientific knowledge and brilliant researching skills

Special merit goes to Prof. Dr Daniel Mandler (*The Hebrew University, Jerusalem, Israel*) and his co-workers for helping me during my two months staying in Israel. I feel that my whole work will be incomplete without their persistent help and encouragement. I would like to thank Dr. Christian Nijhuis and Manon. J. Ludden (*University of Twente, The Netherland*) for providing me samples for SECM experiments. I would like to thank my former and current group colleagues Dr. Oleg Sklyar, Dr. Chuan Zhao, Dr. Yan Shen, Carolina Nunes Kirchner, Malte Burchardt, Sascha E. Pust, Markus Träuble. I am grateful to Dr. Izabella Zawisza for help to obtain spectra in PM-FTIRRAS experiment. Special thanks go to Richard Kaupass, Ehrentraud Schneider-Hassel and Anke Brakenhoff for their technical assistance during my work

I would like to thank my friends Rakes, Sujit, Dillip for their advice, optimism and constant encouragement. I also thank Harekrishna and Monalisa, for creating a family environment around me in Oldenburg for which I will be greatly indebted

Finally, I would like to thank Anindita for everything.

Table of Contents

Introduction	1
1 Interaction of ions and molecules with self-assembled monolayers	5
1.1 Self-assembled monolayers.....	5
1.2 Self-assembly of alkanethiols	6
1.2.1 Interaction of redox active metal ion with SAMs.....	7
1.2.2 Interactions of redox inactive cations with SAMs.....	11
1.3 Self-assembly of supramolecules.....	16
1.3.1 Host-guest complexes	17
1.3.2 Dendrimers.....	18
2 Instruments and techniques for studying reactions at self-assembled monolayers	21
2.1 Scanning probe techniques.....	21
2.2 Scanning tunnelling microscopy.....	22
2.3 Atomic force microscopy	23
2.4 Scanning near field optical microscopy	24
2.5 Scanning electrochemical microscopy.....	26
2.5.1 General operation principles of SECM.....	26
2.5.2 Single potential step chronoamperometry (SPSC) experiment	27
2.5.3 Principle of SPSC at SECM.....	28
2.5.4 Theory of SPSC at SECM.....	30
2.5.5 Double potential step chronoamperometry (DPSC) experiments.....	32
2.5.6 Principle of DPSC at SECM.....	34
2.5.7 Theory of DPSC at SECM.....	36
3 Experimental	41
3.1 Substances and solutions.....	41
3.1.1 Chemicals.....	41
3.1.2 Materials	41
3.1.3 Solutions	42
3.2 Preparation of micro and submicrometer electrodes for SECM	42
3.2.1 Preparation of Au, Pt, Ag ultra microelectrode	42
3.2.2 Preparation of carbon fiber electrode.....	44
3.3 Electrochemical and optical characterization	44
3.3.1 Characterisation of Pt/ Au/ Ag UMEs	44
3.3.2 Characterization of carbon fiber UMEs	46
3.4 Preparation and cleaning of gold substrate	47
3.4.1 Preparation of gold substrate	47
3.4.2 UV/ozone cleaning of gold surfaces.....	47
3.4.3 Al ₂ O ₃ powder / electrochemical cleaning of gold electrodes	47
3.5 Monolayer assembly of thiols on gold substrate.....	47
3.6 Contact angle (CA) measurements	47
3.7 XPS measurements	48
3.7.1 Sample preparation	48

3.8	PM-IRRAS measurements	49
3.9	Experimental set up for SECM imaging experiment	49
3.9.1	SECM experiment.....	49
3.9.2	Optimization of SECM instrument before imaging.....	50
4	Preparation of Cd ultramicroelectrodes for SECM experiment	51
4.1	Preparation of Cd UMEs	53
4.1.1	Preparation of Ag ultramicroelectrodes	53
4.1.2	Chemical and electrochemical etching of Ag UME	54
4.1.3	Deposition of Cd onto the Ag UME from Cd solution.....	54
4.2	Characterisation of Cd UME.....	55
4.2.1	Optical characterization of Cd ultramicroelectrodes	55
4.2.2	Electrochemical characterization of Cd ultramicroelectrodes	56
5	Interaction of Cd metal ions with nonanethiol and 1,9-nonanedithiol SAMs modified gold electrodes	59
5.1	PM-IRRAS characterisation of nonanethiol and 1,9-nonanedithiol monolayers on gold surface	60
5.2	Electrochemical characterisation of thiol-modified and dithiol- modified gold electrodes	62
5.3	Contact angle measurement for nonanethiol and 1,9-nonanedithiol modified gold electrode	63
5.4	Cadmium deposition and stripping at a thiol-modified and dithiol-modified gold electrodes	64
5.5	XPS characterisation of Cd deposition and stripping at di-thiol modified gold electrode	67
5.6	Stripping voltammetry of cadmium using gold electrodes modified with SAMs	73
6	Adsorption, nucleation and growth studies of Ag at gold and thiol, dithiol-modified gold electrodes by SECM	77
6.1	Principle to study adsorption, nucleation and growth of Ag at gold, thiol and dithiol modified gold electrodes	77
6.1.1	Optimization of dissolution potential and pulse time for Ag microelectrode anodic dissolution	78
6.1.2	Optimization of distance for Ag ions generation near to the inert substrate	79
6.2	Deposition of Ag onto gold substrate by using SECM.....	80
6.3	Comparison of single potential step chronoamperometry experiment at gold and glass surface	83
6.4	Double potential step chronoamperometry experiment at gold substrates	85
7	Controlling the supramolecular assembly of redox active dendrimers at molecular printboards by SECM.....	89
7.1	Oxidation of ferrocene dendrimer	91
7.2	Approaching the surface with oxygen reduction	92
7.3	Line scan of the structured surface.....	93

7.4	SECM imaging of Fc dendrimers at molecular printboard at Au surface.....	94
7.5	Optimization of the SECM Imaging for Fc Dendrimers.....	96
7.6	SECM imaging of Fc dendrimers at molecular printboard at SiO ₂ surface.....	97
8	Controlled electrochemical desorption of redox active dendrimers at molecular printboard by SECM	103
8.1	Optimisation of working distance for pulse experiments	104
8.2	Optimisation of the time for pulse experiment for determination of surface concentration.....	107
8.3	Multiple pulse experiments at the same location	108
8.4	Pulse experiment comparison at SiO ₂ and Fc dendrimers covered surface.....	110
8.5	SECM imaging of spots made on SiO ₂ surfaces covered with redox active dendrimers by etching.....	110
8.6	SECM line scans of the etching spots made by different pulse time.....	114
8.7	Determination of surface coverage for different generation dendrimers.....	116
8.8	Electrochemical reduction of cytochrome <i>c</i> on top of streptavidin layers at the molecular printboard	119
	Summary	125
	References	129
	Symbols and Abbreviations	139

Introduction

Metal ions dissolved in an aqueous solution can undergo a large number of interfacial reactions [1-3]. Reductions of the ions and deposition on conducting surfaces are one of the classical themes in electrochemistry. It has been known for a long time that "organic additives" can influence these processes [4]. A large body of empirical knowledge is used in the plating industry, despite the fact that rather little is known about the molecular mechanisms by which the compound influence the interfacial processes. Although it is clear that adsorption of organic molecules is involved in most cases, the diverse and often competing mechanisms by which dissolved metal ions interact with organic layers on electrode surfaces turn the systematic investigation of these processes into a real scientific challenge. Metal ions can be complexed by functional groups of the organic material. Once complexed the immobilized ion may enter into ion exchange processes with dissolved ions. The complexed ion may be diffuse laterally along the solid/liquid interface or being transferred across the organic thin film. Dissolved metal ions can also oxidize solid metals of lower redox potential or compound semiconductors. In some cases the reaction of the metal ion with an organic thin film can induce reversible or irreversible structural changes into the organic thin film. The way these processes occur may depend on the nature of the metal ion and the structure of the organic thin film and perhaps even on the magnitude of the imposed fluxes. Furthermore, metal ions electrostatically attached to organic thin films can be locally reduced by a strong reductant in solution. It is an entire open question, which secondary process will be triggered by this elementary event. It may for instance lead to metal phase formation, which would most likely induce a disturbance in the organic layer.

Besides application in the plating industry, metal layer formation on top of a nonconductive organic monolayer has been an important research subject in recent years because of its connection with an attractive field of molecular electronics in which an organic monolayer will be used in electronic components. Besides technological perspective interactions of dissolved metal ions and organic or semiconductor surfaces are at the heart of a larger number of interfacial processes occurring in nature. The geochemical formation of ore deposits is one example. Interaction of metal ions with complexing functionalities at the surface of particulate organic matter is of outmost importance in understanding the molecular basis of mass balances of trace metals in aquatic ecosystems. These processes are poorly understood on a molecular level and constitute one of the points where chemical (e.g. redox

states) and biological regulation (complexation at the surfaces of cells and extracellular matrix) may overlap.

The discovery of efficient ways to produce model surfaces of organic thin films by formation of self-assembled monolayers (SAM) [5] enabled new studies on this subject using a large variety of spectroscopic, microscopic and diffraction techniques. The advantages of such model monolayer are multifold. The binding motive to the surface can be varied independently from the terminal functional group to which the metal ions will bind. Moreover, such monolayers have also practical application in particular for interfacing artificial microstructured surfaces to biological and biochemical entities where these layers can mimic biological membranes. Most of these SAMs were formed on gold substrate. This is because of the fact that gold does not have a stable oxide, and thus it can be handled in ambient conditions. SAMs of thiols are good candidates to be used as molecular layers for this purpose because of their unique advantages such as ease of preparation, highly ordered structure, and well-documented characteristics.

In order to study the interaction of metal ions with organic monolayer, model system were prepared from alkanethiols and dithiols on gold substrates in this work. Sources for metal ions were obtained by preparing metal electrode probe for SECM. By combining single potential step chronoamperometry and double potential chronoamperometry techniques with SECM, metal-ions were generated at the interest surface and the generated flux of metal-ions were controlled anodically dissolution of these metal probes.

To understand the fundamental interactions between self assembled monolayers of organic molecules with ions, a brief literature overview is given in Chapter 1. Sensing of metal ions at SAMs modified electrode is of particular interest. The review gives an idea to conduct experiment of metal-ion interaction with organic monolayers by SECM. A brief review is also discussed about the supramolecular self assembly via multiple host-guest interaction system.

The first part of the thesis (Chapter 2) deals with the different surface techniques used to study the SAMs. A brief review on different scanning techniques techniques (AFM, STM, SNOM, SECM) is given. Similarities and differences to SECM are pointed out. Of particular interest are single and double chronoamperometric pulse techniques at SECM. They are discussed in detail.

Chapter 3 represents the experimental part of the thesis. Different types of ultra microelectrodes were prepared by conventional method and characterised. Experimental conditions were discussed in details for SECM experiment and other surface characterisation techniques.

Chapter 4 to 8 deal with experimental results and their discussion. A new method was developed to prepare cadmium ultramicroelectrodes for SECM experiment (Chapter 4). Chapter 5 and 6 discuss the interaction of Ag and Cd ions with SAMs of alkanethiols and dithiols. SECM chronoamperometric experiments were explored to study the charge propagation along the monolayers and metal deposition on pure gold and gold substrate modified with alkanethiols and dithiols (Chapter 5). Chapter 6 describes the controlled deposition of cadmium from bulk solution and their stripping analysis via different electrochemical techniques. Further they were characterized by XPS. It also gives an idea how these monolayers on gold can be a useful to sense of Cd ions.

Some of the principles outlined above can also be found in the interaction of other solutes with functionalized surfaces. The advantage of supramolecular system compared to chemi- or physisorption, or covalent chemistry is that the binding kinetics and thermodynamic can be precisely controlled [6]. Additionally supramolecular interactions can also respond to external stimuli to give control over adsorption processes [7, 8].

Scientifically and technologically interesting examples are interfacial supramolecular assemblies with redox-active guest molecules on "molecular printboards" [9]. They have been prepared at the University of Twente and were electrochemically characterized in Oldenburg. Patterned surfaces were imaged (Chapter 7). Further chronoamperometric pulse technique at SECM were explored to measure surface concentration of ferrocene functionalised dendrimers and functional protein cytochrome *c* on molecular printboards quantitatively (Chapter 8). This illustrates the general applicability of the chronomaperometric SECM measurements for the characterisation of these films.

1 Interaction of ions and molecules with self-assembled monolayers

1.1 Self-assembled monolayers

Bare surfaces of metals and metal oxides tend to adsorb adventitious organic materials readily because these adsorbates lower the free energy of the interface between the metal or metal oxide and the ambient environment [10]. These adsorbates also alter interfacial properties and can have a significant influence on the stability of nanostructures of metals and metal oxides. The organic material can act as a physical or electrostatic barrier against aggregation, decrease the reactivity of the surface atoms, or act as an electrically insulating film. Surfaces coated with adventitious materials are, however, not well-defined: they do not present specific chemical functionalities and do not have reproducible physical properties. (e.g. conductivity, wettability, or corrosion resistance).

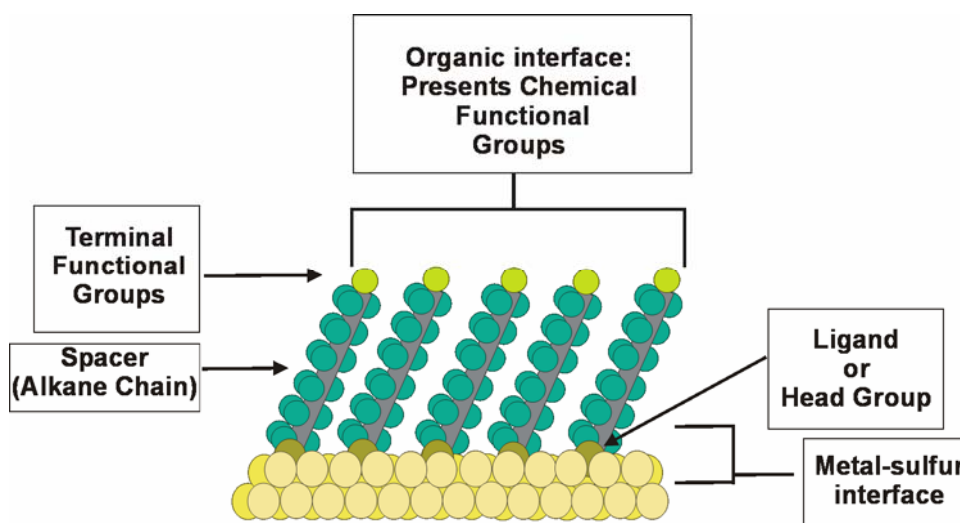


Fig. 1.1: Schematic diagram of an ideal, single-crystalline SAM of alkanethiolates supported on a gold surface with a (111) texture. The structure and characteristics of the SAM are highlighted.

Self-assembled monolayers (SAMs) provide a convenient, flexible, and simple system with which to tailor the interfacial properties of metals, metal oxides, and semiconductors. SAMs are organic assemblies formed by the adsorption of molecular constituents from solution or the gas phase onto the surface of solids or in regular arrays on the surface of liquids (in the case of mercury and probably other liquid metals and alloys). The adsorbates organize spontaneously (and sometimes epitaxially) into crystalline (or semicrystalline) structures

(Fig.1.1). The molecules or ligands that form SAMs have a chemical functionality, or “headgroup”, with a specific affinity for a substrate. In many cases, the headgroup also has a high affinity for the surface and displaces adsorbed adventitious organic materials from the surface. There are a number of headgroups that bind to specific metals, metal oxides, and semiconductors.

1.2 Self-assembly of alkanethiols

The most extensively studied class of SAMs is derived from the adsorption of alkanethiols on gold [11-19], silver [18, 20, 21], copper [18], palladium [22, 23], platinum [24], and mercury [25]. The high affinity of thiols for the surfaces of noble and coinage metals makes it possible to generate well-defined organic surfaces with useful and highly alterable chemical functionalities displayed at the exposed interface [15, 26].

Out of different metals, adsorption of SAMs on gold is the most widely studied. The reason for this are (1) gold forms good (but not uniquely good) SAMs and (2) it is historically the most studied. In fact, for many applications gold may not be the best substrate. There are five characteristics of gold that make it a good choice as a substrate for studying SAMs. First, gold is easy to obtain, both as a thin film and as a colloid. It is straightforward to prepare thin films of gold by physical vapour deposition, sputtering, or electrodeposition. Although expensive and not essential to most studies of SAMs, single crystals are available commercially. Second, gold is exceptionally easy to pattern by a combination of lithographic tools (photolithography, micromachining, others) and chemical etchants. Third, gold is a reasonably inert metal: it does not oxidize at temperatures below its melting point; it does not react with atmospheric O₂, it does not react with most chemicals. These properties make it possible to handle and manipulate samples under atmospheric conditions instead of under ultra high vacuum a great practical convenience for conducting experiments that require “dirty” conditions, e.g. microfabrication (outside of a clean room environment) and cell biology. Gold binds thiols with a high affinity [12], and it does not undergo any unusual reactions with them, e.g. the formation of a substitutional sulfide interphase. Because thiols have a high affinity for gold, they also displace adventitious materials from the surface readily. Fourth, thin films of gold are common substrates used for a number of existing spectroscopies and analytical techniques, including surface plasmon resonance spectroscopy, quartz crystal microbalances, reflection absorption infrared spectroscopy, and ellipsometry.

This characteristic is particularly useful for applications of SAMs as interfaces for studies in biology. Fifth, gold is compatible with cells, that is, cells can adhere and function on gold surfaces without evidence of toxicity. SAMs formed from thiols on gold are stable for periods of days to weeks when in contact with the complex liquid media required for cell studies.

1.2.1 Interaction of redox active metal ion with SAMs

Detection and separation of metal ions from environmental samples is of critical importance due to their toxicity and longevity [27]. Detection of metal ions can be obtained by different methods. Out of different methods, use of electrochemical sensing arrays is the most important one. For instance, highly selective receptor molecules have been immobilized on gold electrodes to bind electrochemically active metal ions, which can be detected using cyclic voltammetry (CV) [28-41]. One of the initial reports of an organized monolayer capable of selectively recognizing redox-active metal ions was published by Rubinstein and co-workers [28]. As shown in Fig. 1.2, different mixed monolayers were prepared, consisting of thio-bis(ethylacetoacetate) (TBEA) and passivating molecules, such as *n*-octadecylmercaptan or *n*-octadecyltrichlorosilane, on gold electrodes. These mixed SAMs were capable of detecting divalent metal ions such as Cu^{2+} or Pb^{2+} on the electrode surfaces even in the presence of Fe^{2+} in 0.1 M aqueous H_2SO_4 . The binding properties of these metal ions to the TBEA monolayer was confirmed by electrochemical and non-electrochemical techniques such as ellipsometry and contact-angle measurements [29], and this selectivity property was ascribed to the complexation between these metal ions and the β -diketonate motif of the receptors. The result also explained that the selectivity exhibited by the immobilized receptor was quite different from that observed in solution. One reason may be the effect of the externally applied potential which seems to provide part of the driving force for metal ion complexation to the immobilized receptor.

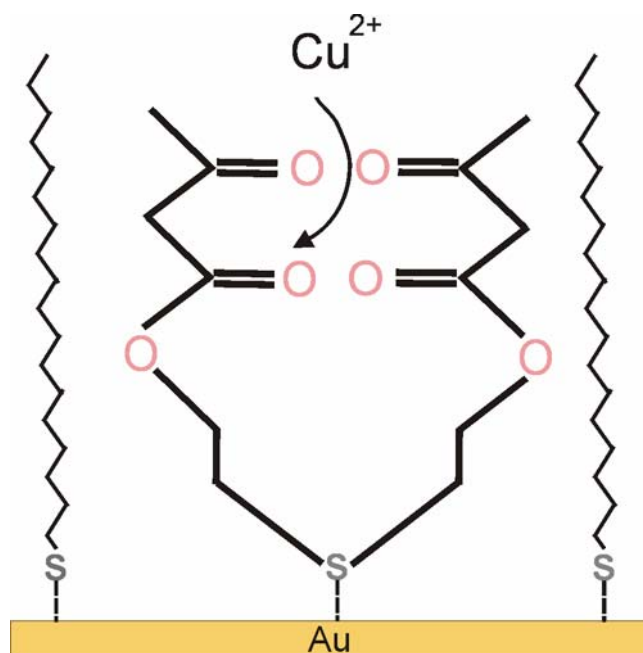


Fig. 1.2: Schematic representation of Cu^{2+} complexation with SAMs of TBEA

Thenceforth, a series of redox-active metal ion sensors based on SAMs were developed. Mandler et al. presented a approach for the electrochemical determination of ultra low levels of Cd^{2+} in an acetate buffer solution using ω -mercaptocarboxylic acid monolayers on mercury and gold electrodes [41]. They determined that shorter ω -mercaptocarboxylic acids produced superior sensitivity (Fig. 1.3a), and they employed both cyclic voltammetry and Osteryoung square wave voltammetry (OSWV) to determine the selectivity and sensitivity of these negatively charged monolayers. This method was successful in determining trace amount of cadmium in seawater with a detection limit as low as 4×10^{-12} M. Recently [41], they investigated further the binding of Cd^{2+} by SAMs of ω -mercaptocarboxylic acids with CV and scanning electrochemical microscopy and concluded that binding of the metal ions by the monolayer affected the kinetics of electron transfer to a negatively charged redox probe in solution [30]. These authors also developed a highly sensitive and selective electrode modified by SAMs of 4-(2-mercaptoethyl)-pyridinium to recognize Cr(VI) in fluoride buffer solutions at pH 7.8 with a detection limit as low as 0.02 nM (Fig. 1.3b) [40]. The high selectivity of these surface immobilized receptors toward Cr(VI) was attributed to both the positive charge of the pyridinium moiety and the hydrogen bonding between the pyridinium and chromate ions.

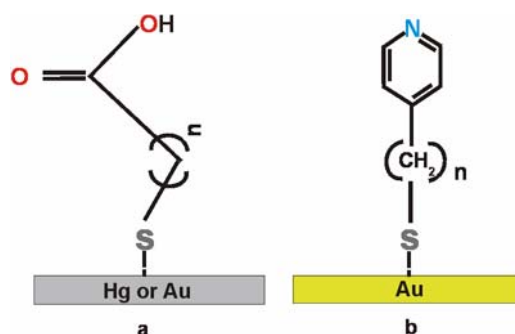


Fig. 1.3: SAMs of ω -mercaptocarboxylic acid monolayers on mercury and gold (a), and 4-(2-mercaptoethyl)-pyridinium on gold.

Electrodes modified with ω -mercaptocarboxylic acids have also been investigated by Shen et al. as Cu^{2+} sensors. They prepared SAMs of 3-mercaptopropionic acid (MPA) and obtained an enhancement in sensitivity and selectivity when the underpotential deposition effect was minimized during the stripping analysis of copper [31]. The structure of MPA (Fig. 1.4(1)) and other organosulfur compounds addressed in this section are depicted in Fig. 1.4. In turn, Nagoaka has employed SAMs consisting of 3,3'-thiodipropionic acid (Fig. 1.4(2)) and 1-decanethiol (Fig. 1.4(3)) for the determination of Cu^{2+} and Ag^+ in aqueous systems in a sensitive and selective manner. Although both Ag^+ and Cu^{2+} bind to the receptor, their different reduction potentials circumvented any interfering detection problems [32], and after optimization of the experimental conditions, detection limits of 2×10^{-9} M and 6×10^{-8} M were obtained for Cu^{2+} and Ag^+ , respectively. Detection of copper ions has also been pursued by Zeng et al. They described the electrochemical response of gold electrodes, which were modified by SAMs of glutathione (Fig. 1.4(4)) to detect copper ions in an acetate buffer solution and found that the sensitivity and selectivity of the Au–glutathione electrode can be improved by including MPA (Fig. 1.4(1)) in these monolayers [33]. More recently, Kubota et al. developed a more sensitive copper ion sensor based also on SAMs of 1 (Fig. 1.4(1)) with a detection limit of 1.8×10^{-14} M. The excellent reproducibility and sensitivity of this sensor facilitated its application in determining the copper content in mineral water and sugar cane spirits [34].

Simple amino acids or short peptides have also proven to be very valuable in the detection of redox active metals. For example, gold electrodes modified with SAMs containing cysteine (Fig. 1.4(5)) have been investigated by several groups to detect copper ions [35-39]. Chen and co-workers have demonstrated the electrochemical sensing abilities of a cysteine monolayer

for Cu^{2+} in aqueous media with a detection limit of 3.9×10^{-10} M [35]. Gold electrodes modified with cysteine monolayers are highly selective towards Cu^{2+} because the binding constant of cysteine with this metal ion is four orders of magnitude larger than with any other metal ion. In terms of reproducibility and sensitivity, the performance of their electrodes was affected by the surface concentration of cysteine and the pH of the copper(II) solution.

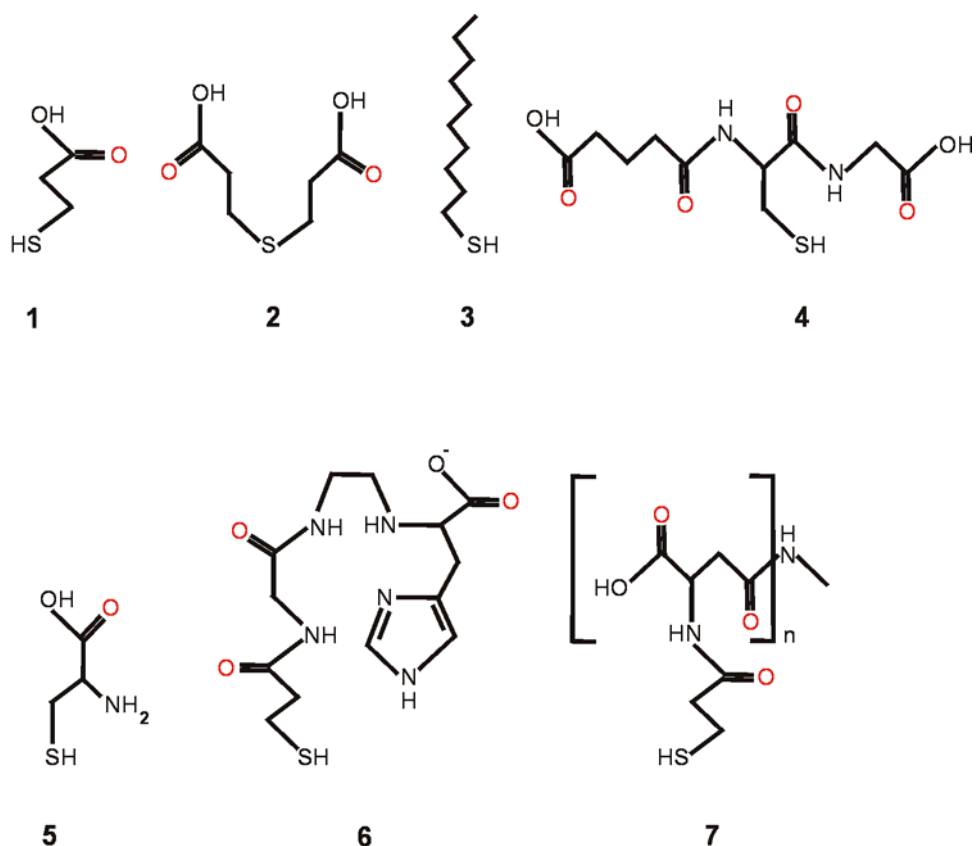


Fig. 1.4: Organosulfur molecules employed in SAMs on gold electrodes to detect redox-active metal ions

These modified electrodes showed optimal performance at pH 5, the isoelectric point of the receptor, suggesting the predominance of the zwitterionic form ($\text{HSCH}_2\text{CH}(\text{NH}_3^+)\text{CO}_2^-$) as the binding motif. The binding affinity of cysteine to Cu^{2+} decreases at pHs lower than its isoelectric point because the carboxylate moiety is then protonated and becomes unable to participate in the binding process. Thus cysteine-modified electrodes have proven to be very specific for Cu^{2+} sensing, and only nickel(II) ions, among all other possible ions, cause significant interference in its detection. Nevertheless, this interference can be prevented with the addition of dimethylglyoxime, which sequesters nickel ions, resulting in total selectivity for Cu^{2+} .

Hibbert and co-workers have also studied gold electrodes modified with SAMs of cysteine for the adsorptive stripping analysis of copper ion in solution and obtained very high selectivity and low detection limits [36]. Techniques such as CV, chronoamperometry, and X-ray photoelectron spectroscopy were employed in the characterization of this system. This group has also achieved the redox sensing of Cu^{2+} with gold electrodes modified with the Gly-Gly-His (GGH, Fig. 1.4(G)) tripeptide with detection limits of sub-parts per billion (sub-ppb) in aqueous media [37]. The complex formed between the surface confined GGH and copper ions was extremely stable as demonstrated by the lack of change in intensity of the Cu^{2+} redox wave upon multiple scans. This stability has been attributed to the binding motif in this system, which is composed of four nitrogen atoms coordinating, in a tetragonal manner, a copper ion. Such an arrangement was confirmed by electrospray ionization Fourier transform ion cyclotron resonance mass spectroscopy, and OSWV was employed to detect low levels of Cu^{2+} in environmental samples with these electrodes [38]. Such an example illustrates the potential of electrodes modified with biomolecules to be employed as metal ion sensors. In their pursuit for lower detection limits, this group also assembled polymeric aspartic acid (PLAA, Fig. 1.4(Z)) onto a MPA-modified gold electrode using an *N*-hydroxysuccinimide intermediate and carbodiimide coupling conditions, and detection limits as low as 0.2 ppb for copper ions in phosphate buffer solutions were obtained. Recently, Profundo et al. detected trace amount of Cu^{2+} ions in tap, spring, and sea water with gold electrodes modified with SAMs, also containing simple amino acids [39]. In this case, the complexing molecules were peptides such as D,L-penicillamine and thiodimethylglyoxime.

1.2.2 Interactions of redox inactive cations with SAMs

So far, the metal ion binding issue described were measured directly by the electrochemical response of the analyte in question. Detection of redox inactive metal ions can also be done directly if the properties of the receptor are altered upon binding, and if this variation can be detected. Such signal transduction can be achieved by electrochemical means either directly or indirectly as discussed in this section, or by other techniques such as fluorescence.

The binding issue can be obtained directly if the SAMs contain a redox active species at the binding site. The electrochemical response of such species depends on the degree of interaction between the redox inactive metal ion and redox active species, and thus, the presence can be obtained directly. Bryce and co-workers have confirmed this approach by utilizing these redox-active monolayers capable of signalling the metal ion binding event by

observing their electrochemical behaviour. They assimilated a redox active species, tetrathiafulvalene (TTF), to the metal binding macrocycle at the 1,2-positions of the TTF species (**8**, Fig. 1.5), and these TTF-macrocycles were coordinated to the gold surfaces using thiol groups [42, 43]. TTF has a characteristic electrochemical behaviour with two reversible one-electron redox couples both in solution and on SAMs [42, 44]. By exposing these SAMs to redox inactive metal ions, an anodic shift of the first oxidation process was obtained which increased from 10–20 mV for Li^+ and K^+ , to 45–55 mV for Na^+ and Ba^{2+} , to 60–90 mV for Ag^+ in acetonitrile [42].

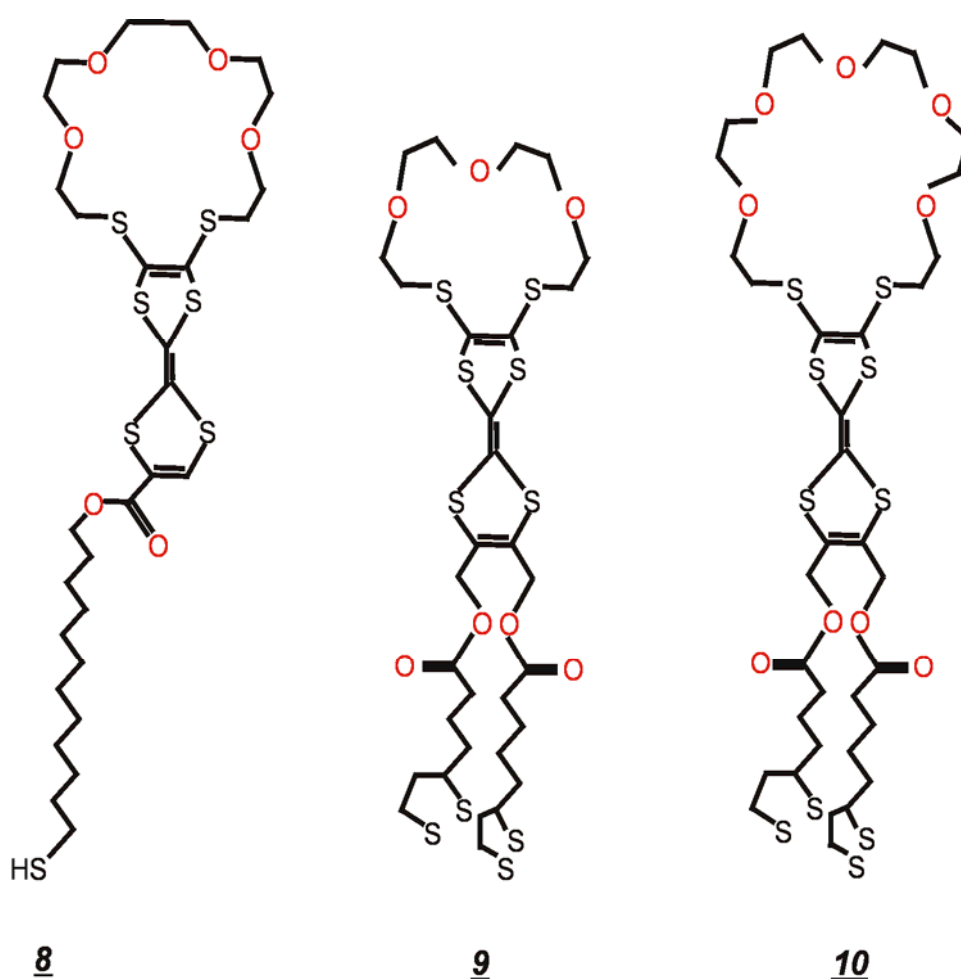


Fig. 1.5: Redox-active macrocycles capable of binding and detecting redox inactive metal ions.

The observations attributed these shifts to the inductive effect on the polarizability of TTF imposed by the bound metal cation. However, the observed responses from electrochemical experiment were weak and poorly resolved. The authors reported that these SAMs were unstable when subjected to potential scan beyond the first oxidation potential.

Echegoyen and co-workers detected well behaved electrochemical responses with crown-1,2-TTF SAMs (Fig. 1.5(**9**) and (**10**)) when they employed multiple anchoring sites or when the crown ether moiety was connected instead at the 2,7-positions of the TTF framework [45-47]. In both cases, the SAMs obtained were extremely stable over a large potential window (from neutral to TTF⁺ to TTF²⁺) unlike those observed before. In order to provide multiple anchoring sites, each molecule of the SAM was composed of a bithioctic ester derivative of the crown-TTF compound, which in turn formed remarkably stable monolayers on gold surfaces due to the dual anchoring approach. These SAMs were characterized by a clear and reversible surface-confined electrochemical behaviour of the TTF moiety, and displayed anodic shifts of both one-electron oxidation processes upon binding Na⁺ and K⁺ in THF [45]. When the crown ether portion is connected at the 2,7-positions of the TTF skeleton, the recognition properties of the ligand are optimized in homogeneous media [47]. SAMs of this receptor on gold electrodes as well as platinum surfaces modified with polymer films incorporating this TTF molecule demonstrated great stability.

Kim et al. also obtained voltammetric recognition of Ba²⁺. The results were obtained in an aqueous medium with well designed SAMs of redox-active calix[4]arenes having diquinone units as electroactive site [48]. They were incorporated into the annular framework as ring members. The binding properties are significantly different before and after the electrochemical reduction. The difference can be attributed to quinone groups which act as a coordination site for the bound metal cations. These SAMs exhibited specific selectivity for Ba²⁺ as compared to Sr²⁺ and Ca²⁺, and displayed no electrochemical response to Mg²⁺.

The examples discussed thus far employed CV as the technique to signal the binding of redox inactive metals by SAMs. Other principles and techniques, such as fluorescence, have been employed in this field because of higher sensitivity, but quenching of fluorescent monolayers by gold surfaces has rendered this type of assemblies ineffective for sensing applications. On the other hand, fluorescent-SAMs have been successfully fabricated on glass surfaces to selectively detect redox-inactive cations [49-51]. In one of these examples, a monolayer of a Na⁺-selective fluoroionophore was prepared by the covalent coupling of the bis-isocyanate derivative of the receptor to a SAM of 3-aminopropyltriethoxysilane on a glass surface [49]. In another example, Reinhoudt and co-workers demonstrated that in some cases there is no need for a pre-organized cavity as long as the SAMs are capped with functionalities containing fluorophores and recognition elements (Fig. 1.6(**11**), (**12**), (**13**), (**14**))

and **(15)**. The interaction between the recognition elements, such as amides, ureas, or sulfonamides, and the metal cations produces changes in the polarity of their immediate environment, which are detected by the fluorophores [50]. For instance, the quenching of the fluorophore (dansyl or coumarin) emission in acetonitrile reports the binding of the cation, and great selectivity for Pb^{2+} ions in the presence of Ca^{2+} and Zn^{2+} was obtained with this system. In addition to fluorescence, electrochemical impedance spectroscopy (EIS) has also proven to be an effective tool in the understanding of interfacial ion recognition phenomena when both the guest ion and the host monolayer are electrochemically inactive. This technique reveals the electrochemical properties of a system and monitors binding events involving charged species through changes of the monolayer capacitance (C_{dl}) and charge transfer resistance (R_{ct}) [27, 52-55]. The advantages of this technique is its capability to detect any changes in the surface charge without disturbing the structure of the monolayer since it applies small potential, in the range of millivolts and its ability to detect binding events in aqueous media, which resembles to a closer extent environmental and biological samples, and thus, it brings SAMs sensors closer to analytical performance.

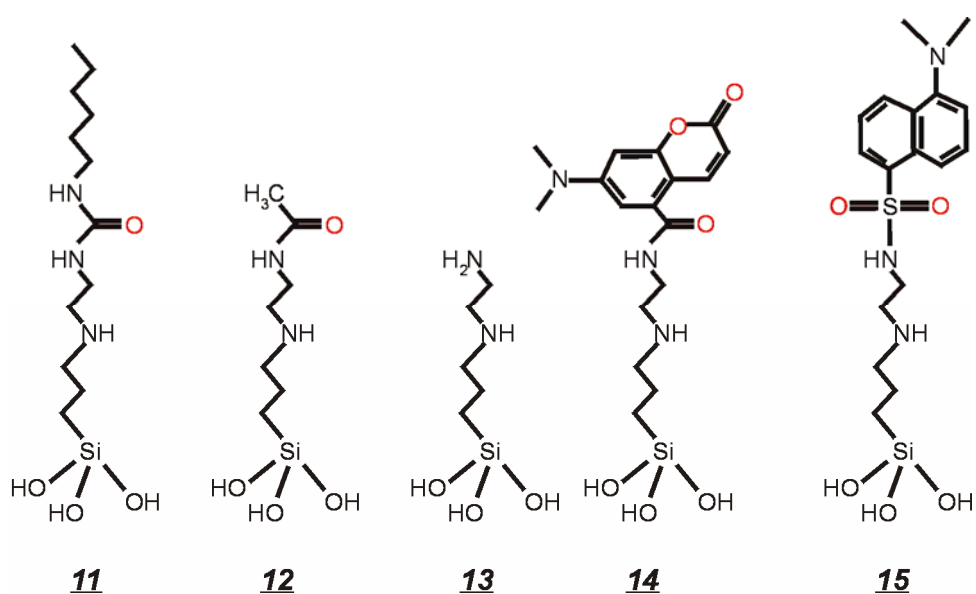


Fig. 1.6: Molecules employed in SAMs to detect redox-inactive metal cations.

Reinhoudt and co-workers were the first to show the significance of impedance spectroscopy to study the binding properties of SAMs containing non-redox active crown ethers as receptors for redox inactive metals in aqueous media (Fig. 1.7**(16)**, **(17)**, **(18)**, **(19)**) [56, 57]. They corroborated their findings with X-ray photoelectron spectroscopy (XPS) and

atomic force microscopy (AFM) [57]. The elegance of their work rests on the simplicity of their systems which self-assemble into monolayers with high concentration of macrocycles on the surface. This surface organization leads to a cooperative binding or “sandwich complexation” which accounts for the high affinity and selectivity of 12-crown-4-capped SAMs for Na^+ ($K = 15800 \text{ M}^{-1}$) and of 15-crown-5-capped SAMs for K^+ ($K = 27100 \text{ M}^{-1}$). Recently, the same principles were applied on CdSe–ZnS quantum dots which were functionalized with 15-crown-5-monolayers and were capable of recognizing potassium ions in water with detection limits on the order of 10^{-6} by fluorescence spectroscopy [58].

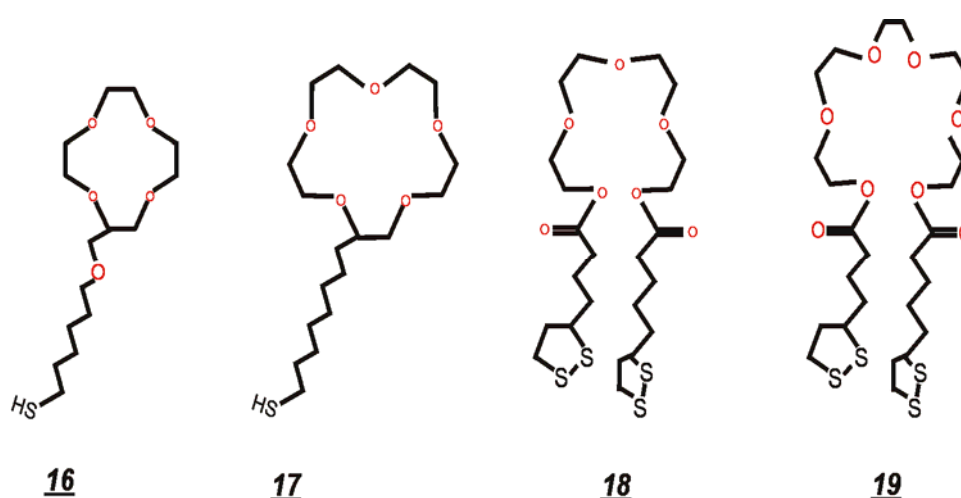


Fig. 1.7: Redox-inactive macrocyclic or pseudo-macrocyclic molecules.

Echegoyen et al. showed that crown ether macrocycles are not needed as the receptors on SAMs in order to detect K^+ or Na^+ ions in aqueous media. Instead, bithioctic ester derivatives of oligoethylene glycols (Fig. 1.7(12, 13)) can be employed to form the monolayers with the idea that the ethylene glycol portion of the molecule, in between the two ending thioctic esters, can fold to form the binding domain on the surface, and the thioctic esters can secure this binding motif to the gold surface of the electrode [59, 60]. These SAMs have shown remarkable stability and selectivity for K^+ or Na^+ suggesting that the ethylene glycol portion folds into pseudocrown ether structures. Monolayers containing hexaethylene glycol portions are selective for K^+ (13), and those containing pentaethylene glycol portions are selective for Na^+ (Fig. 1.7(12)). In this study, impedance spectroscopy played a crucial role in obtaining these results because the structural components of the SAMs are electroinactive. Blocking effects on the CV behaviour of a redox probe, $[\text{Ru}(\text{NH}_3)_6]^{3+/2+}$, confirmed the binding of the redox inactive metal ions in an aqueous system.

Other binding motifs have been incorporated into SAMs to recognize redox inactive cations. For example, the highly selective calix[4]crown-6, in its 1,3-alternate conformation, has shown remarkable efficiency in extracting ^{137}Cs ion from radioactive waste [61], and Echegoyen et al. have shown that this type of receptor retains its selectivity when incorporated into SAMs [62, 63]. Once again, impedance spectroscopy and cyclic voltammetry were employed to detect and to compare the recognition properties of remarkably stable monolayers containing different conformational isomers of *p*-*tert*-butylcalix[4]crown-6 and *p*-*tert*-butylcalix[4]arene bithioctic ester derivatives. SAMs derived from the cone isomer of *p*-*tert*-butylcalix[4]crown-6 derivative do not bind Cs^+ ; however, SAMs derived from its 1,3-alternate isomer recognized Cs^+ selectively [62]. This selective recognition of Cs^+ was confirmed by both CV blocking experiments and EIS in aqueous media. This study clearly showed that the selectivity of the calixcrown SAMs is modulated by the change in conformation. These monolayers are also capable of differentiating between alkaline earth metal cations from alkali metal cations in aqueous solutions [63]. In addition to building monolayer sensors for redox inactive metal ions, the same group has recently developed a calix[6]crown-4 based sensor for redox inactive organic cations in aqueous media[64].

1.3 Self-assembly of supramolecules

Using self-assembly and supramolecular chemistry in nanofabrication is a promising strategy to obtain large scale devices that are organised at the molecular level. One of the key issues in the controlled immobilisation of molecules at surfaces leading to well defined and stable nanostructures. For this purpose, molecular printboards which are self assembled monolayers (SAMs) of host molecules to which guest molecules can be bind in a supramolecular fashion were developed by Nijhuis et al. from University of Twente, The Netherland. The advantage of the supramolecular chemistry, compared to chemisorption, physisorption, or covalent chemistry, is that the binding kinetics and thermodynamics can be precisely controlled. Additionally, supramolecular interaction can also respond to external stimuli to give control over adsorption processes. The local characterisation of such assemblies is described in Chapters 7 and 8.

For a variety of application in molecular electronics, switchable molecules or supramolecular assemblies that can be controlled by external stimuli are a prerequisite.

Redox-switchable molecules are of special interest to incorporate into electronic devices. Moreover, such molecules or supramolecular systems are also of importance in the design of molecular machines, molecular motors, or molecular actuators. Although to date no molecular system exists that can compete with conventional silicon-based technology, a deeper understanding of how molecular scale devices work and differ in properties compared to macroscale devices grows steadily, despite some difficulties in the interpretation of the data.

Single supramolecular interactions are in general relatively weak, but multivalent interaction increases the stability of supramolecular assemblies dramatically. For this reason, a fundamental understanding of multivalency is required which may, for instance, have a profound influence in the design of new protocols for bottom-up nanofabrication.

1.3.1 Host-guest complexes

For example cyclodextrins (CDs) were considered as host molecules which form stable inclusion complexes with redox-active guest molecules such as ferrocene (Fc). The interplay of the cavity size and the nature of the redox-active guest molecules allows precise control over the host-guest complex formation, stoichiometry, and thermodynamics.

CDs are produced by enzymatic conversion of starch. CDs contains a hydrophobic cavity to which small molecules can bind in aqueous media [65]. CDs consists of linked glucose units to yield a chiral macrocycle and the size depends on the number of glucose units. The most common CDs are α -cyclodextrin, β -cyclodextrin (β CD), and γ -cyclodextrin, composed of 6, 7 and 8 glucose units, respectively.

The oxidation state of the guest molecule can strongly affect the stability of CD host-guest complex. One of the first example of a redox-controlled host-guest complex is the β CD-Fc inclusion complex [66, 67]. A detailed electrochemical study by Matsue et al. of ferrocene carboxylic acid in the presence of β CD showed that the peak oxidation potential shifted to higher potentials and the currents decreased upon complexation [68]. These findings were attributed to a CE mechanism, that is dissociation of the inclusion complex occurs prior to oxidation of FcA^- . Also, the currents for the inclusion complex are lower than for the free Fc species due to a lower diffusion constant of the complex. The oxidation mechanism is outlined in the Fig. 1.8. Experimental evidence for the direct oxidation of the β CD-Fc complex could not be found. The oxidised form of FcA^- does not bind to β CD $K_f \gg K'_f$ (Fig. 1.8). The binding behavior is in sharp contrast to the binding of FcA^- to

sulfonatocalix[6]arene which cause a negative shift of the peak oxidation potential and to a smaller extent effects the peak currents [69].

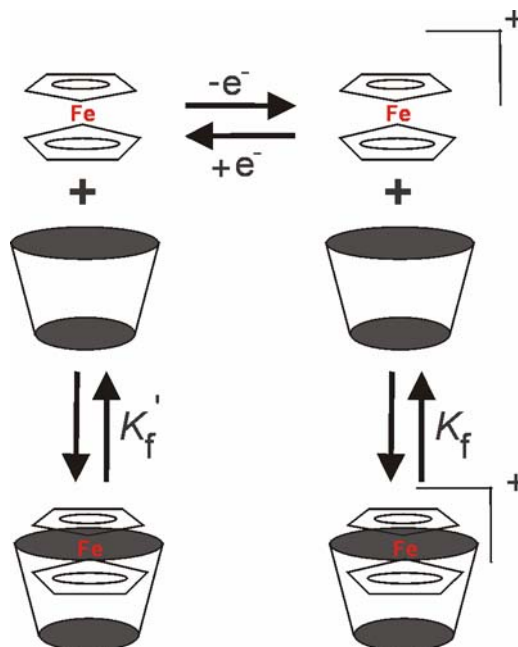


Fig. 1.8: Electrochemical oxidation of Fc and its inclusion complex with β CD.

This indicates that the host interacts more strongly with the oxidised form of FcA^+ , which can be explained by the anionic character of both the guest and the host in the reduced form. Kaifer et al. [70] Reported later that Fc-ammonium salts also can bind effectively to β CD.

1.3.2 Dendrimers

Dendrimers are highly branched monodisperse polymers bearing all functional end groups at the periphery of the molecule [71, 72]. This allows to control the stoichiometry of the host-guest complex. Ideally, dendrimers are defect free with a well defined three-dimensional structure that can be prepared by a sequence of reactions. The dendrimers have internal cavities to which guest molecules can bind, but also binding to the periphery of the molecules is possible. Functional molecules may be incorporated in the dendritic branches or at the focal point of the dendrimers. Due to these interesting properties, a variety of applications have been found for dendrimers in different fields [73]. Dendrimers have been prepared with a wide range of end groups of which especially metallo-dendrimers have attracted considerable interest [74, 75].

Fc-terminated dendrimers Fig. 1.9 have been used in molecular recognition of negatively charged ions [76-79]. Fc-decorated dendrimers or dendritic wedges are electrochemical exoreceptors for inorganic anions, oxo-anions and biological molecules [80]. The neutral dendrimers can only form hydrogen bonds with anionic guests, but the oxidised form of the dendrimers can also have electrostatic interactions to enhance the binding.

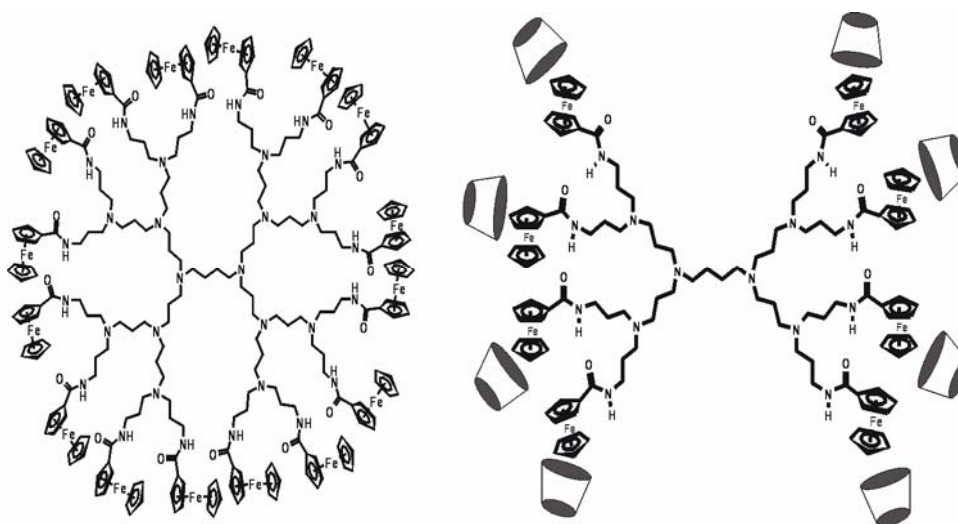


Fig. 1.9: A third generation poly(propylene imine) (PPI) dendrimers with Fc moieties (left). Second generation PPI dendrimers with Fc end groups complexed to β CD resulting in a water soluble supramolecular assembly (right).

Usually, the binding of anions is stronger and selectivity increases by increasing generations. This is the so-called “dendritic effect” which is caused by surface saturation of the higher generation dendrimers, bringing the Fc termini in close proximity with each other, resulting in smaller surface holes.

Simple modification of the linkage of the Fc units to the dendritic core has a profound influence on the binding stoichiometry to anions. Fc functionalised polypropylene imine (PPI) dendrimers linked via urea moieties have also been used in recognition studies of H_2PO_4^- and compared to HSO_4^- and Cl^- [81].

Decorating dendritic molecules with redox-active guest functionalities allows control over the formation of large supramolecular assemblies. PPI dendrimers bearing Fc guest functionalities have been prepared [82, 83], of which a third generation is shown in the Fig. 1.9. PPI dendrimers decorated with Fc units are virtually insoluble in aqueous media, but

complexation of the Fc moieties to β CD resulted in large soluble supramolecular multisite inclusion complexes of well defined stoichiometries [84].

In this work the redox activity of patterned G3-PPI-(Fc)₁₆ dendrimers at β CD SAMs on SiO₂ was mapped by SECM and local oxidation of Fc dendrimers of different generations induced by the ultramicroelectrode resulted in an effective removal of the Fc dendrimers from the host surface since the oxidation of Fc to the oxidised form (Fc⁺) leads to a loss of affinity for β CD were studied. In addition to that the surface coverage of different generation of dendrimers uniformly distributed on β CD SAMs on SiO₂ were calculated by applying SECM pulse technique.

2 Instruments and techniques for studying reactions at self-assembled monolayers

2.1 Scanning probe techniques

Mankind has always been keen about being able to see through the microscope, in order to understand all kinds of natural phenomenon. The degree of resolution of microscopes has indeed increased over the decades from a few hundred to almost a million times. The later techniques like the electron microscope allowed one to be able to see atomic structures. However, only two decades ago a family of new techniques was invented, the scanning probe microscope (SPM), which revolutionalized the whole microscopy application area. Actually the first microscope of this type was the scanning tunnelling microscopy (STM) [85], which resulted in the award of Nobel prize to Gerd Binnig and Heinrich Rohrer in physics in the year 1986. Some years later atomic force microscopy (AFM) [86] was added to these SPMs. And years later other SPM techniques like scanning near field optical microscopy (SNOM) [87], scanning electrochemical microscope (SECM) [88, 89] were added to the SPMs family. SPMs thus allowed one to analyse the physical and chemical properties which were not possible with earlier microscopy technique. These are, for example, distributions of temperature, electrical potential or concentration, course of chemical reactions. With SPMs one could investigate under fluids, in high pressure or in vacuum. The three-dimensional digital images could be analysed by digital procedures, thus enhancing the analyses. Under dynamic conditions one can see details of molecular dynamics, such as gas adsorption. The corresponding SPM images are displayed as false colour images, in which particular physical properties of objects (and not object colour themselves) are presented with a lateral resolution by a colour code or by the intensity of a single colour [90].

Depending on the requirements the following SPMs are used in different fields. Most SPMs techniques provide mapping of physical properties (geometry, topography, local density of states etc). SECM maps distribution of local electrochemical properties of solid-liquid, liquid-liquid and liquid-gas interfaces. This thesis adapted few electrochemical techniques combined with SECM to study this task.

2.2 Scanning tunnelling microscopy

An idea to use current between a local probe and a sample in order to image microscopic structures of conductive surfaces was proposed as early as 1971 by Young et al. [91]. However, a real breakthrough was achieved by Binnig and Rohrer [85] who constructed a corresponding instrument “the scanning tunnelling microscope” [92] that provided atomically resolved images of reconstructed surfaces, which could not be obtained by other techniques.

In STM, a small voltage is applied between a sharp metallic probe (tip) and a conductive sample. If the tip is brought within about 1 nm to the sample surface, this voltage causes a tunnelling current between the tip and the sample. The tunnelling current depends exponentially on the probe-sample distance d [93]. Therefore, the current flows mainly through the foremost atom of the tip and atoms of the sample surface directly beneath it.

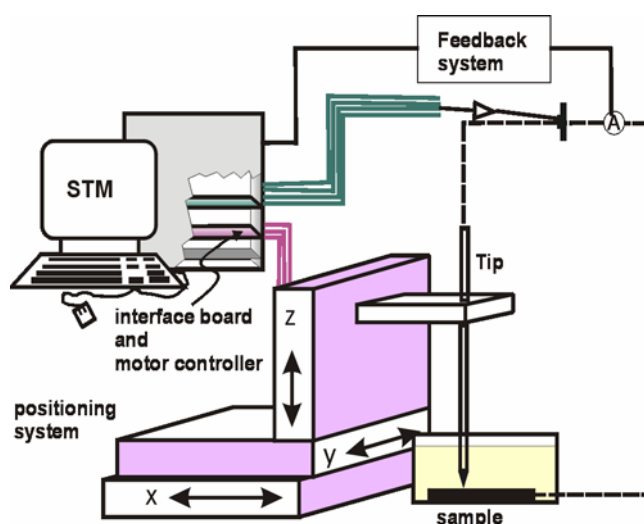


Fig. 2.1: Schematic of STM instrument.

Several components are essential to build an SPM: data acquisition unit, positioning system, and feedback system (Fig. 2.1). These same components will be seen later in other SPMs described in this work. In STM, the tip position in the scanning plane (x, y) and the tip height z above the sample are controlled by a three-dimensional (3D, in Cartesian coordinates $r = (x, y, z)$, where r is the coordinate vector) positioning system using piezoelectric actuators. Computer-controlled data acquisition instruments enable measurements and storage of tunnelling current i_{tun} . The feedback system controls the tip z -position when i_{tun} changes in order to keep i_{tun} constant. The system can operate in two modes. With the feedback on, i_{tun} , and thus d , is kept constant with z adjusted by the feedback system, which results in $z = f_1(x,$

y). It is called constant current mode. With feedback off, z is kept constant (constant height mode) and i_{tun} is measured as $i_{tun} = f_2(x, y)$ which results in $d = f_3(x, y)$. For rough samples, the constant current mode is preferred because it prevents the collision of the tip with the sample. However, the recording speed is limited by the feedback system. For video STM [94] where sequences of images are recorded for objects moving across surfaces, the constant height mode is essential.

If experimental conditions enable obtaining atomic resolution, i_{tun} is a function of both the local states at the sample surface and the atomistic topography. Atomically sharp probes and relatively flat surfaces are the prerequisites for such experiments. The resolution decreases with the decreasing the sharpness of the probe. In this case tunnelling occurs over a large spatial region. Therefore, details of the sample topography are visible on the length scale of the probe surface interacting with the sample reflecting the morphology (topography) of the sample. This is the prevailing situation for the combined STM-SECM images which will be discussed later in this work.

In order to obtain tunnelling current, STM can be used only on conductive or semi-conductive surfaces. Experiments are often carried out in ultra high vacuum (UHV), however it is possible to use STM in electrolyte solution [94]. Even when carried in solutions, electrochemical STM provides chemical information only from changes of topography (metal deposition or dissolution [95] and when the chemical identity at the surface is known from other experiments or controlled by the experimental set up.

2.3 Atomic force microscopy

The first atomic force microscopy (AFM) was invented by Binnig et al. [86] after the they discovered STM. The AFM allows to investigate conductive and non-conductive samples with the resolution close to that of STM. The components of AFM are, a 3D piezoelectric positioning system, a measurement unit, and a feedback system (Fig. 2.2). The principle of AFM is based on a measurement of the force between a scanning probe tip and surface. This force is frequently measured by noting the deflection of cantilever when it approaches the surface. The bending of the cantilever is monitored by the deflection of the laser beam reflected on the back side of the cantilever. As the cantilever scans over the sample, the feedback loop regulates the cantilever z -position to maintain a constant deflection of the laser beam. By storing the z -position as $z = f_4(x, y)$, a topography map is obtained.

Measurements can be carried out both in UHV and in solutions. The latter can be termed as electrochemical AFM.

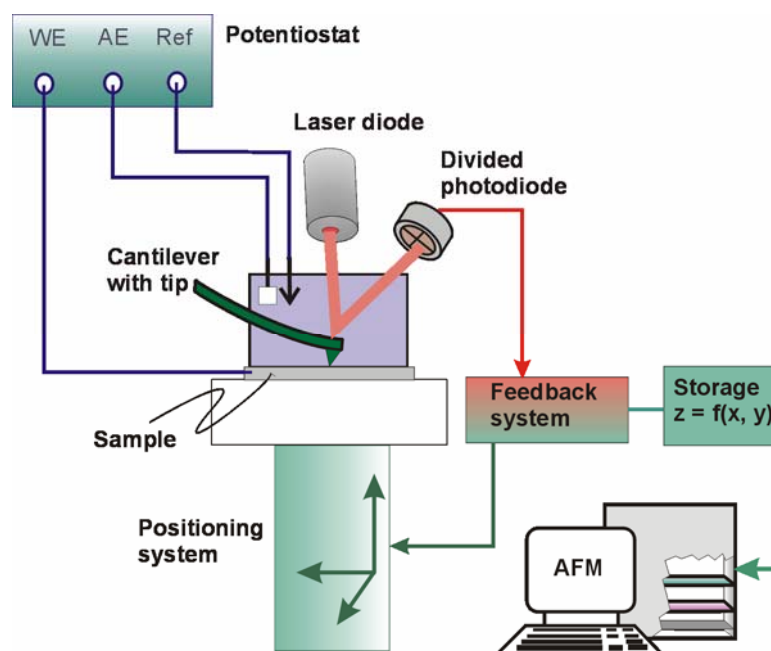


Fig. 2.2: Schematic of an AFM instrument.

The AFM instruments can make use of different cantilever-sample forces in order to obtain the signal. In the contact mode, the tip touches the sample surface permanently and the cantilever is bent because of repulsion of incompletely screened nuclear charges if atoms are pressed together. The contact mode has some practical limitations because the high local pressure of the tip can alter the delicate samples. Therefore many instruments (especially for experiments on biological samples in liquids and thin organic monolayers) use vibrating cantilevers that touch the surface only intermittently. This operation mode was first realised by Digital Instruments under the trade name Tapping Mode, in which the cantilever vibrates at a distance more than 1nm from the sample surface. The amplitude change or the phase shift can be monitored. They can be caused by ionic repulsion, but also by van der Waals, electrostatic, magnetic, or capillary forces [96, 97].

2.4 Scanning near field optical microscopy

Scanning near-field optical microscopy (SNOM) is an imaging technique used to obtain resolution beyond the Abbe diffraction limit. The first citation that this was possible came

from Syngé [87]. Although not strictly feasible with the technology of the time, his technical criteria form an accurate basis for a super-resolution optical microscope.

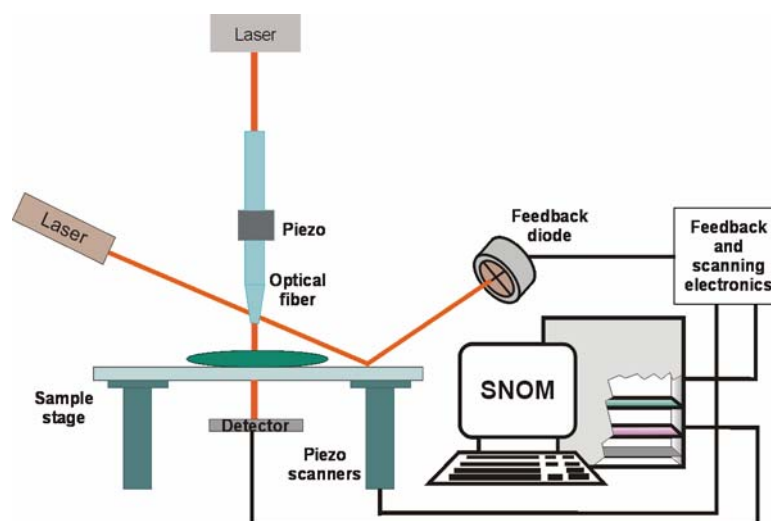


Fig. 2.3: Schematic of SNOM instrument.

The operational principle of SNOM involves illuminating a specimen through a sub-wavelength sized aperture whilst keeping the specimen within the near-field regime (Fig. 2.3) of the source. Broadly speaking, if the aperture-specimen separation is kept roughly less than half the diameter of the aperture, the light does not have the opportunity to diffract before it interacts with the sample and the resolution of the system is determined by the aperture diameter as oppose to the wavelength of light used. An image is built up by raster-scanning the aperture across the sample and recording the optical response of the specimen through a conventional far-field microscope objective. It took almost fifty years for experimental proof that near-field imaging was indeed possible. Ash and Nichols [98] demonstrated this with a system based on microwaves and obtained resolution approaching $\lambda/60$. After few years Pohl et al. [99] achieved this goal with visible light.

The most important advantage of SNOM is that it uses the "light" as the interaction principle. SNOM enables one to obtain a high-resolution micrograph with chemical contrast through spectroscopic measurements. The application of SNOM further extends to determine the phase separation structure of polymer monolayer [100], internal structure of polymer gels [101], high resolution patterning on polymer matrix [102] and single molecule spectroscopy [103].

2.5 Scanning electrochemical microscopy

Although the STM and AFM discussed above result in high-resolution topography maps, no direct information about chemical reactivity can be obtained when using ECAFM, ECSTM or SNOM. However, this kind of information plays a significant role in understanding the nature of localised processes on chemically active surfaces and interfaces.

Scanning electrochemical microscopy (SECM) was developed in order to enable microscopy of chemical processes. Here, the general operating principles and applications of SECM, which are of central importance for this work, are described qualitatively. A detail and through discussion on theory of single potential step and double potential step chronoamperometry SECM is also provided in this chapter.

2.5.1 General operation principles of SECM

SECM was developed by Bard et al. [89, 104] in order to enable investigations of local electrochemical process on the micrometer range. The SECM records Faradic currents at an UME probe in solutions as a measure of the local chemical reactivity at the sample.

The UME is immersed in an electrolyte solution of electrochemically active species (mediator) and is positioned close to the sample surface (Fig. 2.4). A potential that is sufficient for a diffusion-controlled electrochemical reaction of the mediator is applied to the UME. The scans are usually carried out at a constant height. The position of the UME is controlled by a positioning system. Often, high precision stepper motors or piezoelectric actuators with long traveling ranges are used because relevant distances are much larger than in electrochemical STM or electrochemical AFM. Electrochemical reactions at UME and the sample are controlled by a (bi)potentiostat (Fig. 2.4).

Kwak and Bard [105] have demonstrated that the UME current is affected by the sample topography and by UME-sample distances (d). Wipf and Bard [89] have shown that at small d , the Faradic current at the UME depends on the local electrochemical activity of the sample. Therefore, the UME current cannot be a universal measure of d that might be used for distance regulation. Recently, current-independent feedback systems were described for an automated probe positioning [106-108] as opposed to the constant height mode, when no distance-regulating feedback system is used and d may change with the topography of the sample. A thorough description of the SECM instrumentation and application can be found elsewhere [109-111].

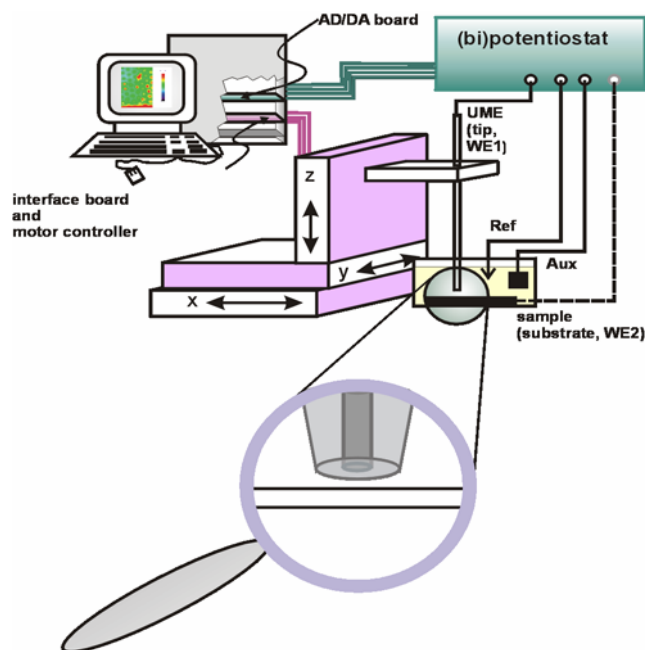


Fig. 2.4: Scheme for an SECM instrument. Main components: electrochemical cell with an UME as a probe, three dimensional positioning system, bipotentiostat to control electrode reactions at the UME and the sample.

Two basic SECM experiments can be distinguished: imaging and line scans in z direction (approach curve). In imaging experiments, the UME scans horizontally along the sample surface, either in the constant height or in the constant distance mode, resulting in a laterally resolved map of the sample reactivity. In approach experiments, the Faradic currents are measured in dependence on d , yielding characteristic curves [112] that reflect the geometry of the UME and the local reaction kinetics of the sample.

2.5.2 Single potential step chronoamperometry (SPSC) experiment

Chronoamperometry is an electrochemical technique in which the potential of the working electrode is stepped, and the resulting current from Faradic processes occurring at the electrode is monitored as a function of time. The potential of the electrode is changed in step-like fashion from a level where no net reaction occurs to a level where there is a net charge transfer reaction in one direction (Fig. 2.5a). The concentration profile during the experiment can be calculated using Fick's law and the appropriate boundary conditions (Fig. 2.5b). Since the Faradic current is governed by the flux of redox molecules, the concentration gradient at ($x = 0$) controls the current. The current at a flat electrode in the semi-infinite diffusion regime, is described by the Cottrell equation:

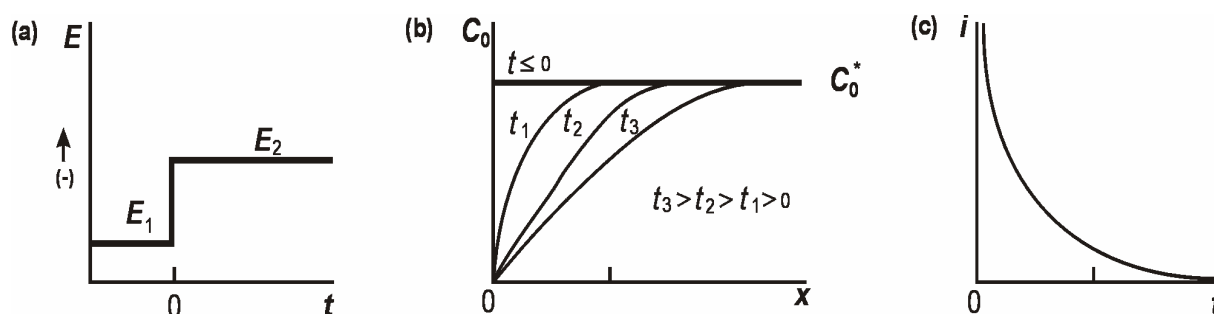


Fig. 2.5: (a) Typical wave form for a SPSC experiment in which species O is electroinactive at E_1 , but is reduced at a diffusion-limited rate at E_2 . (b) concentrations profiles for various times into the experiment. (c) typical current-time response in SPSC experiment.

$$i = \frac{nFAD^{1/2}c^*}{\pi t^{1/2}} \quad (2.1)$$

Here i is the faradic current, n the number of electrons exchanged in the reaction, F the Faraday constant, D the diffusion coefficient, and c^* the concentration in the bulk. According to this equation, the current decays fast. This is caused by the depletion of the diffusion layer close to the surface. If a constant potential is applied, the diffusion layer becomes thicker with time, while the concentration gradient decreases and therefore the diffusion to the surface decreases. Because the current is linearly dependent on the concentration gradient, it will also decrease with time.

By combining with SECM, the single potential step chronoamperometry allow us to monitor the local electrolysis. The chronoamperometric transients are affected by the local reaction at the surface when SPSC is performed in combination with SECM.

2.5.3 Principle of SPSC at SECM

The single potential step chronoamperometric mode has proved to be a particularly powerful method for inducing and monitoring reversible transfer processes at both liquid/solid interfaces [113-119] and immiscible liquid/liquid interfaces [120]. In this application, the UME probe is positioned in a liquid phase, close to the interface of interest at which the transfer process is initially at equilibrium. The electrolysis of a target species at the UME probe depletes its concentration locally, which, in turn, provides the thermodynamic driving force for the interfacial transfer process in the direction of the phase containing the UME probe. This serves to enhance the flux of electroactive material to the UME, compared to the situation where the interface is inert, and the flowing current provides quantitative information on the interfacial transfer kinetics. Reversible reaction studies using this SECM

equilibrium perturbation mode include dissolution [113, 118], adsorption/desorption [119] and solvent extraction/stripping processes [120].

To illustrate the principle of single potential step chronoamperometry mode at SECM, a case is considered where adsorption and desorption of metal ion occurs at the surface of interest.

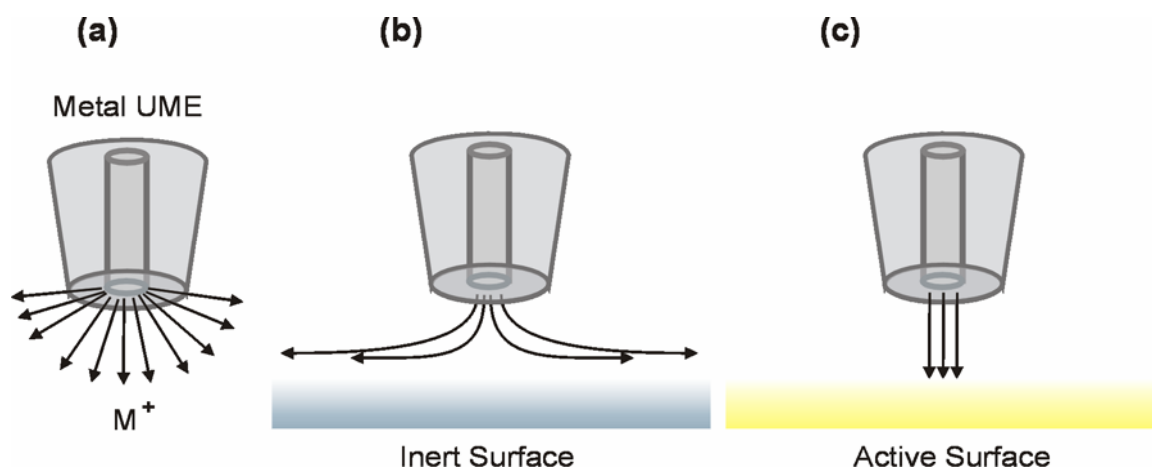


Fig. 2.6: Schematic for SECM-SPSC experiment. In (a) the metal UME is relatively far from the surface and M^+ ions diffuse away from the electrode surface in a hemispherical manner. In close proximity to an inert surface (b), diffusion is hindered and a lower current flows than in (a) at the same electrode potential. If M^+ is taken up by the surface below the UME, there is a concomitant increase in the current flowing at the UME to maintain the electrode surface concentration of M^+ , at a given potential.

To measure local the uptake of metal using the SECM, M^+ ions are electrogenerated via the anodic dissolution of a metal UME, positioned close to the surface of interest (Fig. 2.6). Under potentiostatic control, the current response of the reversible UME process is governed by the rate of M^+ transport away from the probe surface. This, in turn, depends on the extent to which M^+ interacts with the surface. In simple terms, if M^+ is inert with respect to the surface of interest, it simply leaks away from the electrode surface by hindered diffusion (Fig. 2.6b), then a small current flow compared to the case where the UME is in the bulk solution and diffusion is hemispherical (Fig. 2.6a). In contrast, a rapid uptake of M^+ by the surface of interest enhances the flux of M^+ away from the probe, causing a larger current to flow (Fig. 2.6c). In this manner, a specific region of the surface is targeted, and any adsorption or growth behavior involving M^+ is monitored quantitatively and exclusively through the current response at the UME probe.

2.5.4 Theory of SPSC at SECM

To lay out the theory a model system was chosen where irreversible adsorption of electrogenerated metal ion (M^+) onto a substrate surface containing a fixed number of adsorption sites was investigated. The partial differential equations are solved numerically. A model for the adsorption case was developed numerically by Unwin et al.

The axisymmetric cylindrical geometry of the SECM is governed by the following general dimensionless diffusion equation

$$\frac{\partial c}{\partial t} = D \left[\frac{\partial^2 c}{\partial r^2} + \frac{1}{r} \frac{\partial c}{\partial r} + \frac{\partial^2 c}{\partial z^2} \right] \quad (2.2)$$

where c denotes the concentration of the species of the interest, which has a diffusion coefficient, D , r is the radial co-ordinate starting at the center of the UME, z is the co-ordinate normal to the UME surface (again starting at the surface) and t is the time. The electrode radius runs from $r = 0$ to $r = r_T$, with the probe at $z = 0$. The edge of the probe insulation is at $r = r_g$. In the z -direction the substrate location is $z = d$.

The species of interest, M^+ is electrogenerated from the metal UME, in a solution containing supporting electrolyte. M^+ ions diffuse towards the sample interface containing a fixed density of surface sites, N (mol cm^{-2}). For a simple irreversible adsorption process, the flux of M^+ at the substrate/solution interface may be written:

$$z = 0, \text{ all } r: D \frac{\partial c}{\partial z} = k_a (\theta - 1) c \quad (2.3)$$

Where θ is the fraction of the filled surface sites and k_a is the adsorption rate constant. The rate at which the surface sites are filled is given by

$$z = d, \text{ all } r: \frac{\partial \theta}{\partial t} = \frac{k_a c (1 - \theta)}{N} \quad (2.4)$$

The initial condition relates to a concentration of M^+ in the bulk solution at time $t = 0$.

$$0 \leq z \leq d, 0 \leq r \leq r_g: c = 0 \quad (2.5)$$

At $t > 0$, the potential is stepped to a value to affect the oxidation of the metal UME, causing M^+ ions to diffuse from the UME towards the substrate. Assuming this electrolytic

process is reversible, the concentration of M^+ adjacent to the UME surface, $c(d=0)$, is governed by the Nernst equation:

$$z = d, 0 \leq r \leq a: c = c(d=0); E = E^{0'} + \frac{RT}{F} \ln c(d) \quad (2.6)$$

Thus the concentration of M^+ effectively injected by the UME can be controlled via the potential, E , with reference to the formal electrode potential, $E^{0'}$. In equation 2.6, R , T and F each have their usual meaning.

The boundary conditions for this problem are summarized below:

$$z = 0, r_T \leq r \leq r_g: D \frac{\partial c}{\partial z} = 0 \quad (2.7)$$

$$0 \leq z \leq d, r > r_g: c = 0 \quad (2.8)$$

$$0 \leq z \leq d, r = 0: D \frac{\partial c}{\partial r} = 0 \quad (2.9)$$

The boundary condition for the substrate was given by equations 2.3 and 2.4.

The problem can be put into dimensionless form by introducing the following variables:

$$C = c / c(d=0) \quad (2.10)$$

$$R = r / r_T \quad (2.11)$$

$$Z = z / r_T, L = d / r_T \quad (2.12)$$

$$\tau = tD / r_T^2 \quad (2.13)$$

$$K_a = k_a r_T / D \quad (2.14)$$

$$\phi = N / c(d=0) r_T \quad (2.15)$$

The normalized form of the substrate boundary condition is,

$$L = d / r_T, 0 \leq R \leq RG: \frac{\partial C}{\partial Z} = K_a C(\theta - 1) \quad (2.16)$$

Where $RG = r_g / r_T$, coupled with,

$$\phi \frac{\partial \theta}{\partial \tau} = K_a C(1 - \theta) \quad (2.17)$$

The normalized UME current response I_T is calculated from

$$\frac{i_T}{i_{T,\infty}} = \frac{\pi}{2} \int_0^1 \left(\frac{\partial C}{\partial Z} \right)_{Z=0} R dR \quad (2.18)$$

In this equation, i_T is the tip current and $i_{T,\infty}$ is the steady-state diffusion-limited current at an inlaid disk electrode positioned at an effectively infinite distance from the substrate surface. For the present problem, this is given by:

$$i_{T,\infty} = 4nFr_T Dc(d = 0) \quad (2.19)$$

The problem was solved numerically using alternating direction implicit finite difference method by Unwin et al. and has been widely applied to SECM problems [113-116, 118, 121-126].

2.5.5 Double potential step chronoamperometry (DPSC) experiments

In a single potential step chronoamperometry (section 2.5.3) the current of the oxidized or reduced species are monitored at the electrode as a function of time during single potential step of the UME, whereas in double potential step chronoamperometry, the oxidized or reduced species are collected back at the electrode by reversing the potential of the electrode. Such methods comprises a large class of approaches, all featuring an initial generation of an electrolytic product, then a reversal of electrolysis so that the first product is examined electrolytically in a direct fashion. Reversal methods make up a powerful arsenal for studies of complex electrode reactions, and reveal much more about the system. The technique will be discussed further with examples to follow.

Lets consider the effect of the potential program displayed in Fig. 2.7a. The forward potential step, that is, the transition from E_1 to E_2 at $t = 0$, is exactly the chronoamperometric experiment for a single step chronoamperometric experiment. For a period τ , it causes a buildup of the reduction product (e.g., X^- anion radical) in the region near to the electrode. However, in the second phase of the experiment, after $t = \tau$, the potential returns to E_1 , where only the oxidized form (e.g., X) is stable at the electrode. The anion radical cannot coexist there; hence a large anodic current flow as it begins to reoxidize, then the current declines in magnitude (Fig. 2.7b) as the depletion effect sets in.

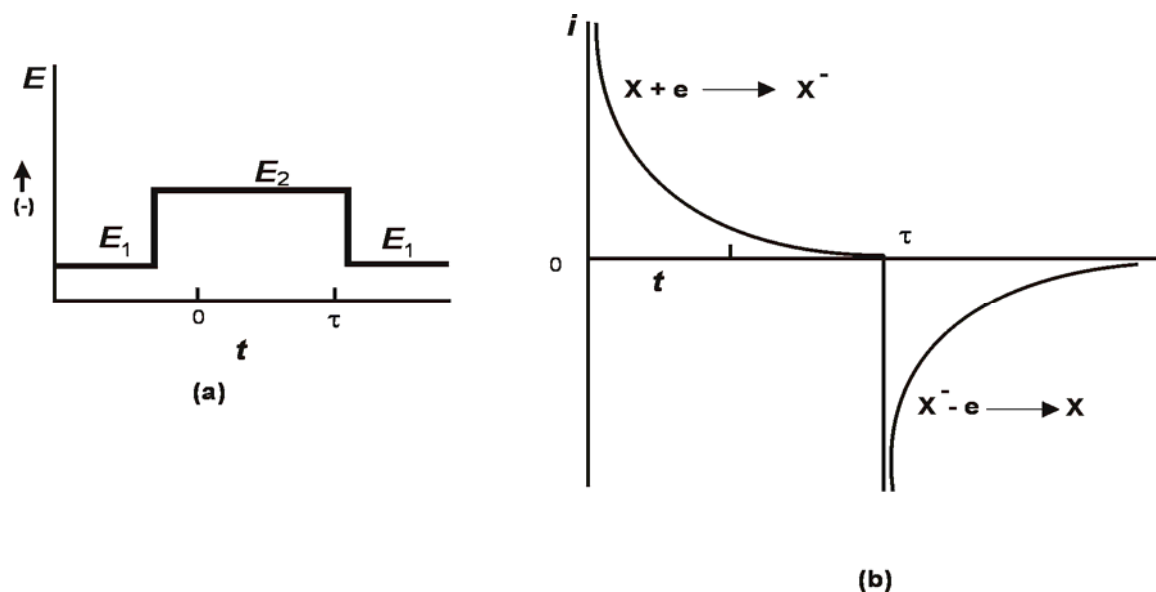


Fig. 2.7: General waveform for a double potential step chronoamperometry experiment (a), current response in double potential step chronoamperometry experiment (b).

In general DPSC has been used to study the rate of a chemical reaction of different chemical species by electrolysis. Birke et al. [127] found the rate constant of a series of alkylcobalamines as a function of temperature in different solution mixture by DPSC technique. Ahlberg et al. [128] studied the kinetics of Lucigenin- 10,1 o-Dimethyl-9,9-biacridylidene redox system by employing the DPSC technique over a temperature range from +23 to -20° C. Electronic properties of the Ph_4P^+ salts of the mixed terminal ligand cubanes $\text{F}_4\text{S}_4(\text{E}_2, \text{Dtc})\text{n}(\text{X}_{4-\text{n}})^{2-}$ ($\text{X} = \text{Cl}^-, \text{PhS}^-$) ($n = 1, 2$) were studied by Kanatzidis et al. [129] Quantitative studies of DPSC shows that the redox processes are diffusion-controlled over the range of 20 ms. The i_c/i_a and i_{pc}/i_{pa} ratios in chronoamperometry and cyclic voltammetry, respectively, show the oxidation product to be unstable. Chronoamperometry indicates that the oxidation product should be stable for about 100 ms. Andrieux et al. [130] studied the electrochemical reduction of dioxygen in dimethyl sulfoxide as a function of the addition of acids by means of DPSC. They analysed the kinetics as a function of dioxygen and acid concentrations and of the measurement time in a series of acids involving five phenols and nitromethane.

Raouf et al. [131] studied the electrocatalytic oxidation of L-cysteine at modified carbon paste electrode by DPSC technique. They come to a conclusion from DPSC measurement that with the redox mediator (Fc/Fc^+), L-cysteine oxidation can be catalyzed at a modified carbon paste electrode. Diffusion coefficient of fullerene C_{60} and C_{60}^- were found out in different

solvent by Hishida et al. [132] by using both single step and double step chronoamperometry technique. Galvez et al. [133-135] has shown simple procedures to determine the values of the rate constants for electrode processes with a slow charge-transfer reaction by using DPSC at plane electrodes. In addition, these procedures provide criteria to assess easily the reversibility of the electrode reaction.

A new method for the determination of the diffusion coefficients of both the substrate (D_S) and the product (D_P) of an electrode process was developed by Hyk et al. [136] by using DPSC over a microelectrode. They explored the two of the unique features of microelectrodes, first the substantial reduction of the ohmic potential drop that allows the electrochemical measurements to be performed at very low ionic strengths, and second the enhancement of the transport of the redox species to the microelectrode surface that makes the electrochemical experiment more sensitive to the transport properties of both substrate and product.

DPSC has also been used for various application [137-148], but when it combined with SECM it allows us to monitor the electrochemical process locally and also to study the kinetic process at an insulating surface by employing a UME close to a surface. The principle and theory of SECM-DPSC will follow in details in further section.

2.5.6 Principle of DPSC at SECM

In order to diversify the range of process that can be studied with SECM transients method, SECM double potential step chronoamperometry (DPSC) as a new methodology were introduced by Unwin et al. [122]. The method was used for initiating and monitoring heterogeneous reactions at the local level. The idea is further used to study metal ion interaction with the organic monolayers at gold substrate via SECM by us.

When used in conjunction with UMEs, DPSC has proved to be a powerful approach for characterizing the diffusion coefficients of electrogenerated species [149] and the lifetime of transient species involved in solution processes [140]. However, DPSC has not been previously used to investigate the kinetics of processes confined to a target interface. The basic concept of SECM DPSC is to employ the UME probe to electrochemically generate a reactive species (**B** in Fig. 2.8) in an initial (forward) potential step for a fixed period. The species could be generated through the electrolysis ($A \rightarrow B + e^-$) of an inert precursor in the solution (**A** in Fig. 2.8) or via the anodic dissolution of a pure or amalgam metal electrode.

During the forward step the electrogenerated species B diffuses away from the probe and intercepts the interface. If B interacts with the interface through either an irreversible or reversible process (Fig. 2.8b(i)), e.g., adsorption, absorption, or a chemical reaction, its concentration profile will be modified compare to the situation where there is no interaction and the species simply slowly leaks out of the probe/interface gap by hindered diffusion [Fig. 2.8a(i)]. Consequently, when the potential is reversed, in a final step to collect the species by electrolysis, the flux of B at the UME and the corresponding current-time characteristics-will be strongly dependent on the nature of the interaction of B with the target interface.

For a particular case of an irreversible process, illustrated using the case of transfer (or absorption) in parts b(i) and b(ii) of Fig. 2.8, it may be anticipated that there will be a decrease in the concentration of B in the probe/interface gap which, in turn, will result in a decrease of the UME current during the reverse potential step. After the mass transport problem is solved for this situation, the reverse current –time behavior provides independent information on the probe/interface separation [150, 151], enabling the quantitative interpretation of the reverse current-time characteristics.

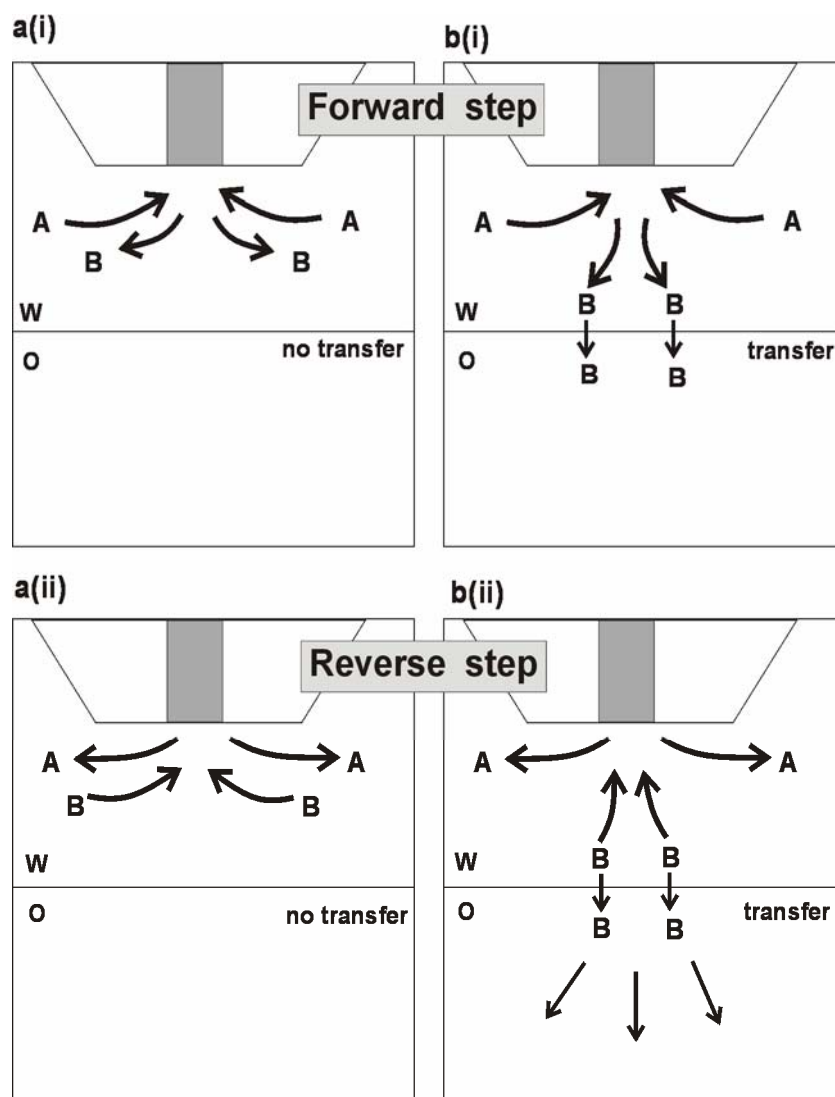


Fig. 2.8: Schematic of the processes in the UME/substrate gap for SECM-DPSC using the irreversible transfer of a solute across a water/organic (w/o) interface as an example. During the forward step, species B is electrogenerated from A [a(i) and b(i)] in the aqueous phase. If B is inert with respect to the target interface, it simply slowly leaks from the UME/interface thin electrochemical cell gap by hindered diffusion [a(i)]. Consequently, when the potential is stepped back to reverse the electrode reaction, much of B is available for collection [a(ii)]. In contrast, if B crosses the w/o interface, as in b(i) and (ii) where it partitions into the o-phase, there is a net depletion of B in the w-phase, resulting in a smaller collector flux [b(ii)] compared to the inert interface case [a(ii)] [122].

2.5.7 Theory of DPSC at SECM

Considering the situation where the solution initially contains only a precursor species A that does not interact with the interface. At time $t = 0$, the potential of the UME probe is stepped to a value to cause the following diffusion-controlled electrolysis:



resulting in the generation of the reactive species B.

The transport of species A and B in the axisymmetric cylindrical geometry of the SECM is governed by the following general dimensionless diffusion equation (where the subscript i denotes A or B):

$$\frac{\partial C_i}{\partial t} = \lambda_i \left[\frac{\partial^2 C_i}{\partial R^2} + \frac{1}{R} \frac{\partial C_i}{\partial R} + \frac{\partial^2 C_i}{\partial Z^2} \right] \quad (2.21)$$

The dimensionless terms in eq. (2.21) are defined in eq. (2.10) – (2.15).

D_A is the diffusion co-efficient of A. The parameter reflects the fact that A and B may have different diffusion coefficients

$$\lambda_i = D_i / D_A \quad (i = A \text{ or } B) \quad (2.22)$$

The concentrations of A and B have been normalised with respect to the bulk concentration of A, c_A^* , such that

$$C_A = C_A / C_A^* \quad (2.23)$$

$$C_B = C_B / C_B^* \quad (2.24)$$

The following boundary conditions hold following the initial potential step at $\tau = 0$ and prior to the reverse step at $\tau = \tau_{\text{switch}}$:

$$0 \leq \tau < \tau_{\text{switch}}, \quad Z = 0, \quad 0 \leq R \leq 1: \\ c_A = 0, \quad -\lambda_B (\partial C_B / \partial Z) = \partial c_A / \partial Z \quad (2.25)$$

$$0 \leq \tau < \tau_{\text{switch}}, \quad Z = 0, \quad 1 < R \leq RG: \\ \partial C_A / \partial Z = 0, \quad \partial C_B / \partial Z = 0 \quad (2.26)$$

$$0 \leq \tau < \tau_{\text{switch}}, \quad R = 0, \quad 0 < Z < L: \\ \partial C_A / \partial R = 0, \quad \partial C_B / \partial R = 0 \quad (2.27)$$

$$0 \leq \tau < \tau_{\text{switch}}, \quad R > RG, \quad 0 < Z < L: \\ C_A = 1, \quad C_B = 0 \quad (2.28)$$

$$0 \leq \tau < \tau_{\text{switch}}, \quad Z = L, \quad 0 < R \leq RG: \\ \partial C_A / \partial Z = 0, \quad \partial C_B / \partial Z = K C_B \quad (2.29)$$

The boundary conditions have the following meanings. Equations (2.25) and (2.26) denote that the electrolysis of A to B at the UME occurs at the diffusion-controlled rate, but both the

species are inert on the insulating sheath surrounding the electrode. Equation (2.27) is a consequence of the axisymmetric cylindrical geometry, while eq. (2.28) assumes that both species recover their bulk solution concentrations outside the thin layer zone formed by the probe and interface. This is reasonable assumptions for the probes used practically in most SECM studies [104, 111, 121, 151-155].

Equation (2.29) reflects the activity of A and B at the interface of interest. Species A is inert on this boundary, while B is lost in a first-order irreversible interfacial process, characterised by a normalised rate constant

$$K = \frac{kr_T}{D_B} \quad (2.30)$$

Where k (cm s^{-1}) is a first-order heterogeneous rate constant.

For the period of the reverse step, in which B is electrolysed to A at the UME at a diffusion-controlled rate, it is only necessary to evaluate the concentration profile of B by solving eq (2.21) with $i = B$ subject to the following boundary conditions:

$$\tau_{\text{switch}} \leq \tau, \quad Z = 0, \quad 0 \leq R \leq 1: \quad C_B = 0 \quad (2.31)$$

$$\tau_{\text{switch}} \leq \tau, \quad Z = 0, \quad 1 < R \leq RG: \quad \partial C_B / \partial Z = 0 \quad (2.32)$$

$$\tau_{\text{switch}} \leq \tau, \quad R = 0, \quad 0 < Z < L: \quad \partial C_B / \partial R = 0 \quad (2.33)$$

$$\tau_{\text{switch}} \leq \tau, \quad R > RG, \quad 0 < Z < L: \quad C_B = 0 \quad (2.34)$$

$$\tau_{\text{switch}} \leq \tau, \quad Z = L, \quad 0 < R \leq RG: \quad \partial C_B / \partial Z = KC_B \quad (2.35)$$

The limiting case of an inert interface can be simulated with $K = 0$ in eqs (2.29) and (2.35).

The aim of the model is to provide a solution for the current-time behaviour during the forward and reverse potential steps. For the forward step, the current i_T , normalised with respect to $i_{T, \infty}$, the steady-state current for the diffusion-controlled electrolysis of A with the UME at an effectively distance from the interface, is given by

$$\frac{i_T}{i_{T, \infty}} = \left(\frac{\pi}{2} \right) \int_0^1 \left(\frac{\partial C_A}{\partial Z} \right)_{Z=0} R dR \quad (2.36)$$

where [156].

$$i_{T, \infty} = 4nFD_A r_T C_{A^*} \quad (2.37)$$

For the period of the reverse step the normalised current ratio is given by

$$\frac{i_T}{i_{T,\infty}} = -\lambda_B \left(\frac{\pi}{2} \right) \int_0^1 \left(\frac{\partial C_B}{\partial Z} \right)_{Z=0} R dR \quad (2.38)$$

The problem was solved numerically using a FORTRAN program based on the ADIFDM algorithm by Unwin et. al. [122].

Both SECM SPSC and SECM DPSC have been shown to be a powerful technique for investigating the chemical kinetics of UME-generated species at liquid/solid, liquid/liquid, and liquid/gas interfaces by Unwin et al. The thesis adapted these techniques and applied them in different systems, also a new simulation is in a developing stage using the boundary elementary method (BEM) in order to interpret experimental data in systems with complex geometries. Both techniques by Unwin et al. complement earlier equilibrium perturbation transient SECM methods by allowing the study of irreversible interfacial chemical processes. The current thesis is limited to the experimental results where SECM SPSC and SECM DPSC were used to study the host-guest interaction at molecular printboards as well the interaction of metal ions with organic monolayers. The DPSC method is well established with a model system used by Unwin et al. where ferrocyanide/ferricyanide redox system was used and also has been used to show that the absorption of Br₂ by both air and DCE from aqueous solutions (under sink conditions) is controlled by diffusion of Br₂ in the aqueous phase, with interfacial processes providing no detectable kinetic resistance to transfer within the range of mass transfer rates attainable by SECM.

Scanning probe techniques represent powerful tools for microscopic investigation of physical and chemical properties of objects down to nanometer range. Using SEM, STM, AFM and SNOM, high resolution topography can be obtained. In addition to that SECM allows microscopic investigation of local electrochemical and chemical processes at interfaces using several electrochemical techniques.

3 Experimental

3.1 Substances and solutions

3.1.1 Chemicals

All chemicals were reagent grade and were used as received. All solutions were prepared with deionized water. The redox mediator used in this study are hydroxymethylferrocene (FcMeOH, ABCR GmbH & Co. KG, Karlsruhe, Germany), hexaamineruthenium(II) ($[\text{Ru}(\text{NH}_3)_6]\text{Cl}_3$, ABCR GmbH & Co. KG, Karlsruhe, Germany), potassium hexachloroirriodate(III), ($\text{K}_3[\text{Ir}(\text{Cl})_6]$ Sigma-Aldrich, Steinheim, Germany), potassium hexacyanoferrous(II), ($\text{K}_4[\text{Fe}(\text{CN})_6]$ Merck, Darmstadt, Germany). Besides FcMeOH all redox mediator are water soluble. To prepare aqueous solution of FcMeOH, first it was dissolved in 500 μl ethanol then diluted to 25 ml with aqueous electrolyte solution. The supporting electrolytes are (KCl, Carl Roth GmbH, Germany), (KClO_4 , Janssen Chimica, Belgium), (Na_2SO_4 , Carl Roth GmbH, Germany), (K_2SO_4 , Merck, Darmstadt, Germany), ($\text{Cd}(\text{OH})_2$, Sigma-Aldrich, Steinheim, Germany), 1,9-nonanedithiol and 1-nonanethiol (Sigma-Aldrich, Steinheim, Germany) were used as received.

3.1.2 Materials

The materials used for the UME preparation are used as received. All the metal (Pt, Au, Ag and carbon fiber) wires for UME preparation were purchased from Goodfellow, Cambridge, England. The glass capillaries were purchased from Hilgenberg, Malsfeld. The outer diameter of the capillary is 1.2 mm, the inner diameter is 0.9 mm. Other materials are Ag epoxy (Epo-tek H24, Polytec, Waldbronn), grinding paper K400, K800, K1200, K2000 (Buehlers GmbH), Al_2O_3 abrasive disk paper with 0.3 and 0.5 μm grain size (Buehlers GmbH).

3.1.3 Solutions

Table: 3.1: List of redox mediators.

redox mediator	mass in mg for redox mediator 10 ml redox mediator solution
2 mM potassium hexachloroiridate(III) ($K_3[IrCl_6]$) in 0.1 M $KClO_4$ (1)	10.4 mg of $K_3[IrCl_6]$
2 mM hexaaminruthenium(III)-chlorid ($[Ru(NH_3)_6]Cl_3$) in 0.1 M Na_2SO_4 (2)	6.4 mg of $[Ru(NH_3)_6]Cl_3$
2 mM hydroxymethylferrocen (FcMeOH) in 0.1 M Na_2SO_4 (3)	4.3 mg of FcMeOH
2 mM potassium hexacyanoferrat(II) ($K_4[Fe(CN)_6]$) in 0.1 M KCl (4)	8.5 mg of $K_4[Fe(CN)_6]$

Table: 3.2: Stock solutions.

electrolyte	mass in g for electrolyte 100 ml solution
0.1 M Na_2SO_4	1.42 of Na_2SO_4 in 100 mL of deionised water
0.1 M $KClO_4$	1.38 of $KClO_4$ in 100 mL of deionised water
0.1 M KCl	0.74 of KCl in 100 mL of deionised water
0.1 M K_2SO_4	1.74 of K_2SO_4 in 100 mL of deionised water

3.2 Preparation of micro and submicrometer electrodes for SECM

3.2.1 Preparation of Au, Pt, Ag ultra microelectrode

The conventional technique frequently used for the preparation of SECM tips is largely based on the fabrication technique for disk-shaped microelectrodes, which have been described in the literature. The procedures for the manufacture of this type of SECM tips have been described in details previously and are only presented briefly.

A wire of Pt, Au and Ag of radius 12.5 μm is placed in a 10 cm long, 1.2 mm outer diameter of glass capillary sealed at one end. The open end of the tube is connected to a vacuum line and heated with tungsten wire helix for approximately 10 minutes to desorb any

impurities or moisture on the wire and glass tube. One end of the wire is then sealed in the glass at the close end of the tube by increasing the heating coil temperature. The glass should melt around the wire for at least 1-2 mm at the tip of assembly. The whole glass tube, including the part that seals the wire, should be straight. After the glass has cooled, the electrode is inspected under a microscope to weather the wire is completely sealed at the tip and to make sure that there are no trapped air bubbles. The sealed end is polished with coarse sand paper until the cross section of the wire exposed and then successively with 0.3 and 0.5 μm Al_2O_3 abrasive disk paper. Electrical connection to the unsealed end of the wire is made with conductive silver paint. After this, a small amount of epoxy is applied to the open end of the glass capillary. This seals the wire and provides a mechanical stability to contact wire. Sometimes slight alteration has been applied during the preparation of these electrodes. After sealing the metal wire inside the glass capillary, an electrical connection was made (normally with a Cu wire with the required diameter) to the metal wire with the help of Ag conductive epoxy. After giving a mechanical stability to the wire with the epoxy, electrodes were subjected to polish with Al_2O_3 abrasive disk paper with 0.3 and 0.5 μm grain size. Two methods were adopted in order to optimise the electrode preparation procedure. The most difficult part is to produce electrodes with required RG (ratio between the insulating part and the metal). A step by step preparation of UME is shown in the Fig 3.1.

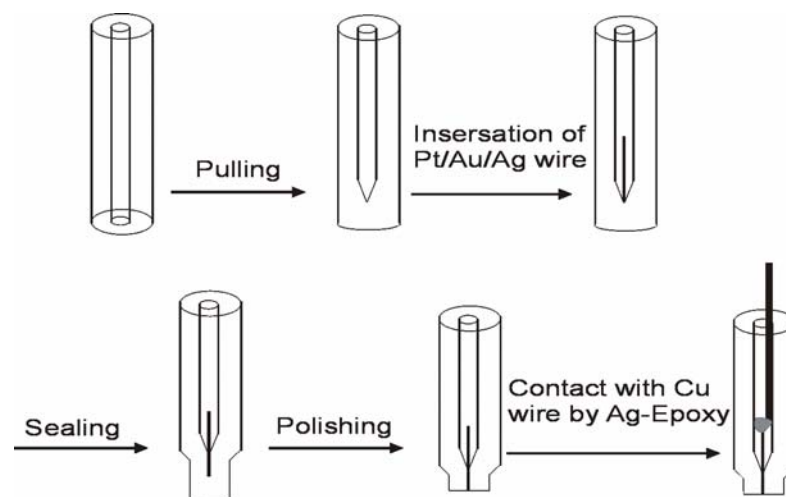


Fig. 3.1: Standard procedure for the preparation of metal UME.

3.2.2 Preparation of carbon fiber electrode

Carbon fibers UME were prepared with slight alteration of the conventional method. At the first step the carbon fibers were attached to a Cu wire with Ag epoxy and dried in an oven for 1 hour. Then they were put inside the glass capillary sealed at one end with great care since they are very fragile. The sealing and polishing steps were done by following the conventional method mentioned in section 3.2.1. A step by step preparation of carbon fiber UME is shown in Fig 3.2

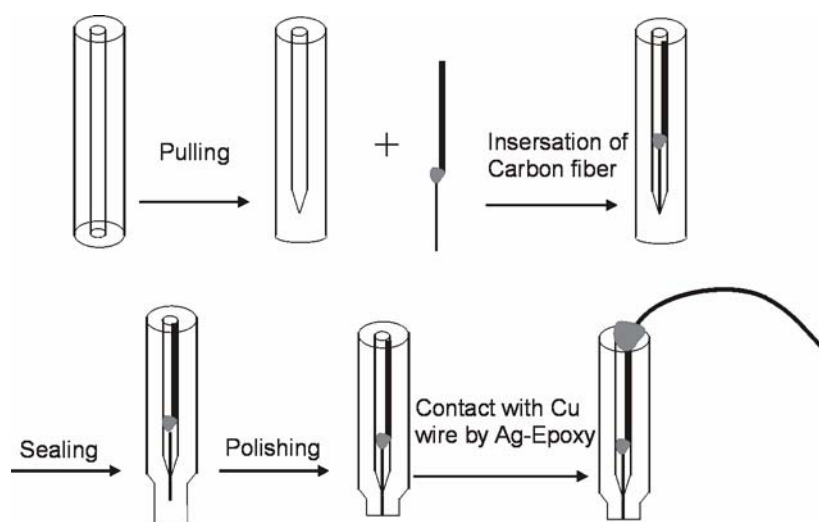


Fig. 3.2: Standard procedure for the preparation of carbon fiber UME.

3.3 Electrochemical and optical characterization

3.3.1 Characterisation of Pt/ Au/ Ag UMEs

UMEs were characterized both electrochemically and optically. The electrochemical characterization of Pt, Au and Ag UMEs were checked by measuring a CV in 1 mM of $[\text{Ru}(\text{NH}_3)_6]^{3+}$. The CV reveals the nature of the UME. The sigmoid curve represents the electrochemical behavior of the electrode. The capacitive current is minimal as can be seen in the CV which indicates a good sealing between the metal wire and glass. The metal wires are exactly at the center as shown in the optical micrograph for each electrode.

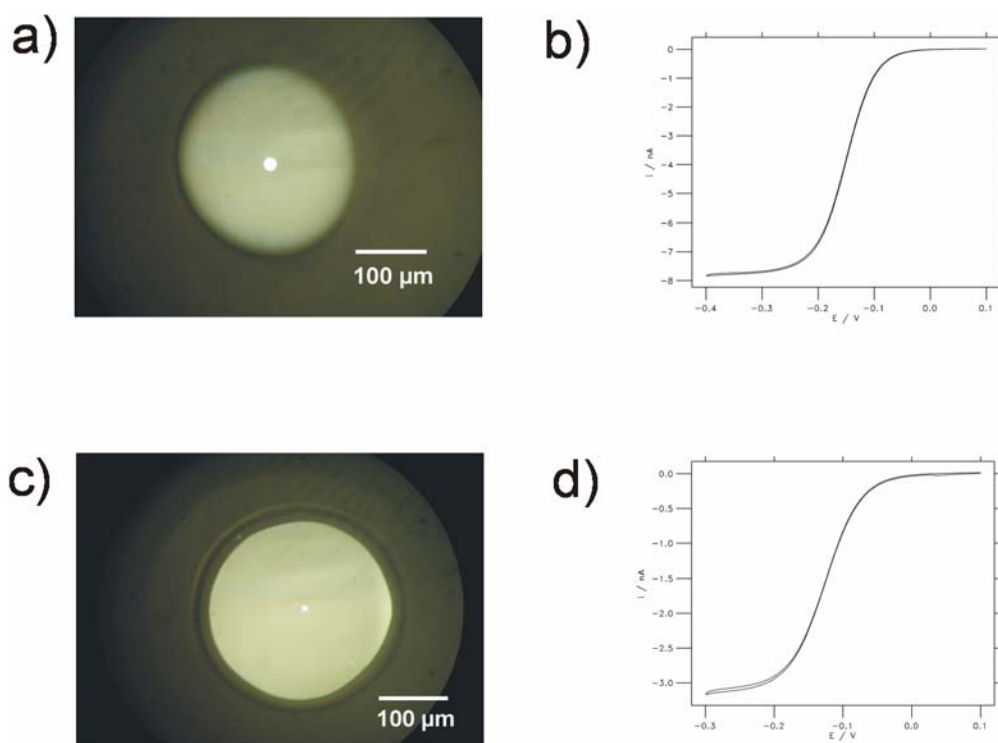


Fig. 3.3: Electrochemical and optical characterization of Pt UME from a-d: a) and c) optical micrograph of Pt 25 μm and 10 μm UME and b) and d) CV of Pt 25 μm and 10 μm UME in 1 mM $\text{Ru}(\text{NH}_3)_6$, scan rate 10mV/s

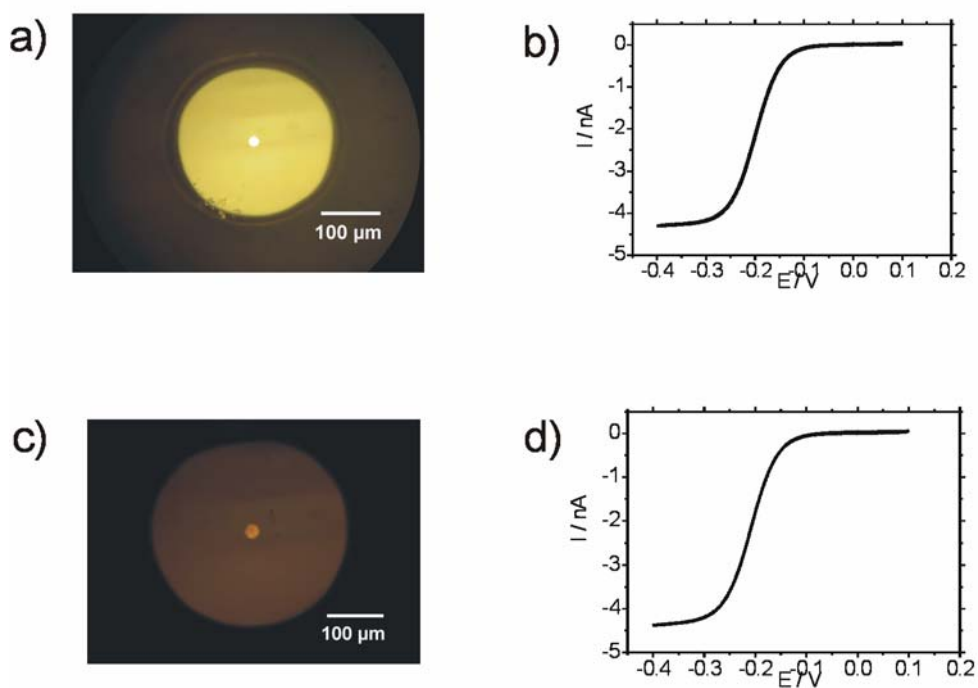


Fig. 3.4: Electrochemical and optical characterization of Au and Ag UME from a-d: a) and c) optical micrograph of Au and Ag UME and b) and d) CV of Au and Ag UME in 1 mM $[\text{Ru}(\text{NH}_3)_6]^{3+}$, scan rate 10 mV/s

3.3.2 Characterization of carbon fiber UMEs

The electrochemical characterization of carbon fiber electrodes were checked by measuring a CV in 1 mM of $\text{Ru}(\text{NH}_3)_6$. The CV reveals the nature of the electrode. The sigmoid curve represents the electrochemical behavior of the electrode (Fig 3.5). The capacitive current is a bit higher as compared to metal UMEs. This is due to the weak sealing between the carbon fiber and glass capillary. However, these UMEs can be used for SECM experiment. The size of the electrode was determined from the profile of the image shown in Fig 3.6

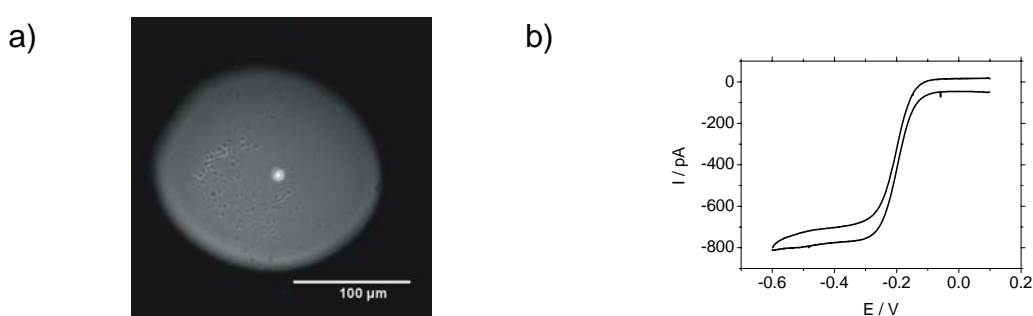


Fig. 3.5: Electrochemical and optical characterization of Carbon fiber UME: a) optical micrograph of Carbon fiber UME and b) CV of Carbon fiber UME in 1 mM $[\text{Ru}(\text{NH}_3)_6]^{3+}$, scan rate 10mV/s

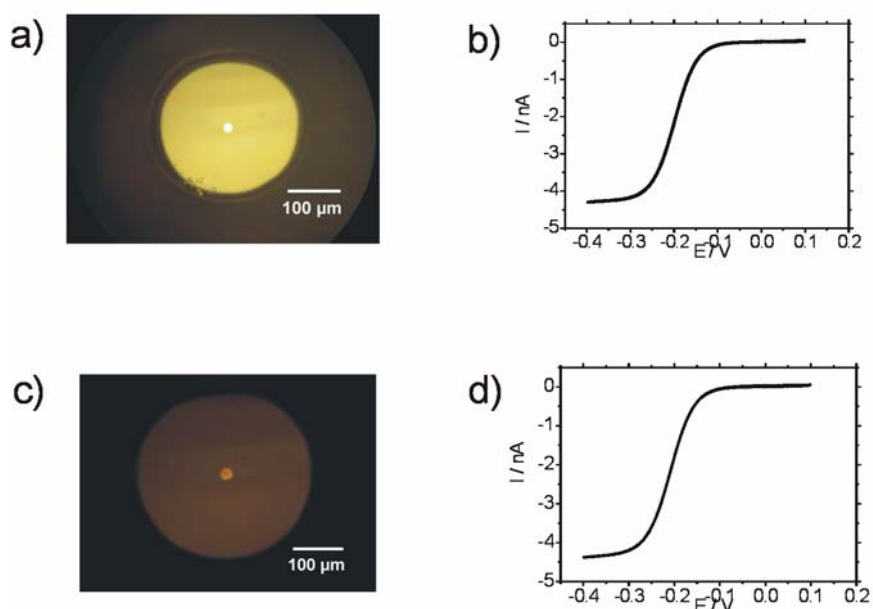


Fig. 3.6: CLSM micrograph of a carbon fiber UME: The profile was obtained from the image shown as a green line.

3.4 Preparation and cleaning of gold substrate

3.4.1 Preparation of gold substrate

All glassware used to prepare gold substrate was immersed in piranha solution. Then the glassware was rinsed with large amounts of deionised water and three times in ethanol. After cleaning the glassware in piranha solution and ethanol, they were subjected to dry in a oven at 100 °C for one hour. Then they were mounted in the gold evaporation chamber quickly to avoid moisture absorption from air.

3.4.2 UV/ozone cleaning of gold surfaces

Gold surfaces were exposed for 30 min to radiation from a low-pressure quartz-mercury vapor lamp, which generates UV emission in the 254- and 185-nm range (Model no. UV.TC.EU 003, Bioforce Nanoscience, USA). The ozone is produced upon absorption of the 185-nm emission by atmospheric oxygen, while the organic moieties are excited and dissociated by the 254-nm radiation. The excited organic molecules react with ozone to form volatile products such as water and carbon dioxide.

3.4.3 Al₂O₃ powder / electrochemical cleaning of gold electrodes

Gold electrodes were cleaned mechanically by using 0.3 and 0.5 µm Al₂O₃ powder on a abrasive disk paper. Then they were electrochemically cleaned in a solution containing 0.5 M of H₂SO₄ aqueous solution before modifying with alkanethiol and dithiol to form SAMs.

3.5 Monolayer assembly of thiols on gold substrate

Self-assembled monolayers of nonanethiol and nonanedithiol on polycrystalline gold electrode and annealed gold substrate were prepared by immersion of the gold sample in a 1 mM of nonanethiol or nonanedithiol solution in ethanol for 2-24 h.

3.6 Contact angle (CA) measurements

Contact angles (advancing and receding) of H₂O was measured immediately (<10 min) after removal of the slides from the alkanethiol or dithiol adsorption solution. Advancing and receding contact angles were measured (contact angle system, OCA 15plus, dataphysics instruments GmbH, Filderstadt, Germany). A drop of H₂O was lowered onto the SAM using the needle of a syringe. The advancing and receding contact angles were measured after increasing or decreasing the volume of the drop. All contact angles reported are the averages

of at least 3 measurements at three different locations on two to five samples. The contact angles were measured within 15 min of removal of the SAMs from the ethanolic solutions in which the SAMs were formed.

3.7 XPS measurements

X-Ray photoelectron spectra (XPS) were recorded for Au, S, Cd and C using an Axis Ultra spectrometer (Kratos), and $AlK\alpha$ radiation of 1486.71 eV at a pressure $< 5 \times 10^{-9}$ Pa. Data were collected and analysed by a vision processing program.

3.7.1 Sample preparation

Four different samples were prepared for XPS measurement. Four samples were modified with 1,9-nonanedithiol over night and then subjected to different potentials for deposition and stripping of Cd before transferred to the XPS instrument for measurement. Samples were prepared as shown in the CV. The deposition time was optimised at polycrystalline gold electrode modified with 1,9-nonanedithiol. 30 seconds time was found to be the suitable time for the deposition of Cd containing 0.1 mM of CdO in 0.1 M of K_2SO_4 and 1 mM of H_2SO_4 .

Sample A: modified with 1,9-nonanedithiol over night, rinsed with ethanol three times and stored in a vacuum.

Sample B: sample B was kept at -0.85 V against Ag/AgCl reference electrode for 30 seconds to deposit Cd onto the monolayers. After deposition samples were removed out from the solution and dried over Ar gas and stored in vacuum.

Sample C: sample C was kept at -0.85 V against Ag/AgCl reference electrode for 30 seconds to deposit Cd and then stripped upto -0.5 V against Ag/AgCl electrode, removed from the electrochemical cell, washed with water, dried and stored in vacuum.

Sample D: sample D was prepared as sample B and C for the deposition of Cd and then stripped upto the -0.2 V against Ag/AgCl reference electrode. Sample was removed from the electrochemical cell, washed with water and dried over Ar gas. After drying, it was stored in vacuum.

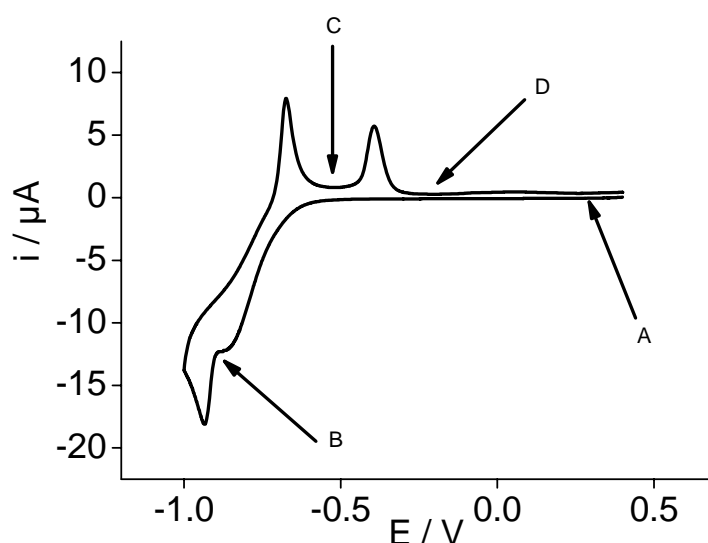


Fig. 3.7: Cyclic voltammetry of Cd deposition and dissolution on Au nonanedithiol-modified surface in 0.1 mM CdO, 1 mM H₂SO₄, 0.1 M of Na₂SO₄ at a potential scan rate of 100 mV s⁻¹: (A) Au-nonanedithiol modified electrode: (B) After bulk deposition of Cd onto the nonanedi-thiol modified gold electrode: (C) after stripping up to the first Cd dissolution peak: (D) after stripping off all the Cd from nonanedi-thiol modified gold electrode.

3.8 PM-IRRAS measurements

All the PM IRRAS spectra were recorded using a Bruker Vertex 70 spectrometer with the Polarization Modulation Set (PMA 50) equipped with photoelastic modulator and demodulaotr (Bruker, Germany, Hinds Instruments, USA). All spectra were recorded with a resolution of 4 cm⁻¹. The PEM maximum efficiency was set for the half-wave retardation at 1500 cm⁻¹ for analysis of CH stretching and bending bands. Each spectrum contains 10.000 averaged spectra. The angle of incident light was set to 80°. All IR spectra were collected in the dry-air atmosphere after 1 hour of incubation in the chamber. The PM IRRAS spectra were processed using OPUS program (Bruker, Germany)

3.9 Experimental set up for SECM imaging experiment

3.9.1 SECM experiment

A home-built SECM instrument was used that consisted of a stepper motor positioning system (Märzhäuser, Wetzlar, Germany) and a CHI701B potentiostat used in a three-electrode configuration and operated via home-built software. The Pt UME had a radius $r_T = 12.5 \mu\text{m}$, and $\text{RG} = r_{\text{glass}}/r_T = 10$ (r_{glass} is the radius of the insulating glass shield). A Pt wire served as an

auxiliary electrode and was used together with a Ag/AgCl reference electrode. Specific settings are discussed in the individual Chapters. The aqueous solution contained 0.1 mM $\text{K}_3[\text{Ir}(\text{Cl})_6]$ and 10 mM KClO_4 . Initially the UME was positioned far from the surface and then approached the surface with the help of the SECM instrument by monitoring the steady-state O_2 reduction current at $E_T = -0.6$ V until the current stayed constant when the insulating sheath of the UME mechanically touched the sample surface. The UME was retracted 10 μm from this point for horizontal scans. The sample tilt was minimized by scanning the UME horizontally over the surface several times while monitoring the steady-state O_2 reduction current and adjusting the tilt table of the SECM instrument. The potential was then switched to $E_T = 0.75$ V to oxidize $[\text{Ir}(\text{Cl})_6]^{3-}$ present in the solution. The translation speed of the UME across the surface was maintained at 200 $\mu\text{m s}^{-1}$ with a step size of 15 μm in the low-frequency scan axis.

3.9.2 Optimization of SECM instrument before imaging

From CV and DPV experiment it is known that after oxidation of Fc moieties, it leaves the surface and diffuses to the solution. Due to the spherical diffusion of the redox mediator at the UME, it not only oxidizes the Fc moieties below the UME but also area close to the UME. In order to overcome this process SECM imaging experiment was optimized by varying the scan speed of UME. The following Fig 3.8 shows the SECM image of the structured area at different scan rate. When SECM was maintained at slow scan rate, 10 $\mu\text{m/s}$ featureless images were obtained (Fig. 7.9, Chapter 7). This is due to the inability of the UME to sample the feedback current having slow scan rate.

4 Preparation of Cd ultramicroelectrodes for SECM experiment

Microelectrode is any electrode whose characteristic dimension is, under the given experimental conditions, comparable to or smaller than the diffusion layer thickness, δ . Under these conditions, a steady state or a pseudo steady state (cylindrical electrodes) is attained. These small-size electrodes have been called microelectrodes. One of their main advantages is the formation of a hemispherical diffusion field that allows more efficient mass transfer than that at macroscopic electrode. The special diffusion properties lead to a rapid establishment of a steady-state diffusion-limited current $i_{T,\infty}$. The current at the disk-shaped electrode surrounded by an insulating sheath which is given in Eq. 4.1 [156], in which n is the number of

$$i_{T,\infty} = gnFDrc^* \quad (4.1)$$

transferred electrons per molecule, F the Faraday constant, the diffusion coefficient, c^* the bulk concentration of the reagent, and r_T the radius of the disk-shaped active electrode area. The geometry-dependent factor g assumes the value of 4 for a disk-shaped electrode embedded in an infinitely large insulator. The properties of such electrodes become apparent in typical experiments when the electrode diameter is smaller than 30 μm . Electrodes with such properties are termed ultramicroelectrodes (UMEs) [157, 158]. UMEs of various geometries have been prepared mechanically or lithographically. The basic properties of UMEs are as follows:

- 1) A steady state for a Faradic process is attained very rapidly.
- 2) The Faradaic-to-charging current ratio, i_T/i_C , is improved, as the charging current decreases in proportion to decreasing area of the electrode, while the steady-state faradaic current is proportional to its characteristic dimension. Therefore, the i_T/i_C ratio increases with the reciprocal of the characteristic dimension.
- 3) The ohmic drop of potential, iR , is decreased as the measured currents are very small.
- 4) The applied potential can be scanned very rapidly because the charging current is suppressed.

- 5) The signal-to-noise ratio is greatly improved when an individual UME performs under steady-state conditions or when the diffusion layers totally overlap in an array of microelectrodes.
- 6) Small size of the electrodes permits measurements in very limited solution volumes and restricted space.

The applications of microelectrodes are based on their typical characteristics. They can be roughly divided into the following fields: 1) To measure electrochemical reaction mechanisms and kinetics [159-161], 2) electrochemical trace analysis, 3) electrochemical reactions in solutions of very high resistance, 4) analytical sensing, 5) *in vivo* measurements on biological objects: [162], 6) detection in flowing liquids [163], and last but not the least for scanning electrochemical microscopy [88, 164]. In addition, there are other specialized uses of UMEs and their arrays, such as the use of interdigitated microelectrode arrays, coated with redox or π -electron conductive polymers, to study the transport of electrons and ions in polymers. The charge transport systems can be potentially employed for construction of electrochemical devices for current rectification, charge storage and amplification, electron-hole pair separation, and for creating gates for ion flow [165].

UMEs and their arrays are usually prepared in the laboratory for a given purpose. The preparation procedures are not complicated but require very careful work and experience. There are several basic approaches to this task. Microcylindrical electrodes are obtained by sealing thin metal wires or carbon fibers in tapered glass capillaries (e.g., micropipettes). The protruding wire or fiber is then cut to the required length (usually less than 1 mm). There are high demands on the quality of the seal which must be tight, without entrapped air bubbles. Epoxy resins that are most often used for sealing must be carefully selected to be sufficiently chemically resistant and noncontaminating. Microdisks are mostly prepared by fixing thin metal wires or carbon fibers in tapered glass capillaries by carefully melting the glass. The disk is then obtained by cutting off the protruding wire or fiber flush with the surface and thorough polishing of the surface to a mirror-like finish. The quality of the seal and of the polishing is decisive for obtaining a good quality UME. Like all solid electrodes, UMEs require suitable pretreatment and activation prior to measurements. The first step always involves the obtaining of a smooth surface (usually by mechanical polishing), followed by chemical or electrochemical conditioning, or by combination of the two. The most common

procedure is electrochemical activation by potential cycling within a suitable range and in a suitable simple (mostly inorganic) electrolyte.

Different UMEs (Pt, Au, Ag and Carbon fiber) were prepared by following the conventional method (Chapter 3). Pt UMEs are exceptionally good in terms of its chemical inertness, rapid response. Ag and Cd UMEs were prepared to study the interaction of the corresponding ions with thin films of organic molecules at interfaces as a source of ions in SECM experiment by anodic dissolution. In this chapter, a new method is described for the fabrication of Cd UME for SECM. For the fabrication of Cd UME, Ag UMEs were prepared by following the conventional method described in the literature [158], then it was modified electrochemically.

4.1 Preparation of Cd UMEs

4.1.1 Preparation of Ag ultramicroelectrodes

The conventional technique frequently used for the preparation of SECM tips is largely based on the fabrication technique for disk-shaped microelectrodes, which have been described in the literature [158]. The procedures for the manufacture of this type of UME have been described in details previously in Chapter 3 and only are presented briefly.

A Ag wire of 25 μm diameter μm is placed in a 10 cm long glass capillary sealed at one end. The outer diameter of the capillary is 1.2 mm, the inner diameter is 0.9 mm. The open end of the tube is connected to a vacuum line and heated with tungsten wire helix for approximately 10 minutes to desorb any impurities or moisture on the wire and glass tube. One end of the wire is then sealed in the glass at the close end of the tube by increasing the heating coil temperature. The glass should melt around the wire for at least 1-2 mm the apex of the assembly. The whole glass tube, including the part that seals the wire, should be straight. After the glass has cooled, the sealed wire is inspected under a microscope, whether the wire is completely sealed at the tip and to make sure that there are no trapped air bubbles. The sealed end is polished with coarse grinding paper until the cross section of the wire is exposed and then polished successively with 0.3 μm and 0.05 μm Al_2O_3 abrasive disk paper. Electrical connection to the unsealed end of the wire is made with conductive silver paint. After this, a small amount of epoxy is applied to the open end of the glass capillary. This seals the wire and provides strain relief for the contact wire.

4.1.2 Chemical and electrochemical etching of Ag UME

The coinage metals Au, Ag are etched by solutions containing 3M NaCN in 1 M NaOH, 1:3 ratio of H₂O and HNO₃, while 1 M NaOH for W. Other metals Pt, Ir or Pt-Ir alloys are etched by solutions containing saturated CaCl₂ (60% by volume), H₂O (36%), and concentrated HCl (4 %). In order to prepare a Cd disk-shaped electrode, the Ag UMEs were chemically and electrochemically etched. The chemical etching was performed in diluted HNO₃ solution. Electrochemical dissolution was carried out by applying a potential to the Ag electrode in solution (Fig. 4.1). The Fig. 4.1 shows the etched silver electrode. The etching has been done by moving the Ag UME up and down inside the diluted HNO₃ solution constantly until some parts of the Ag wire removed. The removal of Ag from the Ag UME is constantly checked under the microscope in order to avoid complete removal of Ag. The rate of removal of Ag in HNO₃ solution depends on the dilution of HNO₃ solution. The following disadvantages were avoided since the Ag metal was etched from a well defined UME and the etching process was controlled under sonication during the chemical and electrochemical etching process.

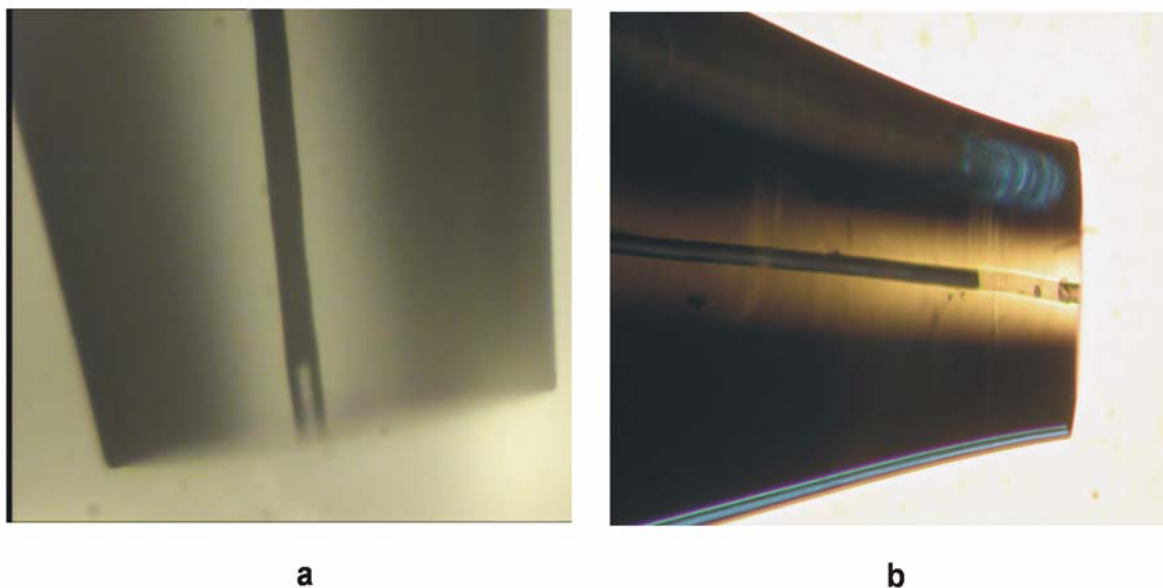


Fig. 4.1: Optical micrograph of a chemically etched Ag UME.

4.1.3 Deposition of Cd onto the Ag UME from Cd solution

After etching of a Ag UME from a dilute HNO₃ solution the electrochemical deposition of cadmium was carried out onto the Ag UME. The cadmium ions were reduced from the bulk

solution by applying a potential of -1 V to the Ag UME in solution. In order to remove trapped air above the recessed Ag UME the deposition was performed under sonication. Sonication also leads to a homogeneous deposition of Cd onto the Ag UME. Without sonication a gas bubble is trapped above the recessed UME and prevents the contact of the Ag UME and the Cd^{2+} solution. Fig 4.2 shows the three-dimensional growth of Cd deposition on to a etched Ag electrode. The etched part of the Ag electrode is nicely covered by Cd and became a Cd UME with good shape and size after polishing the protruding Cd part.

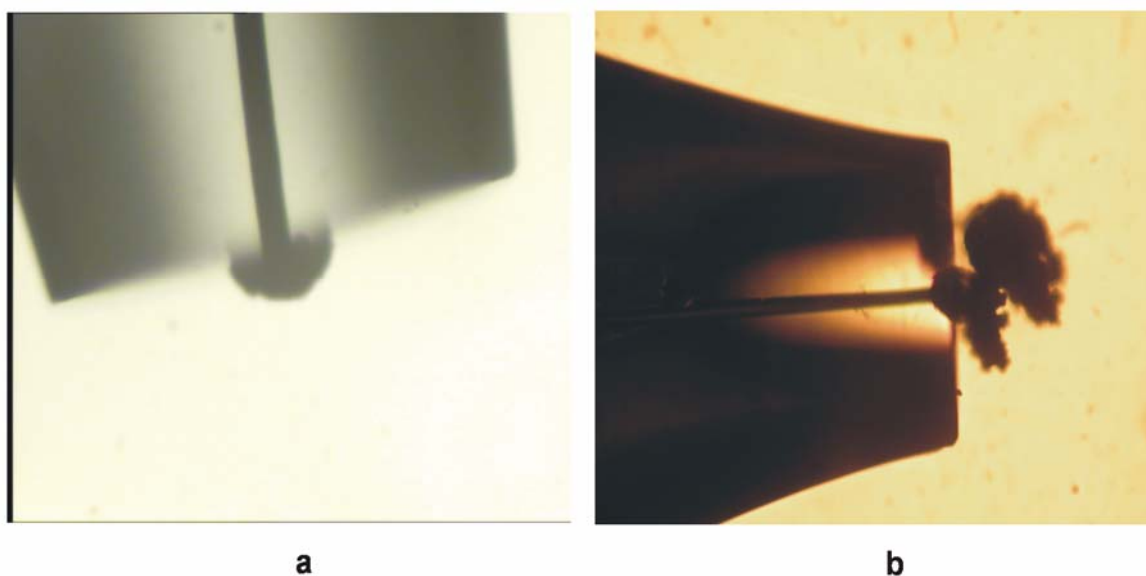


Fig. 4.2: Optical micrograph of an recessed Ag UME after galvanic Cd deposition.

4.2 Characterisation of Cd UME

4.2.1 Optical characterization of Cd ultramicroelectrodes

A top view of the tip of a polished Cd UME is shown in the optical micrograph obtained with confocal laser scanning microscope (Fig 4.3). The images were obtained in reflection mode. The light illumination from the UME is not homogeneous. This could be due to two reasons: 1) the tilting of the sample holder where UME was mounted; 2) the UME was not flat. However, it clearly obtained the image of the UME with distinction of the metal part and the insulating glass part from where RG value ($r_{\text{total}}/r_{\text{Cd disk}}$) can be obtained. The reproducibly, a flat tip geometry was obtained with the $25\ \mu\text{m}$ -diameter Ag UME after electrochemical etching and Cd deposition to the Ag UME. The UME is well centred in the glass insulation (Fig 4.3a). In the particular case shown (Fig 4.3a), the total tip diameter was about $250\ \mu\text{m}$

giving an RG value of about 10. The other electrode (Fig 4.3b) has a diameter of $650\mu\text{m}$ with RG value of about 25.

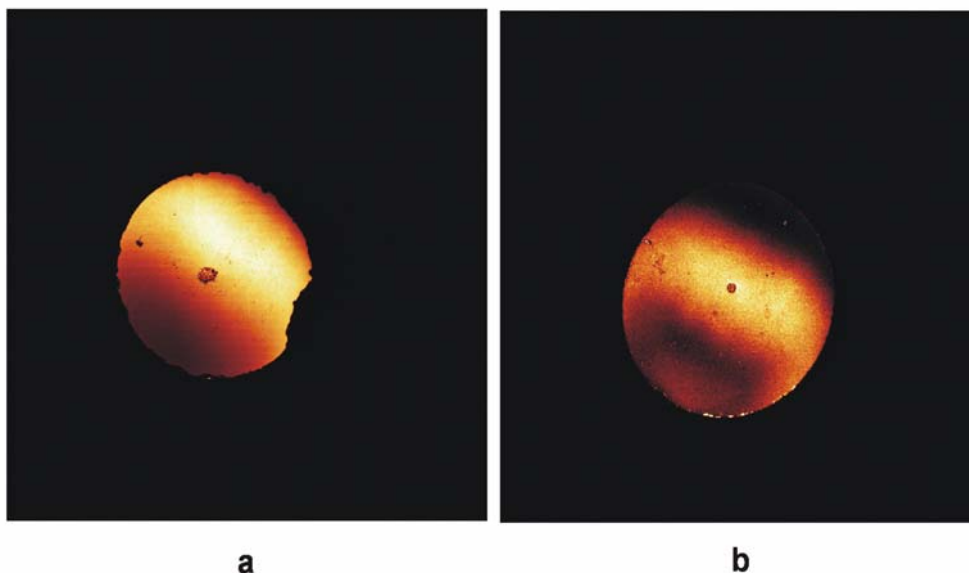


Fig. 4.3: Confocal laser scanning microscope photos of Cd UMEs.

The size and shape of the active electrode area were known since Cd electrodes were prepared from geometrically well defined Ag UME (Section. 4.1.2). The new method of preparing Cd UME turned out to be the best way to prepare this kind of electrodes since it is difficult to prepare Cd UME for SECM in conventional method (Chapter 3). Sealing a Cd directly into glass was impossible due to the evaporation of Cd at the temperatures required for sealing the glass (melting point Cd = 300 K).

4.2.2 Electrochemical characterization of Cd ultramicroelectrodes

In order to characterize the electrochemical behaviour Cd UME, their behaviour was studied by cyclic voltammetry of a redox couple. Since the anodic dissolution potential of Cd is at -0.75 V vs. Ag/AgCl reference electrode, these electrode could not be characterised by most redox couple used for SECM [166]. In order to characterize the electrochemical activity of this electrode, Cd UMEs were subjected to cyclic voltammetry experiment where Cd dissolution and Cd deposition could be studied. When the potentials are scanned from negative to positive potentials, the dissolution of Cd from Cd UME occurs at -0.75 V (Fig 4.4). When the potential is scanned back from the positive to negative potential, the Cd deposited back to the Cd UME at -0.7 V which suggests the presence of Cd on Ag electrode and

behaves as a Cd UME. The scanning potentials were limited to the less positive potential in order to avoid the complete removal of the Cd from the Cd UME. Care was taken that the charge passed in these measurements was small enough to ensure that the Cd UME did not become appreciably recessed. From the CV it is clear that the dissolution of Cd occurs at -0.75 V which agrees with literature value.

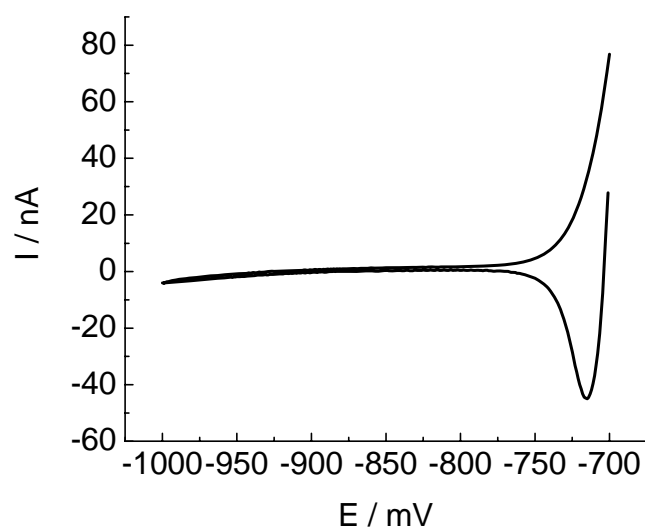


Fig. 4.4: Cyclic voltammetry of Cd UME in 0.1 mM of H₂SO₄ at scan rate 0.1 V/s.

5 Interaction of Cd metal ions with nonanethiol and 1,9-nonanedithiol SAMs modified gold electrodes

Metal layer formation on top of a nonconductive organic monolayer has been an important research subject in recent years because of its connection with an attractive field of molecular electronics in which an organic monolayer will be used in electronic components. Self-assembled monolayers (SAMs) of thiols are good candidates to be used as molecular layers for this purpose because of their unique advantages such as ease of preparation, highly ordered structure, and well-documented characteristics. To build up molecular devices, attention must be paid to the electrical properties of these organic molecules in the SAM. A metal-SAM-metal sandwich structure without a short circuit between the two metals is used to determine the electrical properties of the molecules and is also an essential component of molecule devices. In this geometry, a Au substrate usually serves as a bottom electrode. The top electrode could be metal nanoclusters prepared by vacuum vapour deposition [167-176] or from a suspension of metal nanoparticles [177-179].

Formation of a metal layer on top of an SAM by electrochemical deposition has several advantages over vacuum deposition. For example, electrochemical deposition is less complex, less expensive, and easier to control. However, most attempts to electrochemically deposit a metal on top of a SAM have failed. For example, in order to galvanically deposit copper on thiol-modified Au electrodes, an overpotential is required for nucleation to occur [180], and defect sites on the SAM act as nucleation centres in the under-potential deposition (UPD) region [181, 182].

Metal ions can interact with monolayers through different ways. They can be complexed by functional groups located on the monolayer or diffuse across or laterally along the interface. In some cases the metal ions can react and induce a reversible or irreversible change in the monolayer structure. Interaction of metal ions with complexing functionalities at the surface of particulate organic matter is of utmost importance in understanding the molecular basis of mass balances of trace metals in aquatic eco system. Metal deposition is also important in electrochemical analysis, where metal deposition is used for accumulation of the analyte (stripping analysis). One problem associated with using bare solid metal electrodes,

such as gold and platinum, in stripping analysis to determine heavy metal ions such as lead and copper ions in dilute solutions is that under-potential deposition (UPD) gives multiple stripping peaks in the analysis of mixtures. These peaks are often overlapped and cannot be used. To address this problem firstly Cd^{2+} was deposited onto a gold surface from a bulk solution. Specifically the interaction of Cd^{2+} with self-assembled monolayers located at solid-liquid interface has been studied in this Chapter. Bifunctional alkylthiols, such as 1,9-nanonedithiol, with an sulphide group on both ends of the alkylchain can form SAMs on the surface of the gold electrode. It is shown that such a SAM-modified gold electrode minimizes the UPD effects for the stripping analysis of cadmium. The anodic peak potential shifts and the peak shape changes, indicating that the SAM changes the deposition and stripping steps of these heavy metal ions. Thus, the sensitivity levels for both single species and mixtures can be significantly improved for the conventional solid electrodes. The mechanism of the deposition reaction at the SAM- modified gold electrodes is discussed.

5.1 PM-IRRAS characterisation of nonanethiol and 1,9-nanonedithiol monolayers on gold surface

Polarisation modulation infrared reflection absorption spectroscopy (PM-IRRAS) has been employed for the in situ characterisation of monolayers floating on aqueous solution-air interfaces in a Langmuir film balance [183-187]. Focusing polarized and modulated infrared radiation onto the monolayer surface at a grazing incident angle has permitted the investigation of the effects of changing the surface area by compression [183], hydrogen bonding [184, 185], binding, denaturation and conformational changes of proteins in the monolayer. The effect of the cations on the dissociation of arachidic acid monolayer [186] and the orientation and molecular structure of a mixed monolayers composed of equimolar poly(L-lactide) and poly(D-lactide) [187]. PM-FTIRRAS has also been used to measure orientation of molecules at interfaces. It has also been used to detect the DNA hybridisation in a SAM [188].

Before studying the interaction of cadmium ions with SAM-modified gold electrodes, monolayers of nonanethiol and 1,9-nanonedithiol on gold substrates were characterised by PM-IRRAS. The infrared spectrum of the C-H stretching region is shown in Fig. 5.1. The methyl C-H stretching bands of nonanethiol are located at 2965 and 2878 cm^{-1} and the methylene bands are at 2921 and 2849 cm^{-1} (Fig. 5.1, curve 1). The two peaks at 2965 and

2878 cm^{-1} are assigned to asymmetric and symmetric CH_3 stretching vibration. The highly organised thiol is expected to have asymmetric and symmetric stretching vibration at around 2965 and 2878 cm^{-1} which were previously reported [13, 189]. The wave number of the bands and their relative intensities are in agreement with a previous study of short chain thiols and indicative of an aliphatic chain in an all-trans configuration [5]. More specifically the large intensity of the methyl mode at 2965 cm^{-1} (Fig. 5.1, curve 1) is in agreement with previous studies of aliphatic thiols with an odd number of carbon atoms [190]. The C-H stretching modes at 2965 cm^{-1} and 2878 cm^{-1} (Fig. 5.1 curve 2) of the terminal methyl group are narrow ($\sim 10 \text{ cm}^{-1}$ FWHM). The methylene bands for 1,9-nonanedithiol are located at 2928 cm^{-1} and 2854 cm^{-1} . The assignment of these bands is the same as previously reported [191]. We take these observations as indications that the sample preparation method used here yields the presence of alkanethiols and dithiols, although it would be difficult to predict the homogeneity of the surface by considering the PM-IRRAS results only.

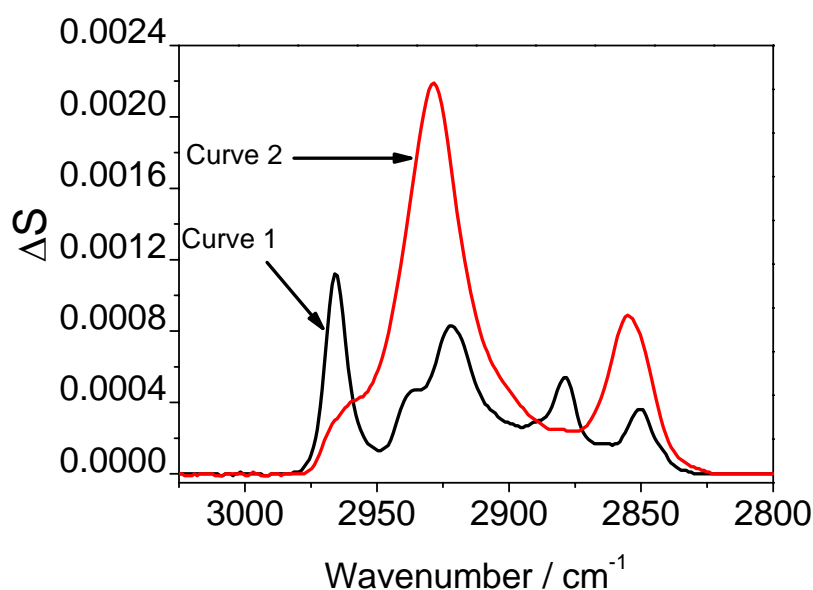


Fig. 5.1: Infrared reflection-absorption spectrum of a nonanethiol (curve 1) and 1,9-nonanedithiol (curve-2) layer chemisorbed on a Au electrode

The infrared spectrum of S-H stretching for nonanedi-thiol is shown in Fig. 5.2. The S-H stretching appeared at 2555 cm^{-1} .

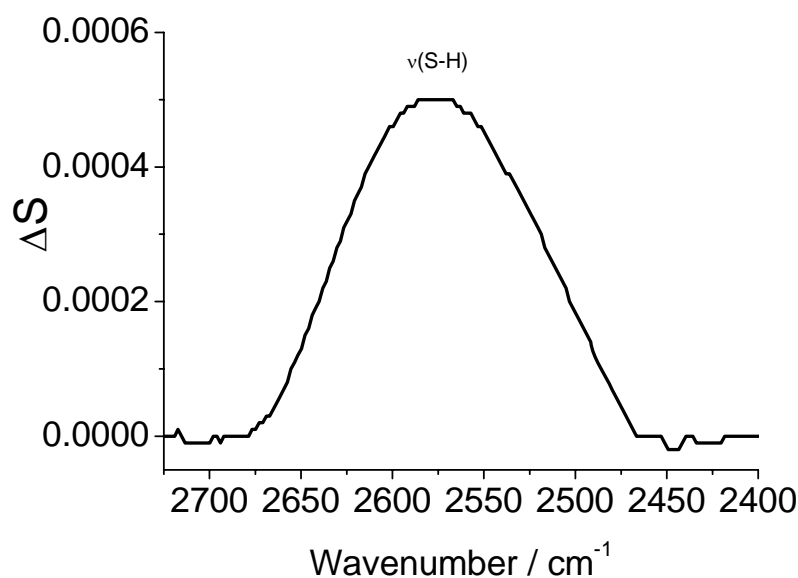


Fig. 5.2: Infrared reflection-absorption spectrum of a 1,9-nonanedithiol layer chemisorbed on a Au electrode at S-H region

It proves that the monolayers exhibit terminal thiol groups. This has to be proved because dithiols could in principle adsorb with both thiol groups to the gold surface. This interpretation demonstrates the importance of terminal groups in dictating the orientation of methylene and sulphur groups in case of nonanethiol and 1,9-nonanedithiol respectively.

5.2 Electrochemical characterisation of thiol-modified and dithiol- modified gold electrodes

CV is one of the tools most frequently used methods to study SAMs on electrodes because of its high sensitivity, which is attributed to its ability to detect currents from the high rates of mass transfer of redox couples on clean electrodes to small pores on a modified electrode [192]. The quality of the nonanethiol and 1,9-nonanedithiol layer was checked qualitatively by recording CVs. Fig. 5.3 shows the cyclic voltammograms obtained for nonanethiol (Fig. 5.3, curve 1) and 1,9-nonanedithiol (Fig. 5.3, curve 2) SAMs on gold electrodes in a 10 mM $[\text{Ru}(\text{NH}_3)_6]^{3+}$ aqueous solution. For comparison the response of the bare gold electrode is also plotted (Fig. 5.3, curve 3). At the nonanethiol or 1,9-nonanedithiol SAM-modified gold electrodes, the Faradic current associated with the redox processes of $[\text{Ru}(\text{NH}_3)_6]^{3+/2+}$ is largely suppressed and, together with the observed mostly capacitive behaviour, testifies for

the highly blocking character of both SAMs [193]. Not unexpectedly, the blocking effect of SAM is more or less similar for both the thiols having same carbon chain length.

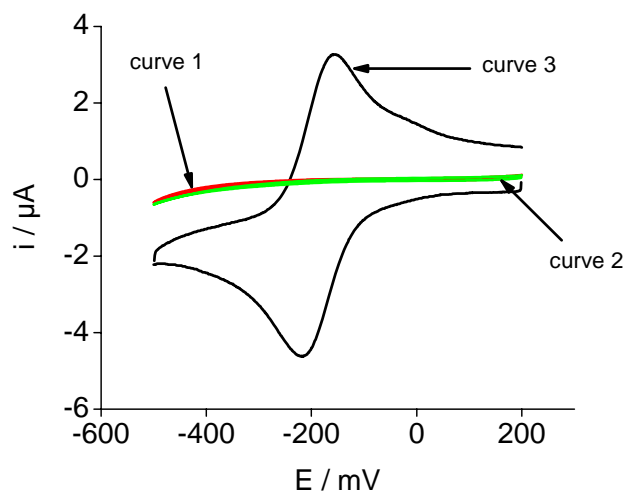


Fig. 5.3: Cyclic voltammograms of Au and modified Au electrodes in 0.1 M Na_2SO_4 and 10 mM of $[\text{Ru}(\text{NH}_3)_6]$ at a potential scan rate of 20 mV s^{-1} : curve 1) nonanethiol modified gold electrode, curve 2) 1,9-nonanedithiol modified gold electrode, curve 3) bare gold electrode.

5.3 Contact angle measurement for nonanethiol and 1,9-nonanedithiol modified gold electrode

The surface hydrophobicity of Au-SAM modified with dithiol was determined by contact angle measurements of a free-standing droplet of water. Fig. 5.4 shows the contact angles of water for 1,9-nonanedithiol and 1-nonanethiol modified gold surface. Clean gold metal surfaces are hydrophilic, which should result in a very small contact angle with water. However, under ambient conditions sessile contact angles for bare gold surfaces have been reported to range from 30 to 70° . This may be caused by easy contamination of freshly prepared metal surfaces by hydrophobic species physisorbed from laboratory air [194]. Contact angles for 1,9-nonanedithiol-modified Au surfaces with H_2O range from 40 to 50° . The measurements were done at different locations of one sample. The results were in close agreement and demonstrate the homogeneity on the length scale of millimetres of the modified surface. These values are characteristic of hydrophobic surfaces, and are similar to that reported for hexanedithiol [195]. The contact angle measurement for 1-nonanethiol obtained to be 91° for over night modification time. The contact angle for a highly organised methylterminated thiol is in between 111° - 115° [196].

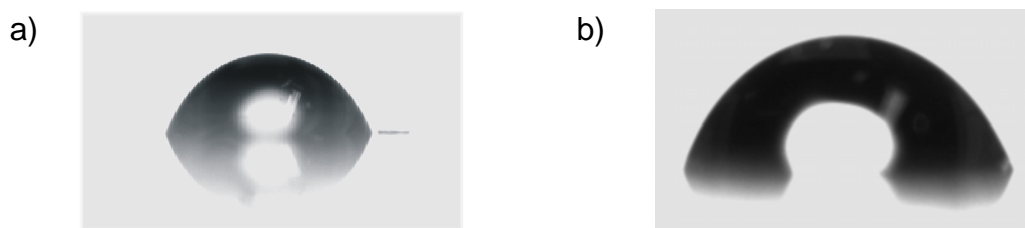


Fig. 5.4: Contact angle measurement at nonanethiol modified gold electrode (a) and 1,9-nonanedithiol modified gold electrode (b)

5.4 Cadmium deposition and stripping at a thiol-modified and dithiol-modified gold electrodes

The technique of stripping analysis [197] is a very sensitive electroanalytical technique. The method consists of two steps. The first one is a preconcentration step where a small portion of the unknown electroactive material is electrodeposited at the electrode surface under controlled mass transport conditions. The second step involves the electrodisolution, or stripping, of the deposit. The technique is used in the determination of trace levels of certain heavy metal ions in solution in particular analysis in remote places can be achieved. In most of these applications the mercury film electrode [198] or the hanging mercury drop electrode [199] has been used. These electrodes have been applicable because amalgam formation is involved. Concerns about the toxicity of Hg and its compounds calls for the use of alternative electrodes. Unfortunately, whenever solid electrodes are used for the determination of other metal ions, the UPD effect represents a major problem. Multiple-peak curves are obtained at lower concentrations as shown by Nicholson [200] in studies of the stripping of micro-deposits of nickel from platinum electrodes. Other investigators [201] concluded that the activities of these deposits could vary with the extent of surface and crystal lattice sites of the electrode. They concluded that bonding forces between the electrode and the deposit of the first monolayer could be stronger than those between the like atoms of the deposit of subsequent layers. Also, some portions of the monolayer deposit could be bonded with different energies at different electrode surface lattice sites. This makes quantitative analysis of dilute solutions virtually impossible. The use of electrochemical STM has opened insight

into the extremely complex interplay between metal lattice structures, bond energies, counter ion adsorption etc. [202-205].

The objective in this work is to use bifunctional thiols to form a SAM on the gold electrode surface to prevent the UPD effects. This should enable the stripping analysis of heavy metal ions at a mercury free electrode.

The cyclic voltammograms of gold electrodes with and without SAM modification were performed. The blue curve represents the CV at a bare gold electrode whereas the red and green curve represents the CV at dithiol and thiol modified gold electrode. The peaks A and B in red the curve is the hydrogen adsorption and bulk deposition of Cd on dithiol SAM-modified gold electrode whereas the peaks C and D is Cd dissolution. The peaks A1, B1, C1 and D1 in the green curve are the same as in the red curve and the peak E corresponds to the UPD of Cd on gold electrodes with and without SAM modified gold electrode. When the potential is scanned from positive to the negative potentials, the deposition of Cd at a dithiol-modified gold electrode occurs through the defects in SAM and then they grow in a three dimensional manner as shown schematically in the Fig 5.6b. When the potential is scanned from the negative to positive potentials, metallic Cd on the gold surface is removed by dissolution of Cd from the surface leading to two peaks (C and D). At the moment peaks C and D cannot be ascribed with certainty to particular processes. From the dependence of the peak height on the amount of deposited metallic Cd, it can be concluded that the first peak (C) leads to the bulk dissolution of Cd. Consequently peak D should result from some fragments of Cd still left on the surface, perhaps by binding to the terminal sulphur atom of the dithiol monolayer (at the monolayer/solution interface) leading to the dissolution peak D. The dissolution peaks at dithiol-modified gold electrode is well defined and there are two clear peaks (C and D). It suggests that the dithiols acts as a catalyst or as an ion exchange sites, which could preconcentrate trace cations prior to the electrodeposition step of Cd leading to the extra dissolution peak (D) and to enhance the sensitivity of the stripping signal.

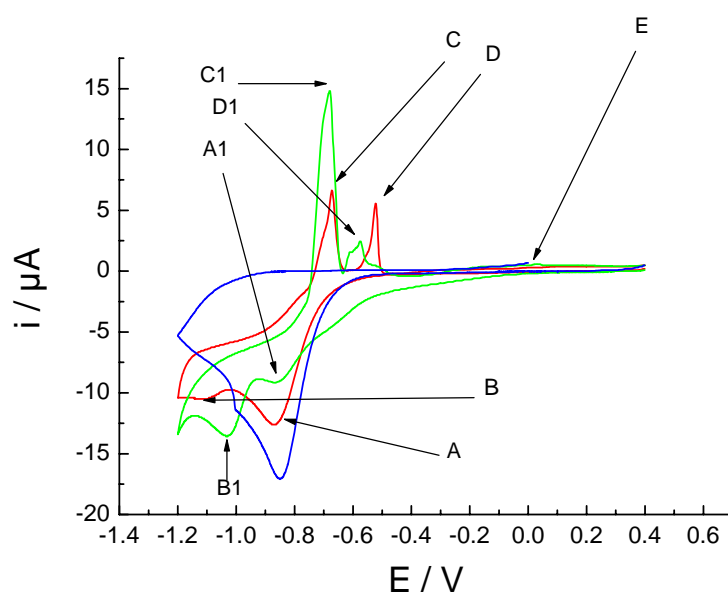


Fig. 5.5: Cyclic voltammograms of Au in 0.1 M Na_2SO_4 , 10 mM of CdSO_4 and 1 mM of H_2SO_4 at a potential scan rate of 100 mV s^{-1} . bare gold blue solid line, nonanethiol-modified gold electrode green solid line and nonanedithiol-modified gold electrode red solid line.

The deposition and dissolution peaks (A1, B1, C1, D1) of Cd in monothiol-modified gold surface were defined earlier. The deposition of Cd and hydrogen adsorption peaks at thiol modified gold electrode occurs at the same potential as in case of the dithiol-modified gold electrode. The only difference is that more Cd is deposited under equivalent conditions, which leads to a higher dissolution peak than at the dithiol-modified electrode. The bulk dissolution peak C occurs at the same potential as in case of dithiol-modified electrodes. The second dissolution peak (D1) is not well separated from C and has a different potential than the dissolution peak C of the dithiol-modified electrodes. It is also much smaller although the amount of metallic Cd deposited is larger than in the case of dithiol-modified surfaces. Probably D1 results from dissolution of Cd from some defects.

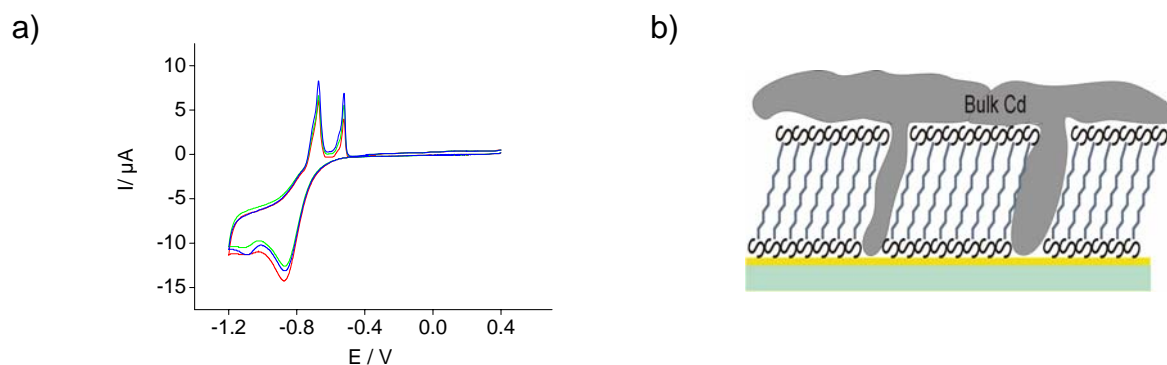


Fig. 5.6: (a) Repeated cyclic voltammograms of 1,9-nonanedithiol-modified Au electrode in 0.1 M Na_2SO_4 , 10 mM of CdSO_4 and 1mM of H_2SO_4 at a potential scan rate of 100 mV s⁻¹. (b) Schematic for Cd deposition on a nonanedithiol-modified gold electrode.

Also in the further experiments Fig 5.6a the dithiol monolayers is quite stable over multiple cycling and both dissolution peaks constantly increase, which indicates that the deposition of Cd does not disrupt the SAM surface. A model consistent with this observation is shown in Fig. 5.6b and can be called "mushroom-growth". After prolonged cycling (6-8 times) slight changes in the peak height and shape occurred indicating some degradation of the dithiol SAM.

5.5 XPS characterisation of Cd deposition and stripping at dithiol modified gold electrode

Formation of a metal layer on top of a SAM by electrochemical deposition has several advantages over vacuum deposition. For example, electrochemical deposition is less complex, less expensive, and easier to control. The deposition and stripping of Cd on to the nonanedithiol-modified gold surface were done. Four different samples were treated at different potential and then characterised by XPS. Four samples were prepared at different deposition potential of Cd onto a modified gold surface (Fig 5.7). Sample A corresponds to the gold modified with nonanedithiol, sample B represents the deposition of Cd to the SAM-modified gold for 30 s, sample C is subjected to the deposition for 30 s at the first stage then stripped up to -0.55 V (1st stripping peak in Fig 5.7) and sample was treated for same 30 s deposition of Cd and then stripped up to -0.2 V (2nd stripping peak in Fig 5.7). Details of the samples preparation are described in Chapter 3.8.1.

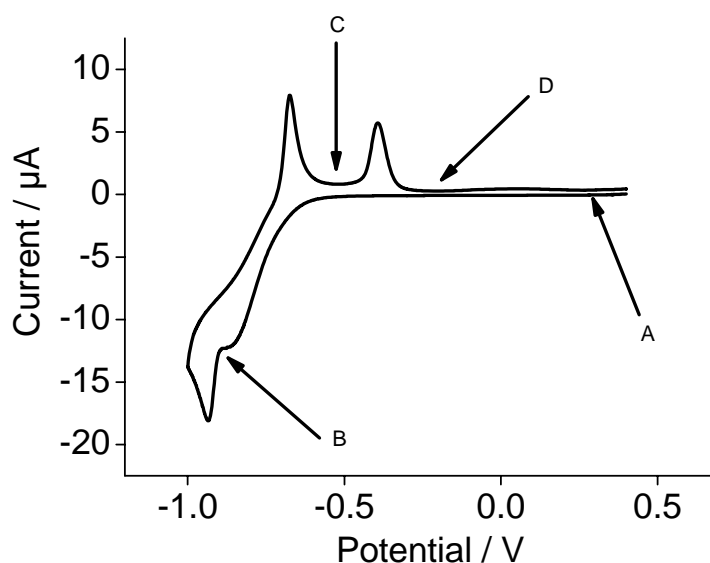


Fig. 5.7. Cyclic voltammetry of Cd deposition and dissolution on Au nonanedithiol-modified surface in 0.1 mM Cd^{2+} , 1 mM H_2SO_4 , 0.1 M of Na_2SO_4 at a potential scan rate of 100 mV s^{-1} . (A) Au-nonanedithiol-modified electrode. (B) After bulk deposition of Cd onto the nonanedithiol-modified gold electrode. (C) After stripping up to the first Cd dissolution peak. (D) After stripping off all the Cd from nonanedithiol-modified gold electrode.

Wide-scan XP spectra of the 1,9-nonanedithiol-modified Au surface are shown in Fig 5.8. The spectra A and B correspond to the samples illustrated in Fig 5.7. In addition to that XPS measurements were done for the elements gold, carbon, cadmium and sulphur over a narrow scan region.

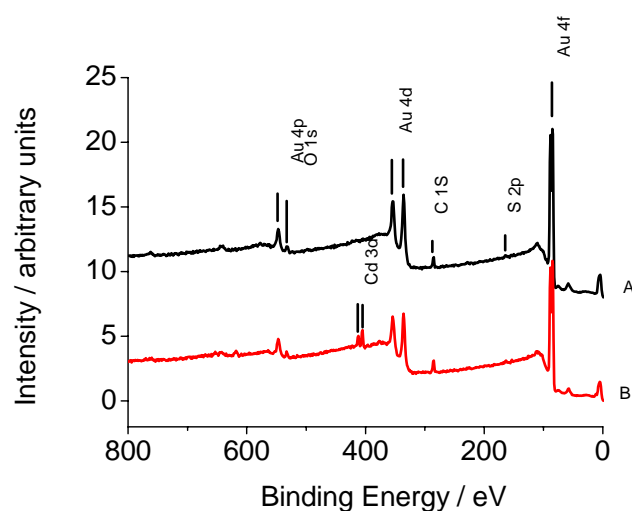


Fig. 5.8: Wide scan XPS spectra of Au modified with nonanedithiol as a binding layer: (a) Au-nonanedithiol modified surface; (b) Au-nonanedithiol-Cd.

Au $4f_{7/2}$ peaks were observed at 84.5 eV BE and 88.1 eV BE, respectively. The BE peak agrees well with that reported in literature for Au [206, 207]. By looking at the peaks for Au in Fig. 5.9 in sample A, B, C and D, it is clear that the Au peaks at sample A and D reappear after removing the Cd from the surface whereas in case of sample B the peak intensity is decreased in comparison to sample C since it is stripped up to the potential -0.55V for sample B and 0.3V for sample C. In case of sample B, where removal of Cd was done partially from the surface. The changes in the intensity of Au peak suggest the formation of Cd layer on Au modified surface during the deposition. The peaks for Au for all the samples appear at the same binding energy which suggest, the Au on the surface does not undergo any changes over the deposition and stripping of Cd onto the dithiol modified gold surface. It would be interesting to calculate the thickness of the Cd layer from XPS and from the change in the voltammograms.

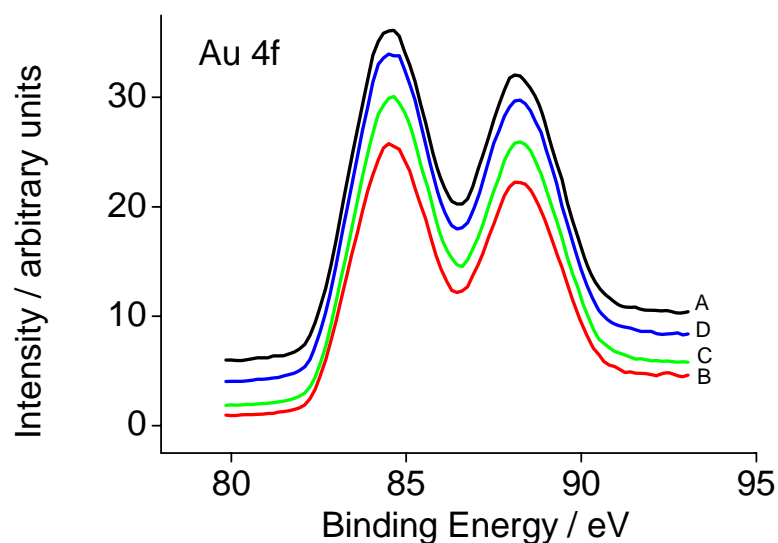


Fig. 5.9: XP spectra of Au 4f of nonanedithiol-modified surface: (A) Au-nonanedithiol-modified electrode. (B) After bulk deposition of Cd onto the nonanedithiol-modified gold electrode. (C) After stripping up to the first Cd dissolution peak. (D) After stripping off all the Cd from nonanedithiol-modified gold electrode.

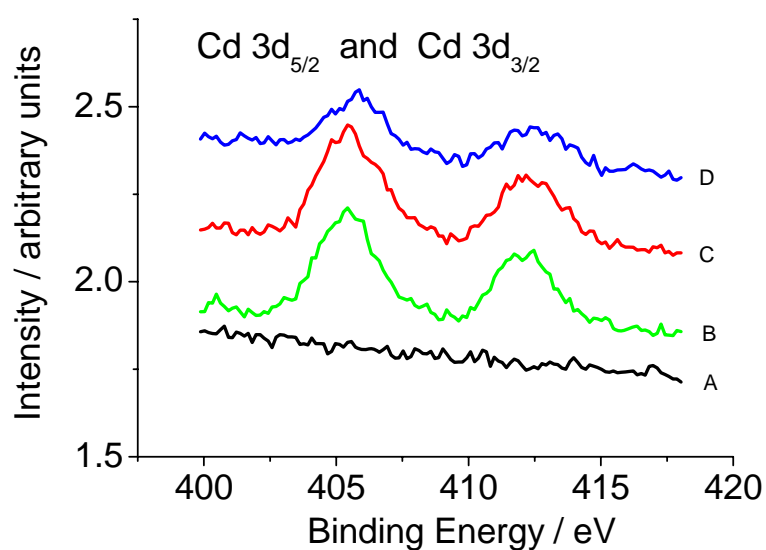


Fig. 5.10: XP spectra of Cd 3d_{5/2} and Cd 3d_{3/2} of nonanedithiol-modified surface. (A) Au-nonanedithiol-modified electrode. (B) After bulk deposition of Cd onto the nonanedithiol-modified gold electrode. (C) After stripping up to the first Cd dissolution peak. (D) After stripping off all the Cd from nonanedithiol-modified gold electrode.

Cd 3d_{5/2} and Cd 3d_{3/2} peaks were observed at 405.7 eV BE and 412.5 eV BE, respectively (Fig 5.10). The BE agrees well with that reported in literature for Cd [206, 207]. The Cd 3d peaks prove the existence of Cd on the surface for sample B, C and D. The peak intensity for

sample B should be more than the sample C. However, peak intensities are almost identical. This could be due to the different samples taken for different experiment or an indication that small Cd islands are formed on the SAM-modified surface. This would also correspond to the general rather low diminution of Au 4f intensities for sample B and C. The Cd 3d signal for sample D shows that there is still some Cd (Cd^0 or Cd^{2+}) present at the surface during emersion at -0.2 V. This suggests the presence of Cd on the surface as some complex with the sulphur groups of the nonanedithiol surface. More detailed statements cannot be made as an oxidation of metallic Cd may also occur during transfer with short air contact (2 s) and the signal to noise ration of the submonolayers Cd coverage does not allow a more precise determination of BE.

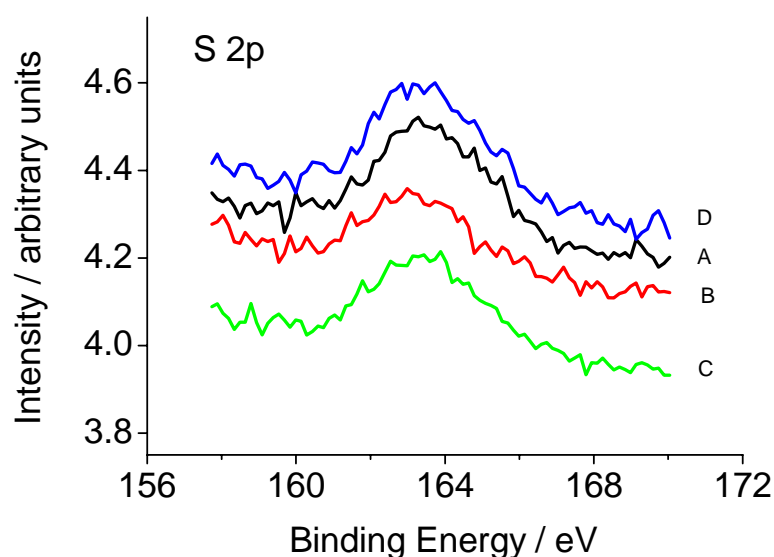


Fig. 5.11: XP spectra of S 2p on nonanedithiol-modified Au: as a binding layer: (A) Au-nonanedithiol-modified electrode. (B) After bulk deposition of Cd onto the nonanedithiol-modified gold electrode. (C) After stripping up to the first Cd dissolution peak. (D) After stripping off all the Cd from nonanedithiol-modified gold electrode.

The S 2p doublet (Fig. 5.11) is not resolved. The peak of the $\text{S}2\text{p}_{3/2}$ appears at 163 eV. The low BE agrees well with literature values for thiol sulfur species on Au substrate [206-208].

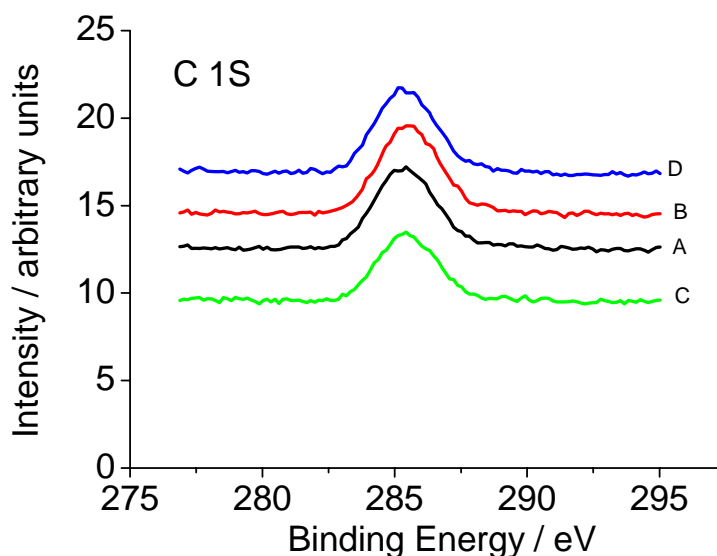


Fig. 5.12: XP spectra of C 1s of nonanedithiol-modified surface: (A) Au-nonanedithiol-modified electrode. (B) After bulk deposition of Cd onto the nonanedithiol-modified gold electrode. (C) After stripping up to the first Cd dissolution peak. (D) After stripping off all the Cd from nonanedithiol-modified gold electrode.

The C 1s spectra (Fig. 5.12) has a main component of sp^3 -hybridized carbon at 285.0 eV [206, 209, 210]. The BE corresponds to that of aliphatic carbon present in the monolayer. There are no peaks at 286.0 eV, 288.2 eV BE which are typically found on samples transferred via air (contamination from air). This suggests the presence of a well packed SAM that prevents adsorption of other organic contamination from air. After observing the peaks for C (Fig. 5.12) in samples A, B, C and D, it is clear that the C peaks did not alter during the deposition and dissolution of Cd from the surface.

The results from XPS measurement are at a preliminary stage. It is difficult to conclude the nature of the 1,9-nonanedithiol-modified surface during the deposition and dissolution of Cd from the surface. Further experiments need to be done in order to obtain a more detailed picture of the deposition and dissolution of Cd surface both as a bulk deposition and Cd deposition at UPD conditions. In particular the signal-noise ratio of the spectra and the spectral resolution must be enhanced to get more detailed information of the S and Cd binding states [211-214]. Quantitative evaluation of the signal intensities require a model of the surface structure (homogeneous layers, island growth) [215].

5.6 Stripping voltammetry of cadmium using gold electrodes modified with SAMs

The interaction of Cd ions with dithiol-modified Au electrodes further explored to use these modified electrodes as a sensing electrode for heavy metal detection. Fig. 5.13 show CV of gold electrodes without and with SAM modification (curve 1 and 2 respectively) in 1 mM of Cd^{2+} and 1 mM of H_2SO_4 solution. The sharp anodic peak at -0.75 V and -0.48 V is the oxidation peak of Cd at a nonanedithiol-modified gold electrode. The reduction peaks at bare gold are not well defined and appear around at -0.6 V . The oxidation of Cd is significantly changed when the gold electrode is modified with 1,9-nonanedithiol. The oxidation peak is sharp and oxidation potential shifts 100 mV in negative direction. This could be the result of some interaction between the self- assembled monolayer and Cd ions at the surface.

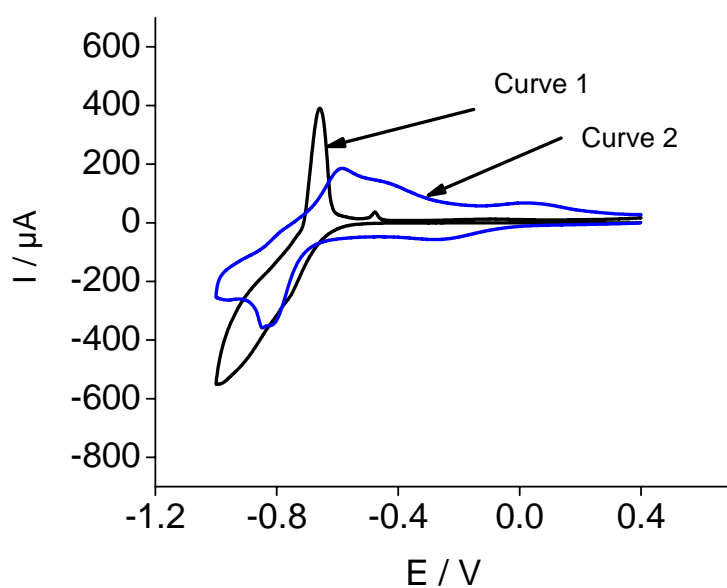


Fig. 5.13: Cyclic voltammograms of Au in 0.1 M Na_2SO_4 , 10 mM of CdSO_4 and 1 mM of H_2SO_4 at a potential scan rate of 100 mV s^{-1} . Nonanedithiol-modified gold electrode (curve 1), bare gold (curve 2).

Further the analyses were performed with variation of deposition time. Figure 5.14 shows stripping voltammograms for the oxidation of a cadmium film formed on deposition in 0.01 mM of Cd^{2+} and 1 mM of H_2SO_4 solution at a nonanedithiol-modified electrode. The potential was initially held at -0.85 V for the deposition of cadmium onto the electrode surface. The stripping peak can only be seen for 90, 120 and 180 s deposition time. The peak intensity

increases for the deposition time from 90 s to 180 s. The peaks are linear with the deposition time which can be used for analysis purpose. For 90 s and 120 s deposition time, the linear sweep voltammetry (LSV) consists of only one stripping peak. The second stripping peak for cadmium appears only for 180 s deposition time at -0.45 V. The peak here is broad as compared to the peak shown in Fig. 5.13 for higher Cd^{2+} concentration.

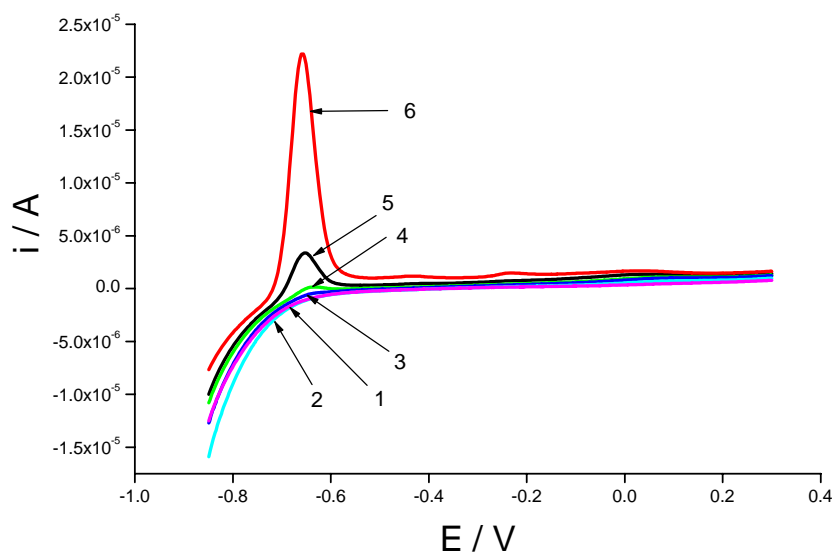


Fig. 5.14: Linear sweep voltammograms of nonanedithiol-modified Au surface in 0.1 M Na_2SO_4 , 0.1 mM of CdSO_4 and 1 mM of H_2SO_4 at a potential scan rate of 100 mV s^{-1} with different deposition time. 10 s (curve 1), 30 s (curve 2), 60 s (curve 3), 90 s (curve 4), 120 s (curve 5), 180 s (curve 6).

After finding the dependency of stripping of cadmium with deposition time, these modified electrodes were further used to perform concentration-dependent experiment. Fig. 5.15 show the dependency of the cadmium stripping peak for different concentration. The concentration dependent experiments were obtained with different deposition time. For lower concentration the deposition time are higher to obtain the stripping peak. With these modified electrodes a concentration of 0.002 mM of cadmium can be detected in linear LSV experiment. The sensing of Cadmium at modified electrodes can be improved by other techniques such as square wave voltammetry.

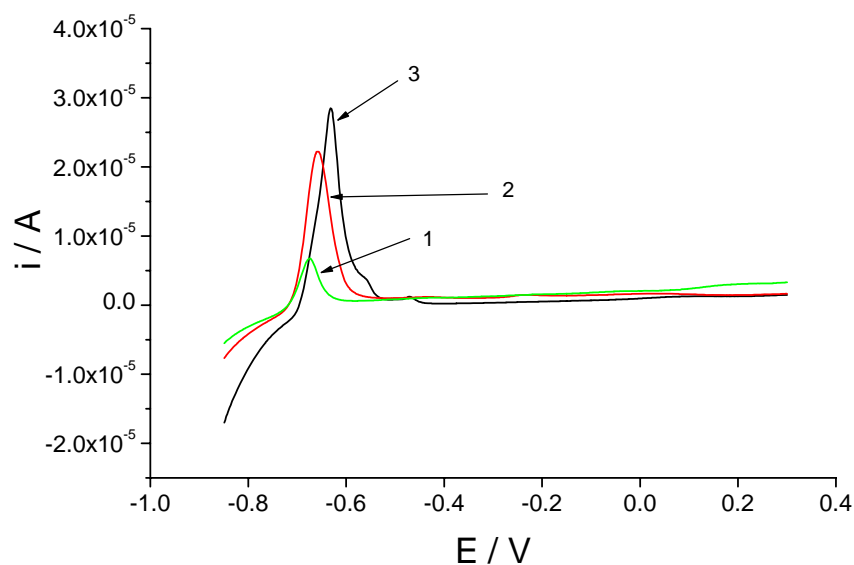


Fig. 5.15: Detection of Cd at a nonanedithiol-modified Au surface in 0.1 M Na₂SO₄, 1 mM of H₂SO₄. 2 μM (curve 1), 10 μM (curve 2), 100 μM (curve 3) at a potential scan rate of 100 mV s⁻¹.

There were some problems occurred during these experiments. The modified electrodes used for the experiment did not produce the same result all the time. Sometime the stripping peaks for Cd oxidation splits into two or three peaks. This observation could be due to the interference of UPD. The detection of Cd was obtained without the presence of any other interfering ions. Further experiments can be done with the presence of interfering ions. The carbon chain length of the dithiol used here is limited to 9. However, it might be interesting to check the behavior of the Cd with other carbon chain length of alkanedithiol family with bi-functional groups.

6 Adsorption, nucleation and growth studies of Ag at gold and thiol, dithiol-modified gold electrodes by SECM

Nucleation and growth kinetics have typically been measured using chronoamperometry or chronocoulometry, with the electrode under potentiostatic control [216], but when the current signal is compromised by background processes, quantitative measurements become difficult. There are also some interfaces which can not be connected. With the view of this problem this Chapter adapts a new approach developed by Unwin et al. [122] To investigate the uptake of metal ions by solid surfaces modified by organic thin films using the scanning electrochemical microscope (SECM). The approach has been explored by Bard et al. [150] and further developed by Unwin et al.[113, 149]. The basic idea is to employ the UME of the SECM – positioned close to the solid/liquid interface under investigation – to quantitatively inject the metal ion (reactant) of interest, and monitor the uptake via the current response. In order to diversify the range of process that can be studied with SECM transients methods, SECM double step potential chronoamperometry (DPSC) as a new methodology for locally initiating and monitoring heterogeneous reaction were introduced. With this both mode of SECM, the interfacial flux of metal ion can be determined directly, free from any artefacts that can arise in conventional approaches, for example, currents from background surface processes or charging currents at short times. Moreover, the technique can be applied to uptake processes that do not involve electron transfer (e.g. adsorption and ion exchange). The use of the SECM to study irreversible phase transfer processes is a new direction in terms of kinetic applications of the instrument, and further expands the range of interfacial processes accessible to study, that already includes electron transfer [217, 218], corrosion [219], dissolution [113-118] and reversible desorption/adsorption [119].

6.1 Principle to study adsorption, nucleation and growth of Ag at gold, thiol and dithiol modified gold electrodes

To measure local uptake of metal ions M^+ using the SECM, M^+ ions are electrogenerated via the anodic dissolution of a metal UME, shown in the (Chapter 2, Fig. 2.6), positioned close to the surface of interest. Under potentiostatic control, the current response of the reversible UME process is governed by the rate of M^+ transport away from the probe surface. This, in

turn, depends on the extent to which M^+ interacts with the surface. In simple terms, if M^+ is inert with respect to the interest surface, and it simply leaks away from the electrode surface by hindered diffusion (Chapter 2, Fig. 2.6b), then small current flows compared to the case where the UME is in bulk solution and diffusion is hemispherical (Chapter 2, Fig. 2.6a). In contrast, a rapid uptake of M^+ by the interest surface enhances the flux of M^+ away from the probe, causing a larger current to flow (Chapter 2, Fig. 2.6c). In this manner, a specific region of the surface is targeted, and any adsorption or growth behavior involving M^+ is monitored quantitatively and exclusively through the current response at the UME probe.

6.1.1 Optimization of dissolution potential and pulse time for Ag microelectrode anodic dissolution

In order to find out the anodic dissolution potential for Ag UME, linear sweep voltammetry experiments were done against Ag/AgCl reference electrode. Different fluxes of Ag ions were produced according to the potential chosen as shown in the Fig. 6.1. To examine the chronoamperometric behaviour, with the UME positioned far from the gold surface, the UME potential was stepped from open circuit potential to the chosen potential for Ag^+ generation as shown in the Fig. 6.1.

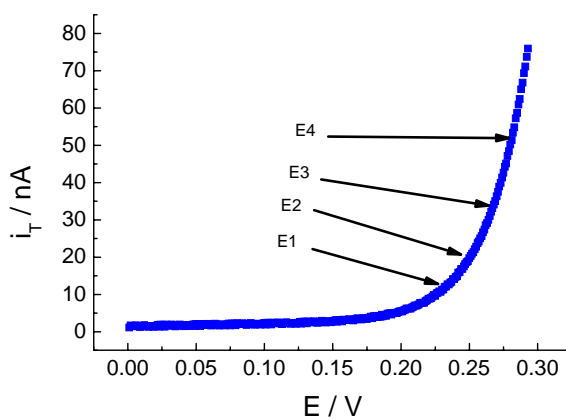


Fig. 6.1: Linear sweep voltammetry for Ag dissolution in 0.1M KNO_3 . E1, E2, E3, E4 are the potentials used for the generation of different flux of Ag at the Ag UME close to the surface.

Preliminary experiments on the anodic dissolution of Ag under potential step chronoamperometric, conditions were carried out with a 25 μm radius probe UME positioned at a large distance (several millimetres) above glass and gold surface. Care was taken that the charge passed in these measurements was small enough to ensure that the Ag electrode did

not become appreciably recessed and the corresponding current-time behaviour recorded. A typical transient plotted $i_T = f(t)$ is shown in Fig. 6.2

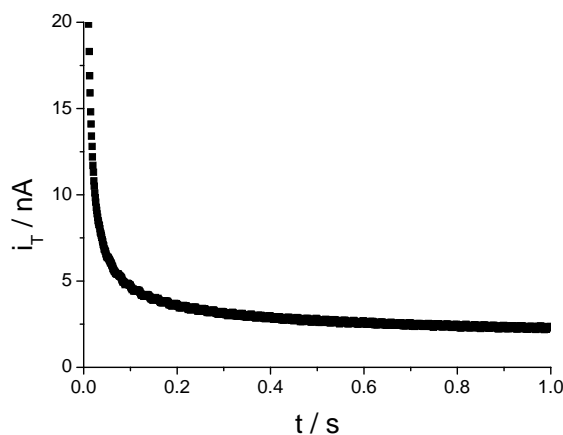


Fig. 6.2: Current-time behavior at an Ag UME positioned far from the gold surface. The data have been plotted as current versus time.

6.1.2 Optimization of distance for Ag ions generation near to the inert substrate

The distance between UME and surface was optimised in order to find a suitable and close distance to an inert surface in order to perform chronoamperometry single and double pulse experiments. A typical set of chronoamperometric transients for the anodic dissolution of Ag, measured at several UME-substrate separations is shown in Fig. 6.3. These data were obtained by stepping the UME potential from -200 mV to the 350 mV vs. Ag/AgCl reference electrode, where the oxidation of Ag is diffusion controlled. The behaviour is as expected, in that the current decreases with decreasing tip/substrate separation, as a consequence of the inert substrate hindering diffusion to the UME [88, 119, 150, 151, 220, 221]. This is important because the process of Ag dissolution at Ag UME and has to be monitored by the UME in order to find the surface concentration to deposit in later experiments, silver on to the metallic gold and modified gold electrodes with thiol and dithiol SAMs. It was found that up to $20 \mu\text{m}$ distance between UME and the surface is suitable for the pulse experiment.

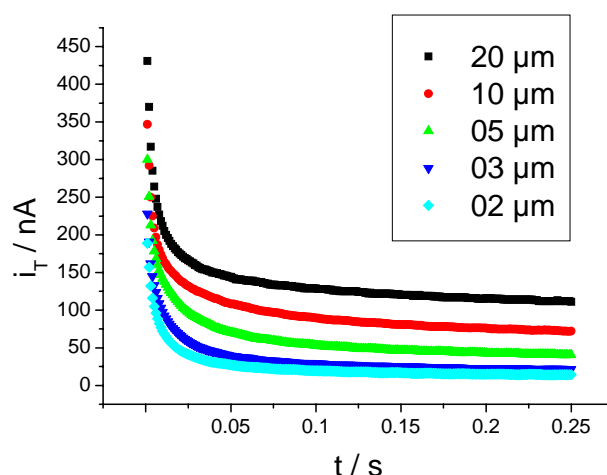


Fig. 6.3: A series of SECM chronoamperometric transients for the anodic dissolution of Ag UME with the UME positioned at distances of 2 μm (lower curve), 3, 5, 10, 20 μm above a glass (inert) surface.

6.2 Deposition of Ag onto gold substrate by using SECM

The electrodeposition of Ag on gold has been investigated in different methods [222-225]. Before studying the silver absorption on gold and modified gold surfaces, silver deposition was carried out on gold and a gold surface modified with thiol or dithiol self-assembled monolayers. The following figures show the silver deposition on a gold surface biased at -200 mV. Deposition of metal ions on different substrate has been investigated by SECM before. The SECM has been used to fabricate microstructures by deposition or etching via two different approaches, direct mode and feedback mode. In the direct mode a faradic current is passed between a UME and a metal substrate electrode. Deposition of silver metal on polymer films was done by SECM direct mode where the probe is a tip penetrating into a polymer film having Ag^+ over a Ag substrate. When potentials were applied across the tip and substrate, Ag is deposited in the polymer films in contact with the SECM tip. The counter current is provided etching the Ag substrate below the polymer film [226]. In feedback mode the substrate is a reactive surface which can irreversible react with the UME generated species. The electron transfer that takes place on this surface can drive a net electrochemical reaction on the surface, if the net reaction is thermodynamically and kinetically feasible [227].

As an example silver deposition was performed on gold surface [228]. The silver cations are complexed by an excess of ammonia to form the diamine complex. This shifts the potential necessary for the deposition of silver to more negative values. The complexation

represents an equilibrium reaction that depends on the concentration of protons. Protons can be generated at the UME by oxidising nitrite to nitrate ions. This increases the local concentration of free silver cations. The deposition of silver only occurs at locations with a high concentration of free silver cations.



SECM has also been used to deposit different metal ions, Au, Co, Ni on different substrate by a sacrificial microelectrode [229-232]. Besides using the feedback and direct mode in SECM to deposit metal on substrate, a new approach was made by Yatziv et al. [233] to deposit Ag micro patterns by SECM which is based on ion transfer across a micro interface between two immiscible electrolyte solution. The approach is based on the transfer of silver ions, across a liquid/liquid interface at the tip of a micropipette that is dipped in an outer organic solution of nitro benzene consisting of the electrolyte tetrabutylammonium tetrakis [4-chlorophenyl] borate (TBATPBCl). In this approach Ag ions were released from the pipette, stabilised by the ligand and get deposited onto the gold surface during the approach when the gold surface is unbiased and biased at 0 V. The deposition does not occur when the Au substrate is biased at 0.6 V preventing the reduction of Ag^+ at the surface. The advantage of this approach is to produce high resolution micro pattern but the shape and size of the structures is not well defined due to the size of the micro pipette and difficult to control the size growth of the pattern below the pipette, whereas the deposition of Ag metal on gold surface by using a sacrificial Ag UME is more easy and the pattern formed are well defined as shown in the Fig 6.4. Although the current study doesnot focus on formation of Ag patterns on gold or gold surfaces modified with thiol or dithiol SAM surfaces rather it mainly focus on absorption of Ag^+ on gold and gold modified surfaces limited to one or two monolayers and if possible the kinetics involve in this reaction.

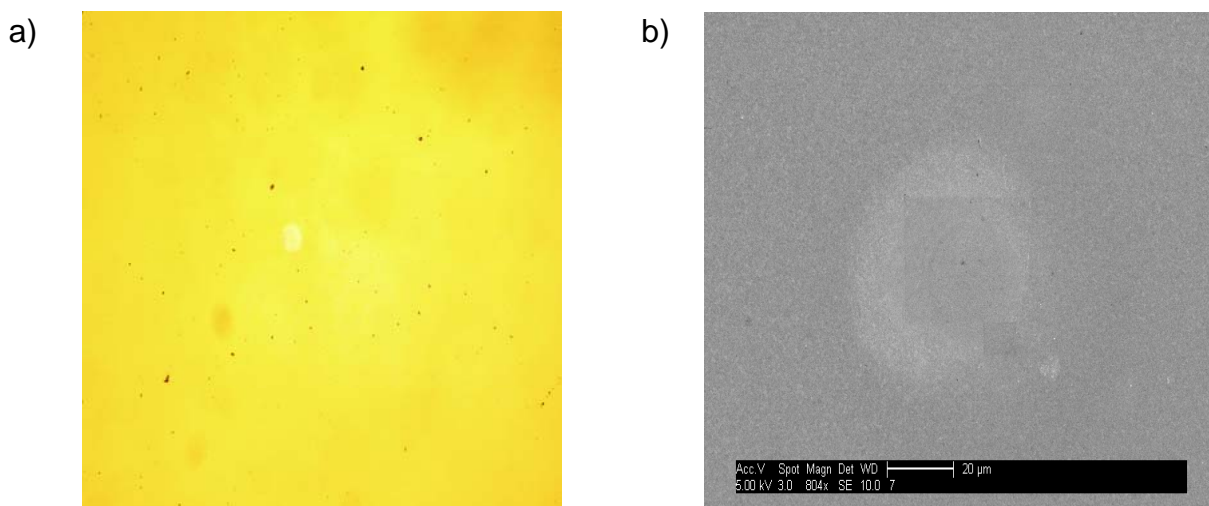


Fig. 6.4: Optical (a) and SEM (b) images of Ag pattern deposited locally by the SECM. The Ag UME was held 5 μm above a gold surface, which was biased at -200mV vs. Ag / AgCl.

Fig. 6.4 show the patterns that were formed on the gold substrate as a result of stepping the potential of the Ag UME into the Ag silver dissolution potential. Clear circular patterns of a crystalline material can be seen that match reasonably well with the UME size of 25 μm. The deposits within the disk shaped patterns are not homogeneous, as can be seen in the magnified images shown in the Fig 6.5. This inhomogeneous distribution of Ag on gold could be due to a mechanism associated with electrolyte diffusion present in the solution into the gap between the UME and the gold substrate. The dependence of the anodic dissolution on the radial diffusion of the electrolyte would result in a flux of Ag^+ generated at the UME that was higher at the edge than the centre, as reflected in the distribution the deposit. The evidence of the pattern limited to the confined region is an excellent evidence for a diffusion- controlled process.

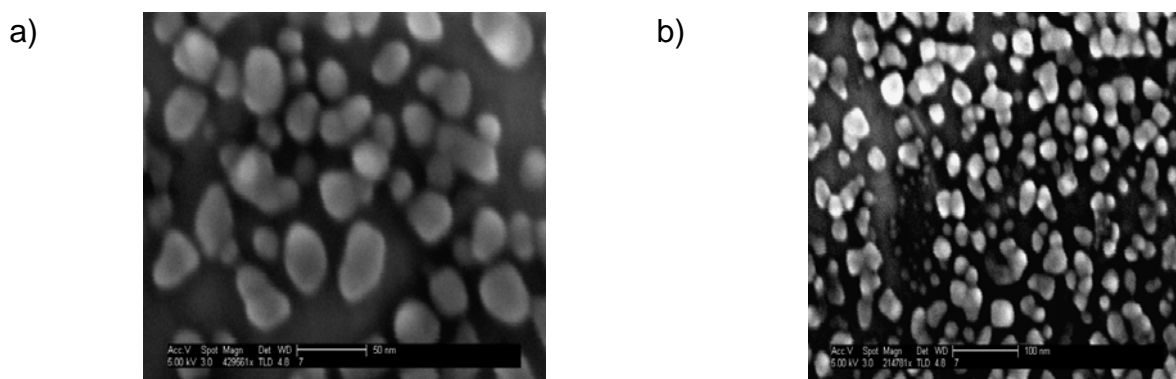


Fig. 6.5: Magnified SEM images of Ag patterns deposited locally by the SECM at two different places of the pattern

Preparation of such patterns on thiol-modified and dithiol-modified gold surface is relatively difficult. The resulting metal structures are not well defined as shown in the Fig. 6.6 (a) and (b). This could be due to the insulation of the gold surface by the self-assembled thiol or dithiol monolayers. Certainly there is Ag^+ adsorption [234] to the dithiol-modified gold electrode in an alkaline solution, where Ag^+ was absorbed to the dithiol-modified gold surface. This gives an excellent opportunity to study the adsorption kinetics of Ag ions by using the SECM. If some absorption of Ag occurs on dithiol-modified or thiol-modified gold electrodes, it would be difficult to see the presence of pattern in a low resolution SEM as shown in Fig. 6.6. In contrast to the results shown in Fig. 6.4, no Ag particles were detected by SEM when low potentials were applied to the Ag UME, such that the flux of Ag^+ was only sufficient for Ag adsorption, but not high enough for Ag nucleation on gold. This suggests that a route to investigate the adsorption process, largely free from nucleation and growth is to employ a low driving potential to the UME probe.

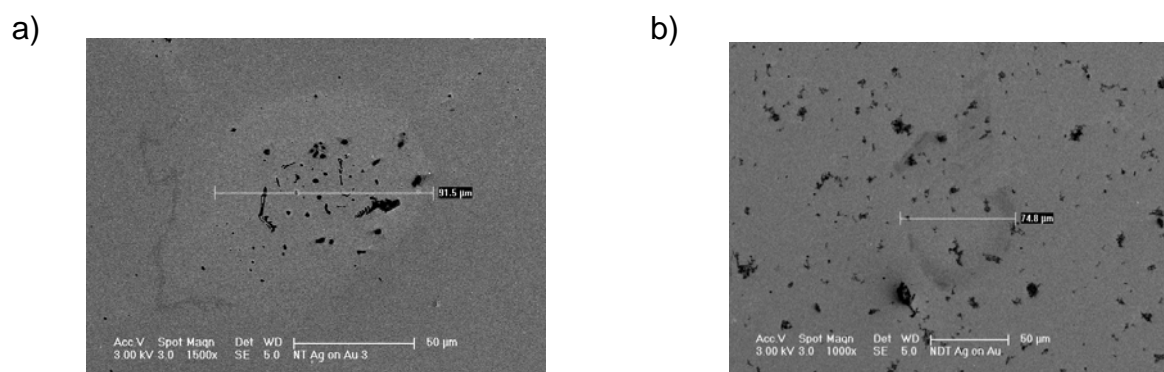


Fig. 6.6: SEM images of Ag patterns deposited locally by the SECM at modified gold electrode, (a) modified with nonanethiol, (b) modified with nonanedithiol.

6.3 Comparison of single potential step chronoamperometry experiment at gold and glass surface

To measure local silver uptake using the SECM, Ag^+ are electrogenerated via the anodic dissolution of a silver ultra microelectrode (UME), shown in Fig 6.7, positioned close to the gold/aqueous solution or glass/aqueous solution interface. Under potentiostatic control, the current response of the reversible UME process is governed by the rate of Ag^+ transport away from the probe surface. This, in turn, depends on the extent to which Ag^+ interacts with the gold sample. In simple terms, if Ag^+ is generated close to a glass surface, it simply leaks away from the electrode surface by hindered diffusion (Fig. 6.71c), then a small current flows

compared to the case where the UME is in bulk solution and diffusion is hemispherical. In contrast, a rapid uptake of Ag^+ by the target surface enhances the flux of Ag^+ away from the probe, causing a larger current to flow (Fig. 6.71a and Fig. 6.71b).

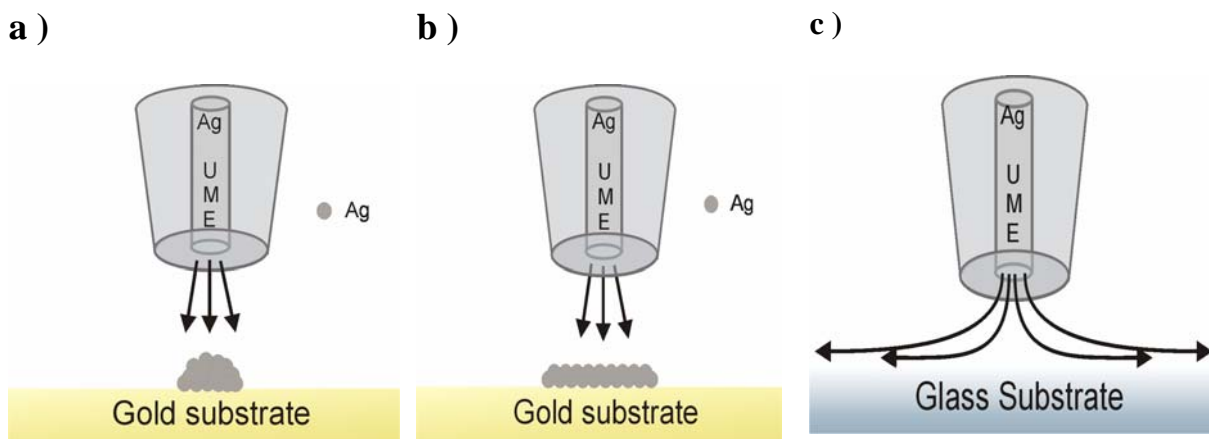


Fig 6.7: Schematic for SECM single pulse chronoamperometric experiment. In (a) Ag^+ is taken up by the substrate when gold is biased at -200mV , (b) when gold is biased at 600mV , (c) diffusion is hindered at an inert (glass) surface.

In this manner, a specific region of the surface is targeted, and any adsorption or growth behaviour involving Ag^+ is monitored quantitatively and exclusively through the current response at the UME probe. After having been confirmed that the anodic dissolution of Ag was a reversible diffusion controlled process, the next stage was to investigate the chronoamperometry characteristic for Ag^+ electrogeneration when the UME probe was placed in close proximity to the gold and glass substrate. Fig. 6.8 show a typical set of transients at the UME above gold and glass surfaces with UME/substrate separation of $5\ \mu\text{m}$.

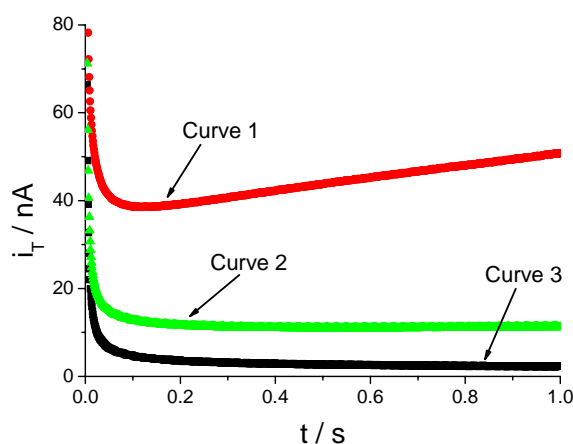


Fig. 6.8: Current – time behavior at an Ag UME positioned 5 μm from the surface. (1) gold surface biased at -200 mV, (2) gold surface biased at 600 mV, (3) glass surface.

Figure 6.8 (curve 1) shows the rapid growth of Ag on gold when gold substrate was biased at -200 mV. This is in contrast to the transient where the substrate was held at 600 mV only allowing the adsorption of Ag on gold in the UPD region Fig 6.8 (curve 2). The curve 3 shows the transients at an inert substrate glass. The steady state current for gold substrate at different potential is higher in comparison to the glass substrate since transients of the UME is affected by the potential of the gold substrate, due to the partial reversibility of the Ag dissolution process under the chosen conditions.

6.4 Double potential step chronoamperometry experiment at gold substrates

In order to find out the Ag^+ UPD on gold substrate double potential step chronoamperometry experiments were done with a sacrificial Ag UME at gold substrate at different potentials. Distinct difference between the chronoamperometry can be seen for the two substrate potential. When the potential of the surface was 600 mV the generation and collection transients are very similar and the collection efficiency, which may be defined as the ratio of the integrated charge between the collection and the generation steps, is fairly high. This is readily explained given previous double potential step chronoamperometry studies using SECM [122, 230-235]. When the substrate is inert it simply acts to trap the electrogenerated materials, i.e., Ag^+ ions, close to the UME, leading to a highly efficient collection step when the potential is reversed.

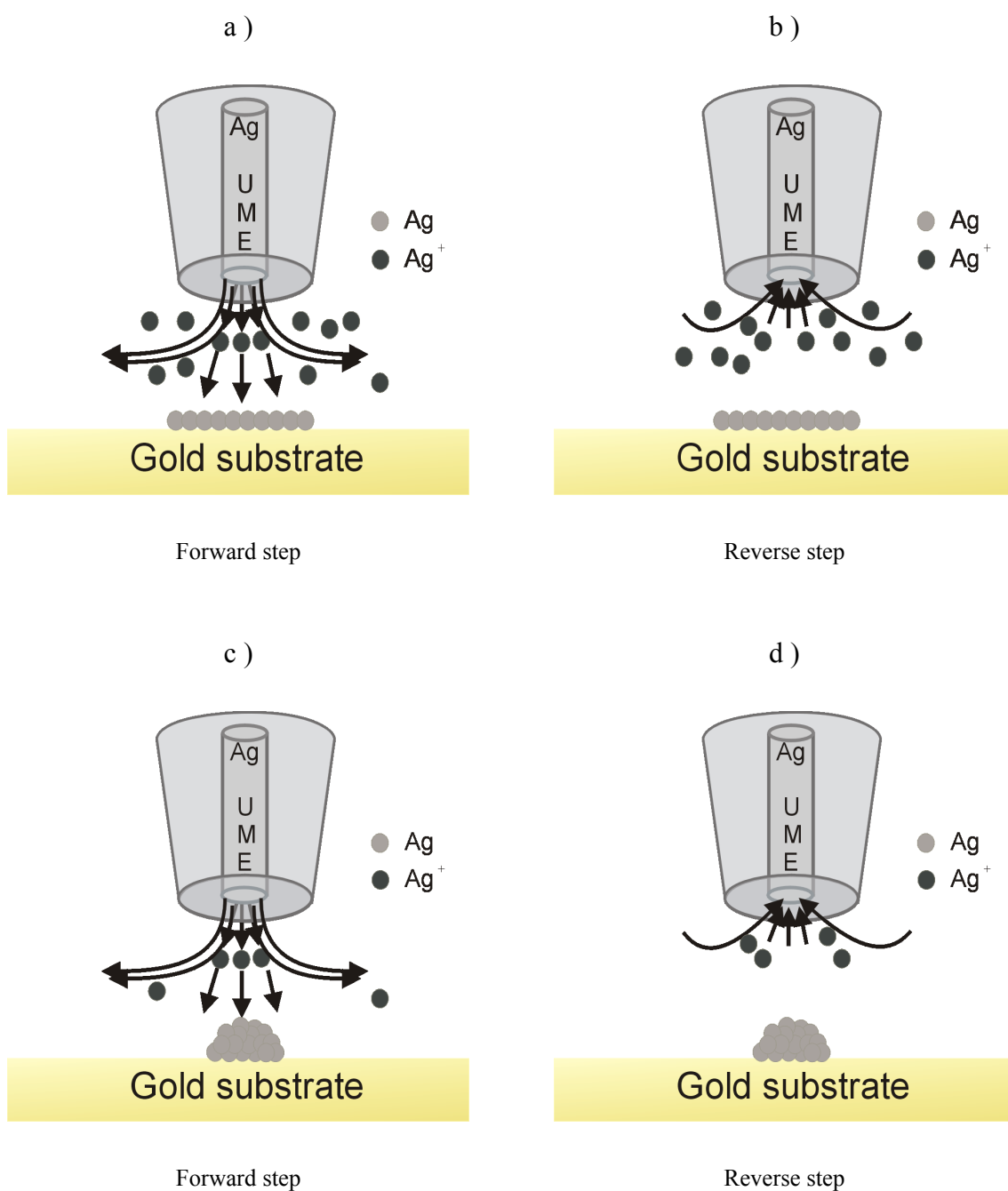


Fig. 6.9: Schematic of the process in the UME/substrate gap for SECM double potential step chronoamperometry. During the forward step Ag⁺ ion is produced by an electrolysis of the sacrificial Ag microelectrode close to the gold substrate (a) biased at 600mV (c) biased at -200mV. During the reverse step Ag⁺ ion reduced at the microelectrode by reversing the potential.

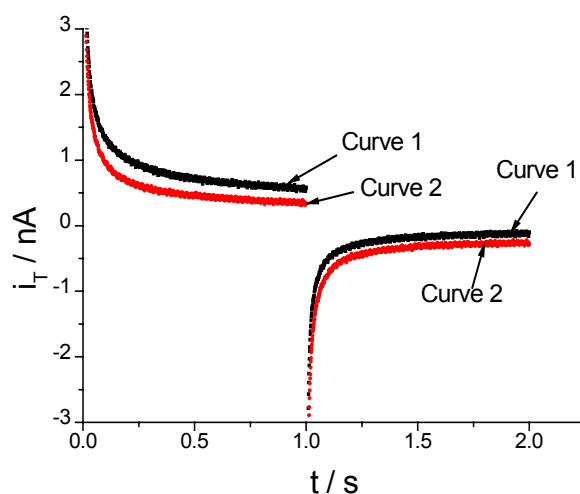


Fig. 6.10: Current – time behavior at an Ag UME positioned 5 μm from the surface in SECM-DPSC mode, (1) gold surface biased at -200 mV, (2) gold surface biased at 600 mV.

The collection efficiency is much higher when the gold substrate is biased at 600 mV as compared to when it is biased at -200 mV. When the gold substrate is biased at 600 mV only Ag UPD occurs, the rest of the Ag^+ are available for the collection in the reverse pulse (Fig. 6.10, curve 1). When the Au substrate is biased at -200 mV, Ag deposition occur at the gold substrate which can be seen in Fig 6.10 (curve 1) having higher steady-state current at the UME during Ag dissolution . In the reverse pulse less Ag^+ is left and current in the reverse pulse is smaller than in curve 2. The fact that the collection efficiency is lower than the half can be explained by the absorption of one or two molecular layer of Ag^+ on gold substrate which is held at UPD range of Ag on gold and also by the partial leaking of the generated species from the thin layer cell that is formed between the UME and the surface. On the other hand when the substrate potential is made sufficiently negative, -200 mV to drive the deposition of silver, less Ag^+ ions are available for collection and redeposition on the microelectrode in the reverse step. Accordingly the collection efficiency decreases to ca. 0.32, which is significantly lower than obtained when Ag^+ were adsorbed on the substrate to one or two monolayer. It is interesting to note that the generation transients for $E_s = -200$ mV is higher than the when the surface is inert or allowed to absorb one or two molecular layer which is attributed to the continuous depletion of Ag^+ from the gap between the microelectrode and the surface during the forward step. The fact that the generation transients

of the microelectrode are affected by the potential of the gold substrate is due to the partial reversibility of the Ag dissolution process under the chosen conditions.

7 Controlling the supramolecular assembly of redox active dendrimers at molecular printboards by SECM

A key issue in molecular electronics [236-241], sensors [242, 243], and biological [244-246] arrays is the positioning of molecules with high accuracy and stability at solid substrates. In this context “molecular printboards” of β CD at gold and SiO_2 surface were developed by Nijhuis et al. from University of Twente, The Netherland. “Molecular printboards” are regular arrays of receptor sites to which, molecules can bind via multiple host-guest supramolecular interaction. Particularly dendrimers serve as a suitable class of polyfunctional guest molecules since the number of end groups can be exactly controlled and all end groups are exposed at the periphery of the molecule [247-249]. Furthermore, the unique properties of dendrimers find applications in many fields such as drug delivery [250], optoelectronics [251], catalysis [252], molecular recognition [253, 254] and molecular encapsulation [255, 256]. In this regard different generations of ferrocenyl (Fc)-functionalised 18 poly (propylenimine) (PPI) dendrimer as a guest molecules were synthesised at University of Twente, The Netherland. Dendrimers of generation 1 to generation 5 have 4, 8, 16, 32, or 64 end groups (Fig. 7.1), respectively, and form multiple host-guest interactions with the molecular printboard. Electrochemical studies of these Fc dendrimers reveals that upon oxidation, the dendrimers leaves the host surface and diffuse to the solution since Fc in oxidised form (Fc^+) has less affinity towards β CD [257]. This process gives an excellent opportunity to SECM to not only to characterize the binding properties, but also to locally modify the electrochemical properties with the help of a suitable redox mediator. The redox-controlled binding can also be done if the printboard is generated on an insulating support such as glass where an electrochemical switching via the support surface would not be possible. It also allows SECM to map the surface in order to check the distribution of these dendrimers on patterned surface at gold and insulating surfaces like SiO_2 .

Measuring the concentration of redox active dendrimers at Au surface by SECM is difficult from the data interpretation view, since the mediator is not only oxidised and reduced at the redox dendrimers at the Au surface and at Au surface that can be reached via pinholes in the monolayers [258]. This leads to complicity of the data interpretation by SECM. This problem can be avoided if the receptors are immobilized on an insulating surface; e.g. SiO_2 .

This work also represents a new SECM imaging technique where a monolayer of a surface-bound species is redox-titrated by the SECM mediator. Traditionally, SECM image is performed by maintaining a steady state current at UME, whereas here the image was obtained with a decrease of the steady state current at the UME since the current decreases due to the constant removal of Fc moieties from the pattern surface upon oxidation. Due to the constant removal of Fc moieties from the surface during the imaging, SECM imaging was optimised with respect to speed and also the step size in both forward and backward direction.

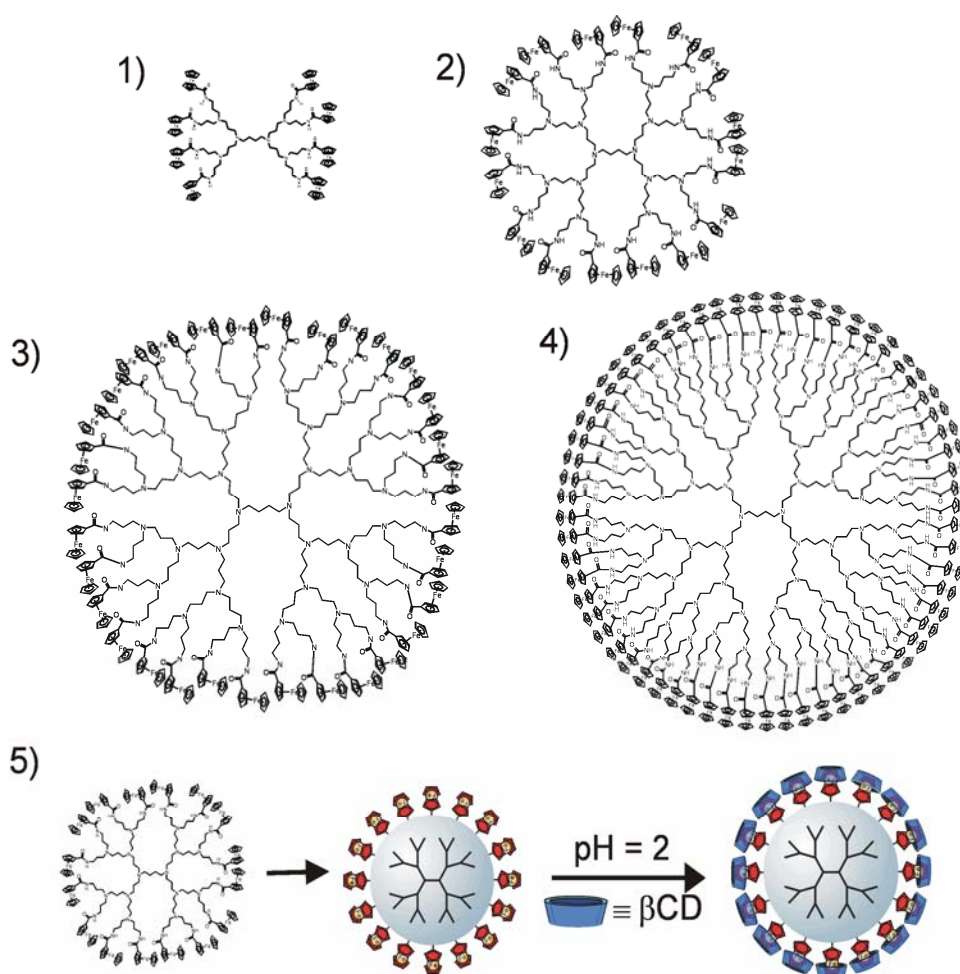


Fig. 7.1: Different generation poly(propylene imine) (PPI) dendrimer decorated with Fc moieties. (1) 2nd generation (G2) PPI dendrimer with 8 Fc end groups, (2) 3rd generation (G3) PPI dendrimer with 16 Fc end groups, (3) 4th generation (G4) PPI dendrimer with 32 Fc end groups, (4) 5th generation (G5) PPI dendrimer with 64 Fc end groups, (5) 3rd generation (G3) PPI dendrimer with Fc end groups complexed to β CD resulting in water soluble supramolecular assembly.

7.1 Oxidation of ferrocene dendrimer

The interaction of five generations PPI dendrimers- β CD assemblies in aqueous solutions with β CD SAMs at Au was characterized by CV and differential pulse voltammetry [257]. The oxidation potential of Fc dendrimers was found to be 0.540 V vs. Ag/AgCl. As the potential increases, the Fc groups are oxidized to ferrocenium cations which are not able to form inclusion complexes with β CD leading to desorption of the dendrimers from the β CD SAM (Fig. 7.2) and subsequent diffusion into the solution. Upon reduction, only dendrimers that remained close to the surface can be reduced back to the surface, resulting in concomitant decrease in intensity during the cyclic voltammetry scan [257]. Scan rate-dependent cyclic voltammetry revealed almost reversible behavior at low scan rates for all generation of Fc dendrimers, but irreversible behavior at high scan rates for lower generation of dendrimers (G1 and G2), because of diffusion of small size Fc dendrimers. Higher generation Fc dendrimers can be trapped during the fast scan rate cyclic voltammetry due to their larger size. Out of five generations of PPI dendrimers, generation-3 (G3) dendrimer was used for SECM experiment, since G4 and G5 showed a complex electrochemical behavior and G1 and G2 do not form stable host-guest interaction of β CD immobilized at SiO_2 surface.

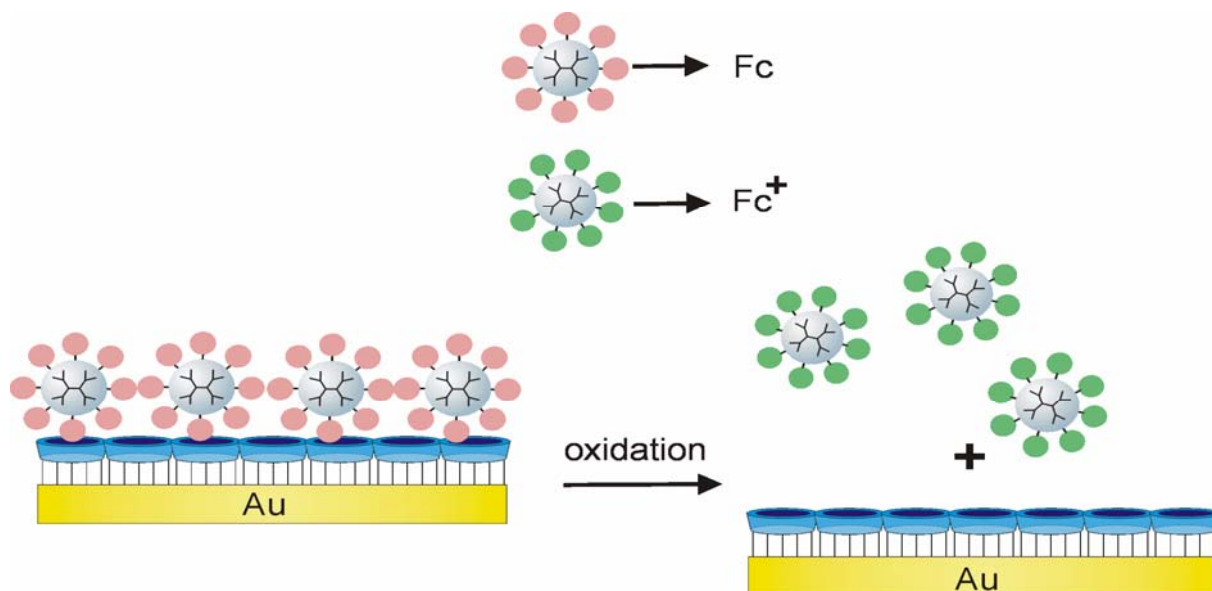


Fig. 7.2: Electrochemical desorption of Fc dendrimer from β CD assemblies at gold surface.

In order to oxidize Fc dendrimers at the surface, a mediator is required that has a higher formal potential than that of the Fc dendrimers $E^{\circ'} = 0.540$ V. In addition the mediator has to be suitable for SECM experiments, i.e. both redox forms of the mediator must be stable in

aqueous solution. Potassium hexacyanoferrate-II, ferrocene methanol and potassium hexachloroiridiate-III were tested. The formal potential was obtained by cyclic voltammetry (Table 7.1). From the tested mediators potassium hexachloroiridiate-II was found to be a suitable redox couple, since it has a higher formal potential, 0.65 V than the Fc dendrimer.

Table 7.1: Formal potential of different redox couple obtained at a Pt UME in solution 1 against Ag/AgCl reference electrode.

Redox Couple	Formal Potential / $E^{\bullet\bullet}$ (V)
$K_4[Fe(CN)_6]$	0.3
Fc-CH ₃ OH	0.1
$K_3[Ir(Cl)_6]$	0.65

7.2 Approaching the surface with oxygen reduction

In order to conduct a SECM experiment, the UME has to be brought close to the specimen surface. Doing so with the mediator selected for oxidation of the Fc dendrimers would already alter the surface (Fig. 7.3). Therefore, a second redox mediator was used. Dissolved oxygen can be reduced at the UME. Because the oxygen reduction is an irreversible reaction, no reaction occurs at the sample and an approach curve is controlled by the hindered diffusion of oxygen to the UME (Fig 7.4). The current will follow Eq. 2.19. An example is given in Fig. 7.5. The UME reduced O₂ at -0.6 V.

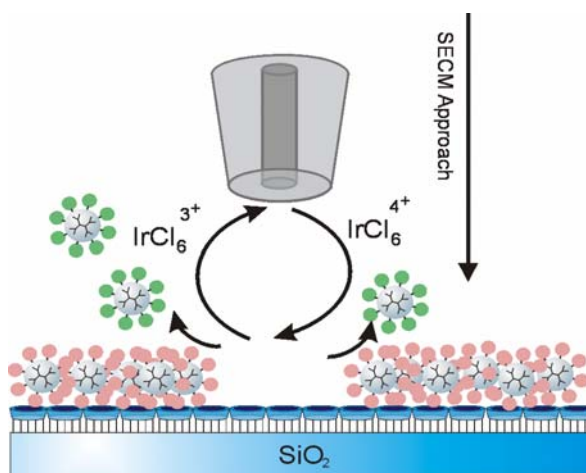


Fig. 7.3: Approaching of the UME to the surface with the mediator selected for the oxidation of the Fc dendrimer.

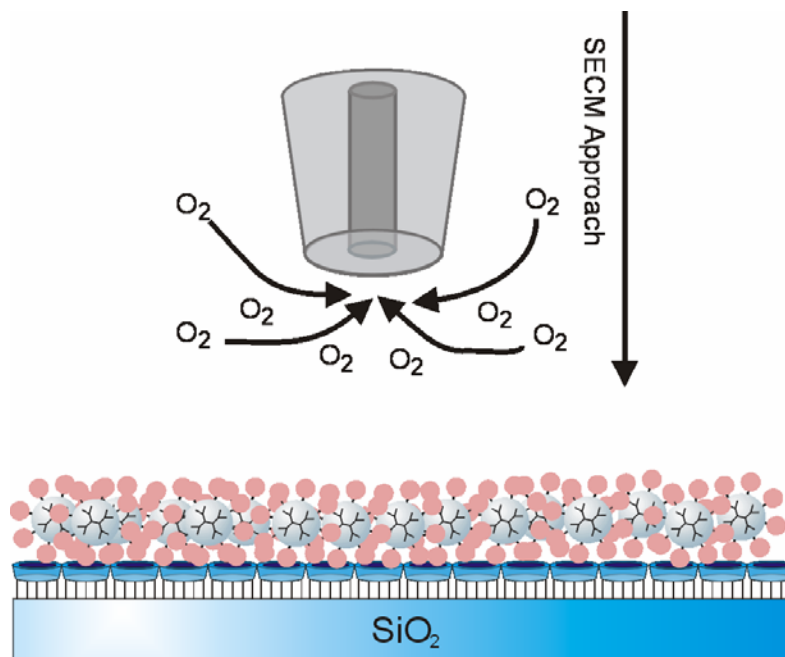


Fig. 7.4: Approaching of the UME to the surface with O₂ reduction present in the solution.

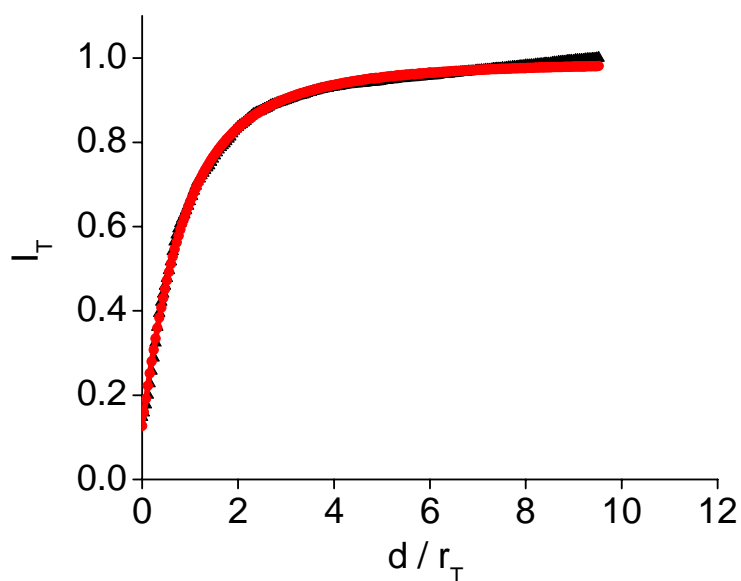


Fig. 7.5: Approach of the UME with steady-state O₂ reduction current. The experimental points (▲) are plotted filled symbols. The line with symbol (●) is a fit using Eq (2.19) with the following parameters: $r_T = 12.5$, $RG = 15.2$, $i_{T\infty} = 3.2$ nA.

7.3 Line scan of the structured surface

Since the sample has one life time for SECM imaging it was foremost important to find the patterned area for the imaging, therefore multiple line scans were preformed in x and y axis.

Multiple line scans were done in order to image patterned surface. Care was taken to avoid the situation as shown in the Fig. 7.6a (situation B) before imaging. The situation A is more acceptable than the situation B for SECM imaging. If SECM image will start with the situation B then the feedback current sampled at the UME would be less and it would be more difficult further when UME will be allowed to map the whole surface. Because the redox mediator will diffuse spherically and oxidize the Fc moieties before the UME samples the surface during the next step.

The UME records a higher feedback current during a forward scan (Fig. 7.6b, curve 1) than the backward scan (Fig. 7.6b, curve 2). This is due to the removal of Fc dendrimers from the patterned surface upon oxidation during the forward scan. This further proves the observation as previously mentioned (Chapter 7.1).

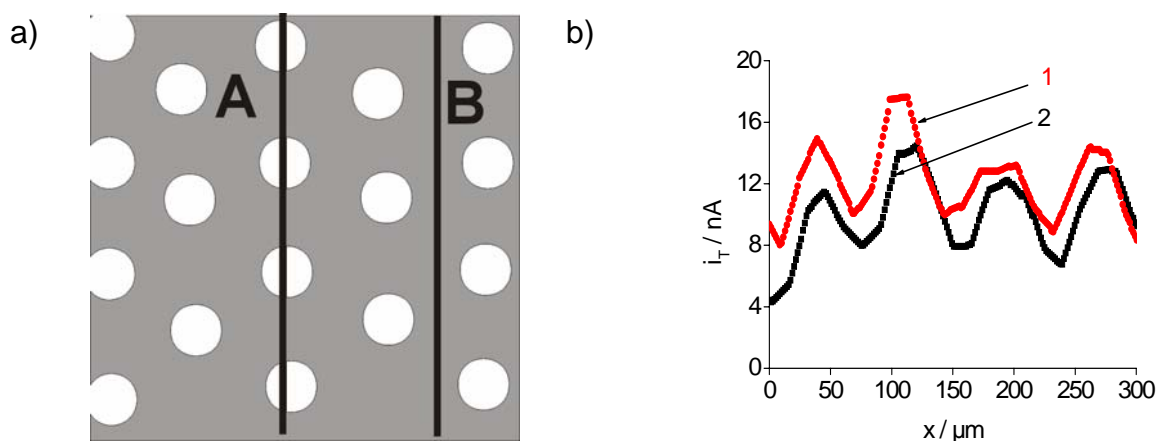


Fig. 7.6: (a) Ideal situation (A) to start SECM imaging, non-ideal situation (B) to start SECM imaging, (b) Forward (1) and backward (2) lines scan over the structured surface.

7.4 SECM imaging of Fc dendrimers at molecular printboard at Au surface

In initial experiments the patterns were obtained on a gold surface. The dendrimers were printed in line with gaps of 15 μm . The SECM image was obtained by scanning the surface with the presence of $[\text{Ru}(\text{NH}_3)_6]^{3+}$ as a redox mediator. The image was obtained with the idea to get an SECM image with the hindered diffusion of redox mediator at the patterned surface. At location where only bare βCD monolayer is present the current at UME is larger than where the pattern of Fc is present. This is due to the higher electron transfer kinetics of the mediator at βCD monolayer without Fc-dendrimers than at the Fc-dendrimers loaded

monolayers. The Fig 7.8 shows the hindered diffusion of mediator rather than oxidation of Fc moieties from the surface since the reduced species $[\text{Ru}(\text{NH}_3)_6]^{2+}$ of the mediator was unable to oxidize Fc moieties from the surface because the formal potential of the redox mediator is negative with respect to the formal potential of the Fc moieties.

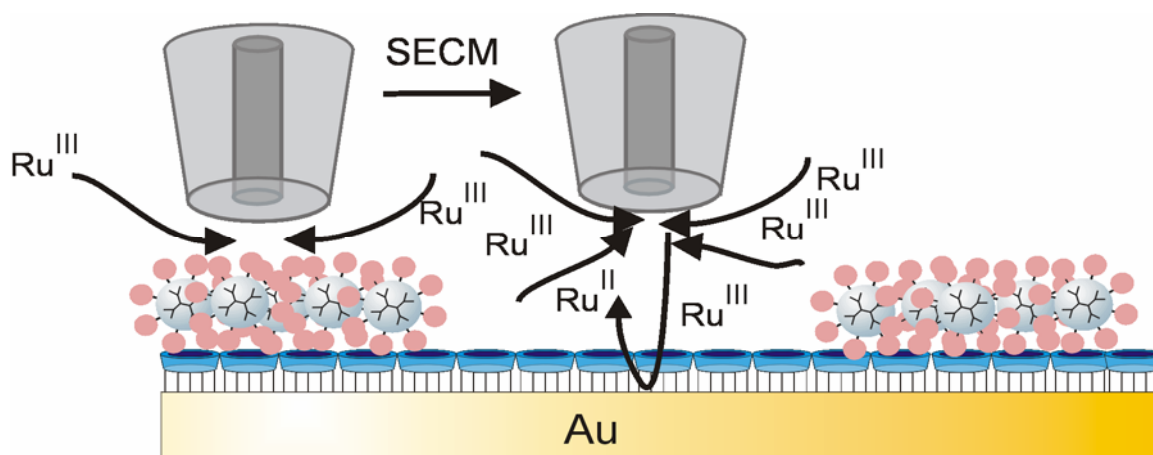


Fig. 7.7: Schematic of the mechanism of SECM imaging with the hindered diffusion of the redox mediator at molecular printboard on gold. The regeneration Ru^{2+} from Ru^{3+} occurs through the defect present in the βCD monolayer at Au surface.

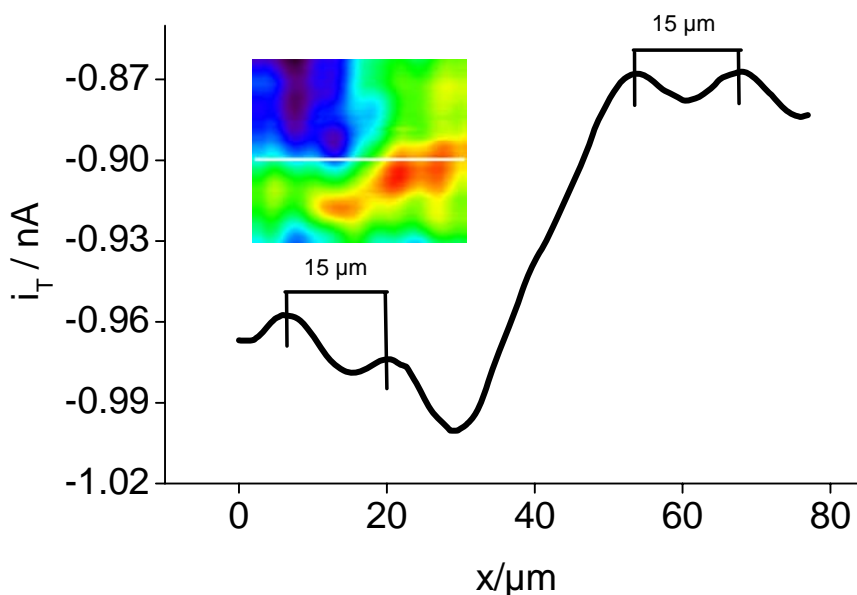


Fig. 7.8: Line scan (right) obtained from the profile of the image (left) indicated by the white line in the image showing the line pattern of Fc on Au surface with irregular periodicity. $E_T = -0.4 \text{ V}$, $v_T = 10 \mu\text{m s}^{-1}$, $0.1 \text{ mM } [\text{Ru}(\text{NH}_3)_6]^{3+}$.

Although the oxidation of Fc moieties from the surface was not possible by $[\text{Ru}(\text{NH}_3)_6]^{3+}$ but still an image of the patterned surface can be obtained (Fig. 7.8). The periodicity of the sample found out to be $15\ \mu\text{m}$ from the line scan obtained from the profile of the image as shown in the Fig. 7.8, which agrees with the way the samples were prepared.

7.5 Optimization of the SECM Imaging for Fc Dendrimers

From previous studies [257] and line scans of the patterned surface, it is clear that after oxidation of Fc moieties, it leaves the surface and diffuse to the solution. Due to the spherical diffusion of the redox mediator at the UME, it not only oxidizes the Fc moieties below the UME but also in areas close to the UME. This situation creates a problem for SECM imaging. In general SECM imaging has been done with monitoring the constant steady state current at the UME whereas the current decreases here with time since the Fc moieties leaves the surface after oxidation and diffuse to the solution. In order to avoid this problem, the SECM instrument was optimised with respect to speed and the step size in both directions. When SECM image was performed with a slower scan rate (Fig 7.9a), featureless images were obtained. Because the dendrimers have already released and the current is sampled at UME. Finally when the SECM scan rate was increased to $200\ \mu\text{m}\ \text{s}^{-1}$, the patterned surface of Fc-dendrimers is successfully imaged (Fig 7.9b), because the redox capacity of the Fc-dendrimers is sufficient to sustain the feedback current during the short time the UME is located above a specific region of the surface.

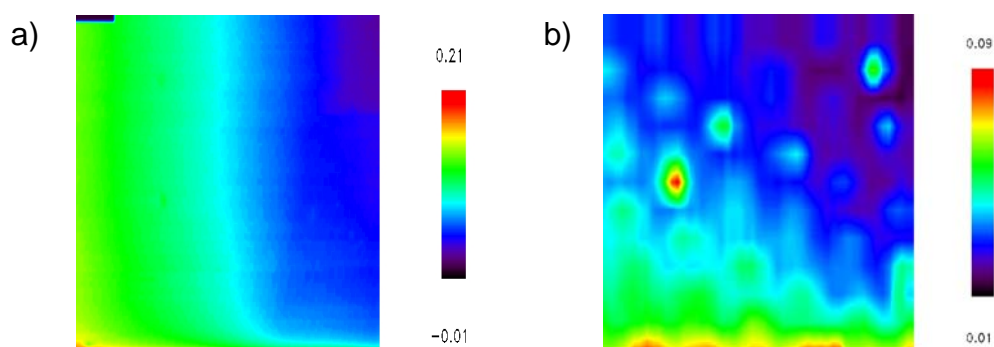


Fig. 7.9: SECM images of the patterned Fc-dendrimers βCD on SiO_2 with $[\text{IrCl}_6]^{3-}$ as redox mediator, $E_T = 0.75\ \text{V}$: a) translation rate $10\ \mu\text{m}\ \text{s}^{-1}$ and b) translation rate $200\ \mu\text{m}\ \text{s}^{-1}$.

Even at higher scan rates the first line scans have the highest feedback current compared to the successive line scans in all obtained images. This could be due to the partial leakage or

diffuse of the oxidised species to other part of the sample and subsequent oxidation of the Fc moieties before it could be mapped at the UME during the line scan.

7.6 SECM imaging of Fc dendrimers at molecular printboard at SiO₂ surface

The dendrimers were printed in dots with a diameter of 50 μm and gaps of 30 μm and verified by AFM [259]. The SECM images were obtained by scanning the surface in aqueous solutions containing $[\text{IrCl}_6]^{3-}$ as a mediator in the positive feedback mode. The UME potential E_T was kept at 0.75 V vs. Ag/AgCl such that $[\text{IrCl}_6]^{3-}$ is oxidized at the UME under diffusion-controlled conditions. The oxidized species $[\text{IrCl}_6]^{2-}$ diffuses to the surface and may accept an electron from Fc moieties of the dendrimers which have a lower E° . During this process Fc^+ would be released and $[\text{IrCl}_6]^{3-}$ regenerated. Subsequently, $[\text{IrCl}_6]^{3-}$ may diffuse back to the UME giving rise to positive feedback current. At locations where only a bare βCD monolayer is present the $[\text{IrCl}_6]^{2-}$ can not be reduced, since no dendrimers are present, resulting in an UME current i_T that can be described by pure hindered diffusion of $[\text{IrCl}_6]^{3-}$ from the solution bulk to the UME. The redox processes that occur at Fc-dendrimers loaded part of the surface are outlined in Fig. 7.10.

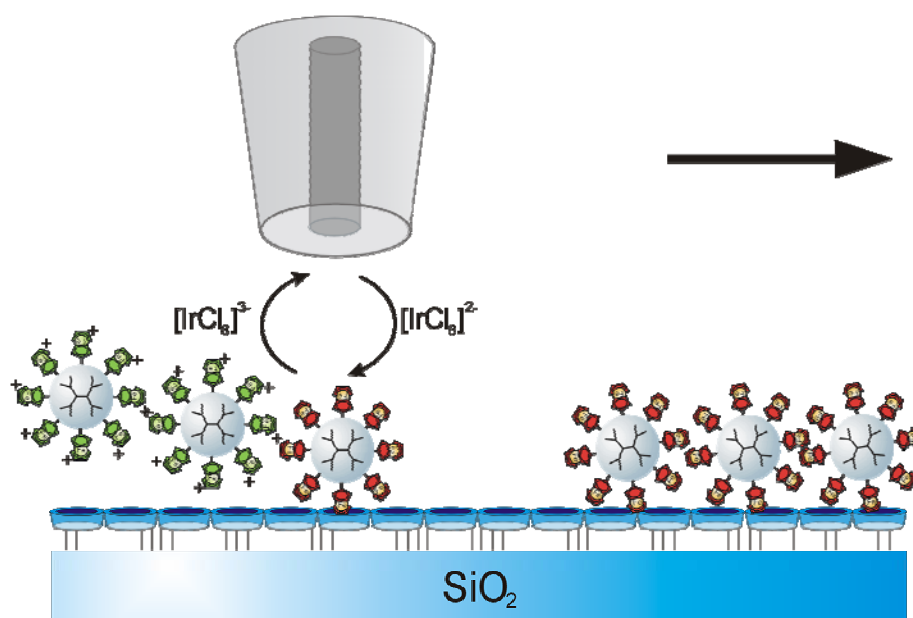


Fig. 7.10: Schematic of the mechanism of SECM induced desorption of the dendrimers from the molecular printboard on glass. $[\text{IrCl}_6]^{3-}$ is oxidized at the UME and diffuses to the molecular printboard where it oxidizes the patterns of Fc dendrimers. Subsequently, the oxidized Fc dendrimers desorb from the host surface and the reduced $[\text{IrCl}_6]^{3-}$ diffuses back to the UME giving rise to positive feedback currents only at the Fc dendrimer-covered regions.

A SECM image is shown Fig. 7.11. The image clearly shows a hexagonal pattern of dots, which appear with a higher feedback current, compared to the background. The periodicity was determined from the profile extracted along the white line from the image and the corresponding line scan is also shown in Fig. 7.11. The observed periodicity of 80 μm corresponds exactly to the printed dendrimer dots (50 μm in diameter and 30 μm gaps). Hence, SECM faithfully reveals the hexagonal pattern of a monolayer of dendrimers printed on the molecular printboard. The peak intensities of the line scan are not uniform probably due to an inhomogeneous distribution of G3-PPI-(Fc)₁₆ at the surface.

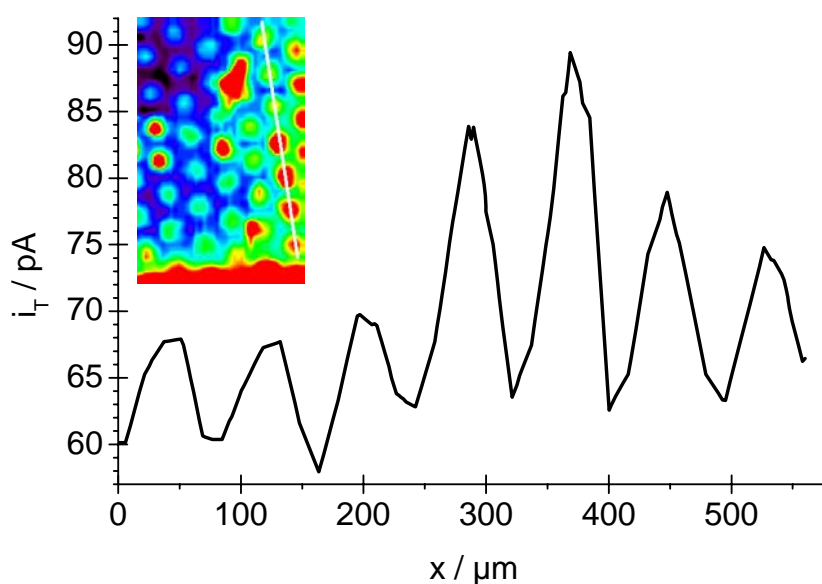


Fig. 7.11: Line scan (right) obtained from the profile of the image (left) indicated by the white line in the image showing the periodicity of the printed features. $E_T = 0.75$ V, $v_T = 200$ $\mu\text{m s}^{-1}$, 0.1 mM $[\text{IrCl}_6]^{3-}$.

In order to obtain the image in Fig. 7.11, a very high scan rate and step size had to be used. The translation speed was 200 $\mu\text{m s}^{-1}$ and the step size in the low frequency axis (y) was 15 μm . At slower scan rates featureless images were obtained because the Fc-dendrimers were completely released during the scan and mediator regeneration ceased before the current values were sampled. Even at higher scan rates the first line scans have the highest feedback current compared to the successive line scans in all obtained images. This is nicely demonstrated by the surface plot shown in Fig. 7.12. Individual line scans are displayed as black lines. The first line scan is placed in the rear part of the plot. The first line scan is more intense because during the first line scan also some of the Fc-dendrimers are oxidized that are

located in the area later probed by the UME. In subsequent images sample regions outside the imaging frame can contribute to the mediator regeneration, whereas the imaged region is successively depleted.

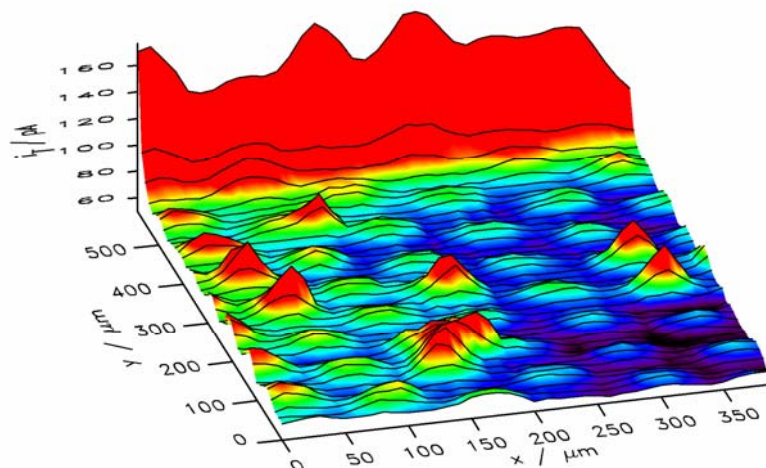


Fig. 7.12: SECM image of a Fc-dendrimer-modified printboard illustrating the higher intensity of the first line scan (shown in the background). Black lines correspond to individual line scans. The false color was interpolated; $E_T = 0.75$ V, $v_T = 200$ $\mu\text{m s}^{-1}$, 0.1 mM $[\text{IrCl}_6]^{3-}$.

Upon imaging by SECM the feedback currents decreased significantly due to the depletion of Fc-loaded dendrimers on the surface. This is illustrated in Fig. 7.13.

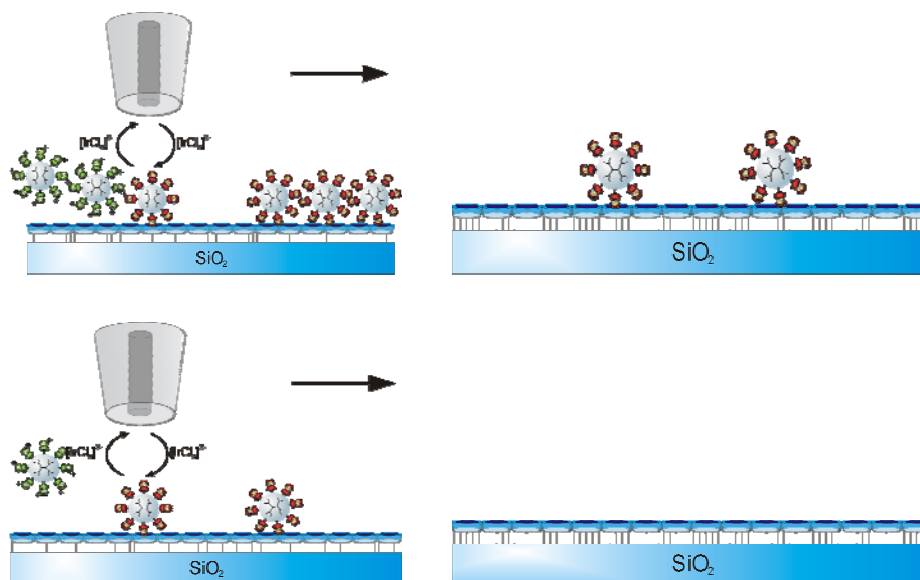


Fig. 7.13: Schematic of repeated imaging by SECM at the same place.

Moreover, repeated imaging of the same area showed a further decrease in feedback currents. Fig 7.14 shows four images of the same sample regions. Fig 7.14b and Fig 7.14d are assembled from the reverse line scans of Fig 7.14a and Fig. 7.14c, respectively. The features are hardly visible in the last image.

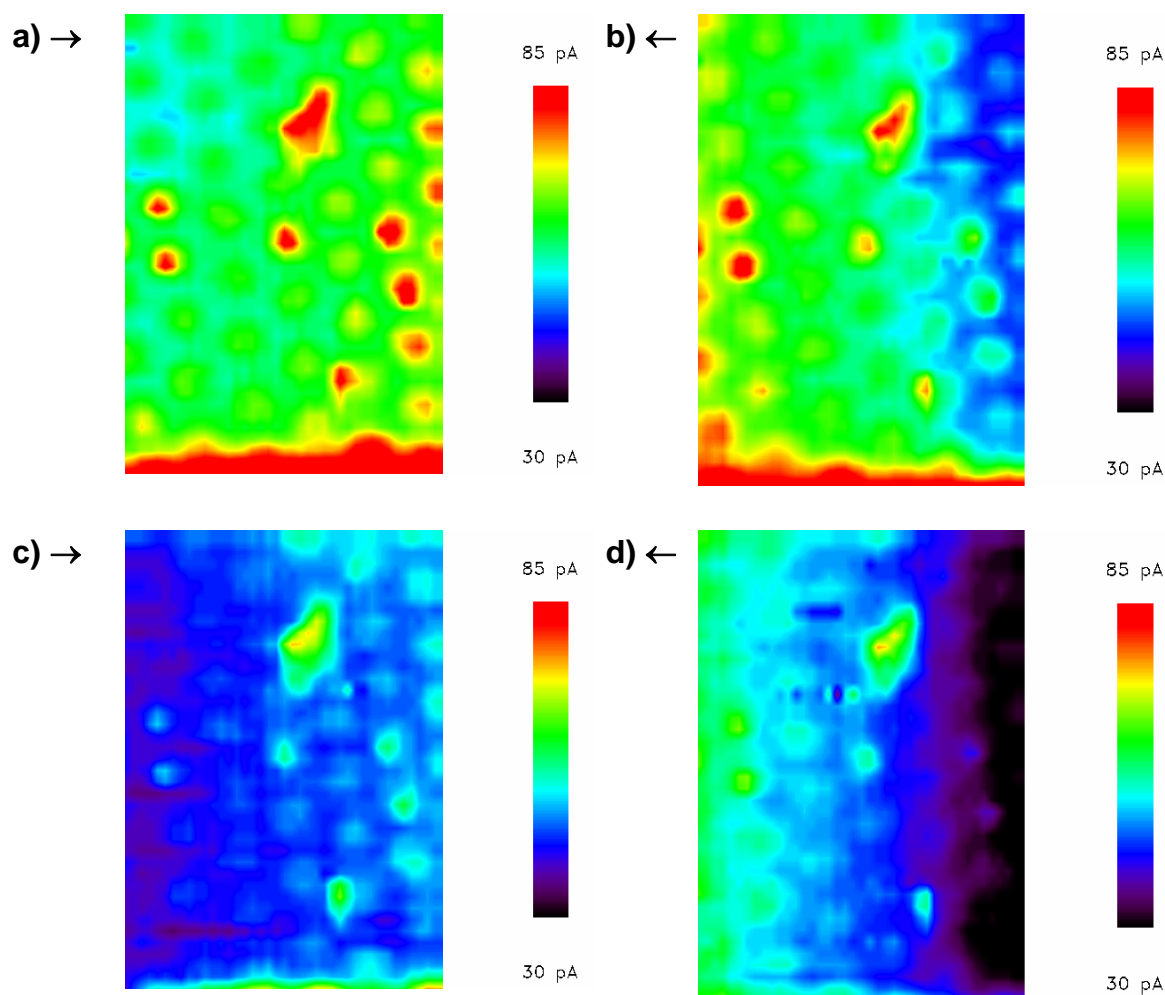
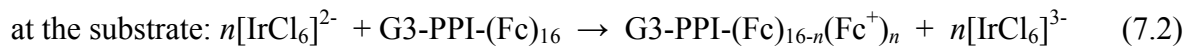
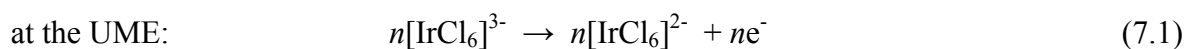


Fig. 7.14: SECM images of G3-PPI-(Fc)16 printed at a β CD SAM on glass: a) image composed of the forward line scans and b) backward line scans; a second SECM image of the same area composed of the forward line scans (c) and backward line scans (d); $E_T = 0.75$ V, $v_T = 200 \mu\text{m s}^{-1}$, $0.1 \text{ mM } [\text{IrCl}_6]^{3-}$.

The observations, *i*) the relatively high intensity of the first line scan, *ii*) the pattern disappearing upon scanning, and *iii*) the high scan rate necessary to visualize the structures, all suggest that upon scanning, the dendrimers desorb from the host surface. The proposed mechanism is outlined in equation (7.1) and (7.2). At the UME the mediator is oxidized and diffuses to the surface where it may oxidize Fc groups of the dendrimers. The reduced form of the mediator may diffuse back to UME. It is well-known that the oxidized form of the Fc is not able to form inclusion complexes [257] with the β CD at the surface resulting in an

effective desorption of the dendrimers from the surface. The reactions at the UME and at the substrate are thus:



Therefore, subsequent scans and backward scans show a significant decrease in intensity of the feedback currents. The high scan rate is required to reduce the number of redox equivalents imposed per surface area, where it oxidizes the Fc units of the dendrimers. The dendrimers desorb from the host surface and diffuse into the bulk solution or oxidize neighbouring dendrimers. Consequently, scanning slowly may impose more redox equivalent per sample surface area than Fc units be present in the dendrimer-modified areas. For similar reasons the step size in the low frequency direction had to be relatively large in order to minimize oxidation during scanning the previous line scan. This also explains why the very first scan gives a substantially higher positive feedback currents than the remaining line scans. SECM-induced oxidation of the dendrimers resulted in an effective desorption of the dendrimers from the β CD SAM at SiO_2 and also provided images of the desorption process at different stages by repetitively recording images until all Fc-dendrimers were desorbed. This observation implies that the dendrimers are primarily bound via specific host-guest interactions to the β -CD at the host surface on SiO_2 [260]. In principle, the monolayer is less ordered compared to monolayers on Au since the monolayer is covalently bound, but nevertheless, the binding behaviour of the dendrimers is in full agreement to that found in studies of Fc dendrimers binding to printboards on gold surfaces [257] and of divalent guests binding to printboards on glass.

8 Controlled electrochemical desorption of redox active dendrimers at molecular printboard by SECM

In this chapter an attempt was made to calculate the surface concentration of different generations of Fc-functionalised dendrimers by chronoamperometric pulse technique. Three different types of Fc-functionalised dendrimers of generation 3 to 5 were adsorbed at self-assembled monolayers of heptathioether-functionalised β CD host surface at SiO_2 . The samples were obtained in collaboration with Nijhuis et al. from University of Twente.

The general idea of the experiment is outlined in Fig. 8.1. The UME generates an oxidant that converts the ferrocene units to ferrocinium units leading to a release from the host surface. By estimation of the charge transferred to the Fc units at the surface, the surface concentration of the dendrimers should be accessible. The process is similar to a titration known as redox titration. Redox titration (also called oxidation-reduction titration) is a type of titration based on a redox reaction between the analyte and titrant. The redox titration process is followed by the change in UME current. In Chapter 7 it was shown that SECM provides a way to induce local desorption of redox active dendrimers from SiO_2 surface. In addition imaging possibilities can be used to determine the size of the modified area. In addition to that the local desorption were made with different chronoamperometric pulse time in order to find the relation between pulse time and area of the spots made by local desorption. On a completely different chemical system, Mandler et al. [261-264] deposited metal and etched semiconductors material by using a pulse technique similar to the chronoamperometric pulse technique used here. The UME was held for a certain period of time at the formal potential of the mediator to produce a strong oxidant. On a similar note Unwin et al. [119, 265] used this technique to study the adsorption and desorption kinetics and as well as surface diffusion rates at solid-liquid interfaces.

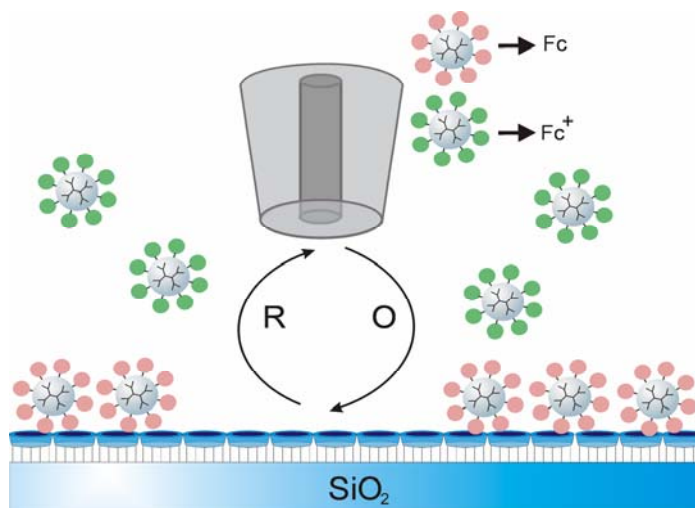


Fig. 8.1: Local redox titration of Fc modified-surface by SECM redox mediator, the oxidized form of ferrocene (Fc⁺) marked as green colour, ferrocene (Fc) marked as red colour, upon oxidation Fc-dendrimers depart from the surface and diffuse to the solution.

8.1 Optimisation of working distance for pulse experiments

The distance d between UME and surface was optimised in order to find a suitable and close distance to the surface to perform chronoamperometric pulse experiment. This is important because the oxidation and reduction process occur at the UME, and the surface has to be monitored by the UME in order to find the surface coverage of different generation of dendrimers at SiO₂ surface. The working distance has two effects. It controls indirectly the area exposed to the UME-generated oxidant. It also has a big effect on the time required for the mediators to diffuse between UME and sample. The Fig. 8.3 shows the pulse experiment done at UME at different distances with respect to the functionalised surface. The general features of such current traces are described below. The current at long times approaches the steady state current measured over an insulating surface. For a given UME, it depends only on the distance d and the concentration c and diffusion coefficient D of the mediator. At long time all the ferrocene units are oxidised (Fig. 8.2b). The surface behaves like an inert or insulating surface. Therefore the currents for $t \rightarrow \infty$ follow a sequence from small distances (Fig. 8.3 curve 1, $d = 2 \mu\text{m}$) to large distances (Fig. 8.3, curve 5, $d \rightarrow \infty$). At short times the situation is different because the mediator is regenerated by the redox reaction with the Fc dendrimers (Fig. 8.3, curve 1-4). This situation is illustrated by Fig. 8.2a. The process are summarised in Fig. 8.2

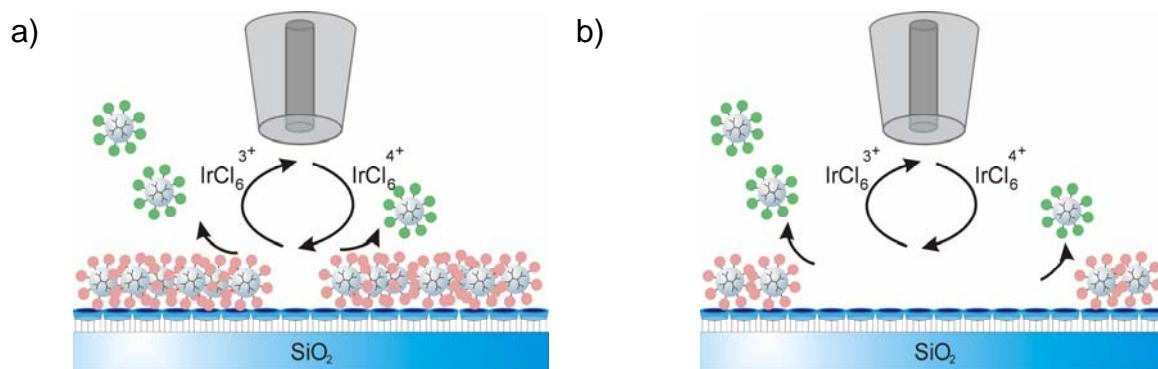


Fig. 8.2: Chronoamperometric pulse experiment at UME, (a) at short pulse time, (b) at long pulse time. Pt UME positioned at $15\mu\text{m}$ distance from the surface for both the pulse experiment.

A distance of $15\mu\text{m}$ was selected for further experiments. This distance can be relocated with an acceptable relative uncertainty $\Delta d/d$. Smaller distances turned out to be difficult to work with since a comparison must be made between the pulse experiment over the Fc-modified and a bare surface. Larger working distances did not show good mediators regeneration. The redox processes occurring at the UME and the surface are described in Chapter 7 (Eq. 7.1 and 7.2).

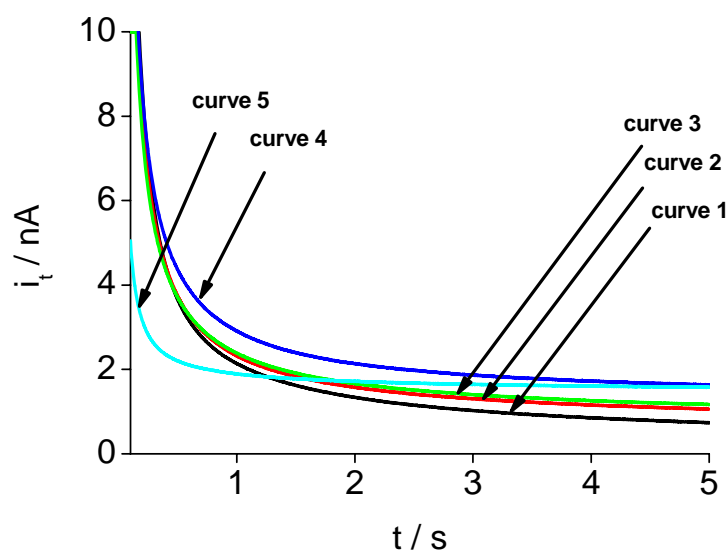


Fig. 8.3: Chronoamperometric pulse experiment at different distances from the an insulating glass surface, 1) $2\mu\text{m}$, 2) $5\mu\text{m}$, 3) $10\mu\text{m}$, 4) $15\mu\text{m}$ and 5) UME in bulk solution

A comparison of pulse experiments were performed for large and small d . The purpose of this experiment is to prove that the feedback current measured close to the surface is higher

than the feedback current measured far from the surface. The feedback current measured close to the surface is higher at the beginning of the pulse (Fig. 8.4 curve 1). After a certain time it decreases below the response recorded far from the surface (Fig. 8.4, curve 5). This is due to the removal of Fc moieties from the surface upon oxidation, which could not contribute to the feedback current, measured at UME at longer time. The current measured at the UME at longer time is only due to the hindered diffusion of the redox mediator. Diffusion is more effectively hindered at smaller d . The current measured at the UME far from the surface corresponds to the steady state current of the redox mediator. The current at $t < 0.05$ s is influenced by charging currents and is not considered here. The behaviour for $t > 0.05$ s can be explained by considering steady state feedback current experiments and the limited redox capacity of the immobilized Fc-dendrimers. At $0.1 > t < 1$, the response is controlled by almost diffusion controlled positive feedback due to the reaction between immobilized Fc-dendrimers and the oxidised mediator. The response depends on the distance and at smaller working distances (Fig. 8.5, curve 1) a much higher current is recorded. At later times the redox equivalents at the surface are exhausted. This situation is reduced faster at small d since the flux of the oxidant is focussed on a smaller sample region. After exhaustion the remaining UME current results from hindered diffusion of $[\text{Ir}(\text{Cl})_6]^{3-}$ from the solution bulk to the UME.

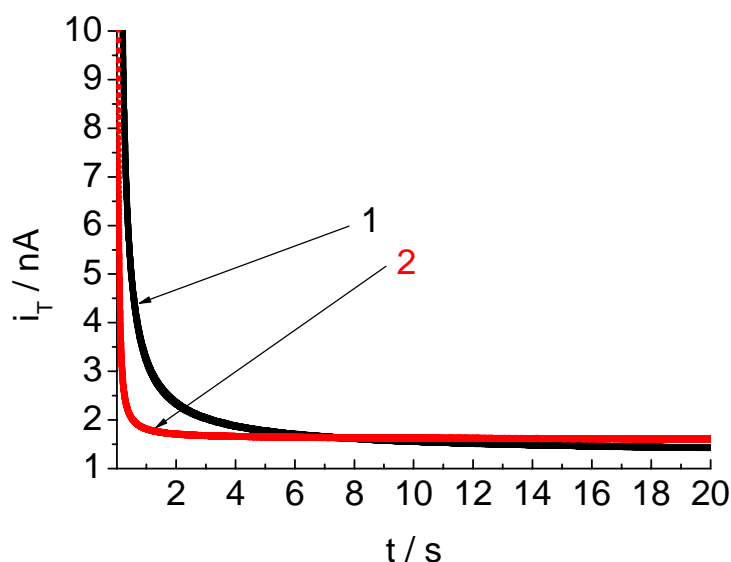


Fig. 8.4: Chronoamperometric pulse experiment at two distances with respect to G3 Fc dendrimer-modified surface, (1) $15 \mu\text{m}$ from the surface, (2) far from the surface.

This current will be smaller if d is decreased. As a consequence the two chronoamperometric curves in Fig. 8.4 cross each other at around 8 s. This method could be applied to determine the surface concentration of the Fc moieties by performing the pulse experiment close to the surface.

8.2 Optimisation of the time for pulse experiment for determination of surface concentration

The general idea of this experiment consists in a two pulse experiment at identical distance. During the first pulse, the Fc-dendrimers are completely oxidized. A second pulse shall provide the background signal originating from hindered diffusion of $[\text{Ir}(\text{Cl})_6]^{3-}$ from the bulk. The optimisation task is to find a suitable pulse time, where the pulse time should be long enough to oxidize the Fc moieties from the surface during the first pulse under diffusion-controlled conditions affecting a certain area of surface below the UME. When the second pulse would be performed, no more Fc should be there to be oxidised. The difference of the charges measured at the UME during both pulses would correspond to the oxidation of Fc moieties from the surface. The charges of the both pulses are obtained by integration of the recorded UME current. From the charge the surface concentration of Fc-dendrimers can be estimated.

The potential of the UME should be well above the formal potential of the redox mediator (0.75 V) in order to get a steady state diffusion-controlled current upon the oxidation of the reduced species (R) present in the solution. During the pulse experiment, UME was kept at this potential for certain period of time so that oxidised species produced at the UME can diffuse to the surface and can oxidise Fc moieties. The optimisation of the pulse time was done after optimising the distance between UME and the surface. The complete removal of Fc moieties is not possible during the short pulse experiment (Fig. 8.5a and Fig. 8.5b). The chronoamperometric curve during the first pulse meets the second chronamperometric curve only after 20s pulse experiment. This situation corresponds to the complete removal of Fc dendrimers from the surface during the first pulse under the area below UME, which is shown in Fig. 8.5c.

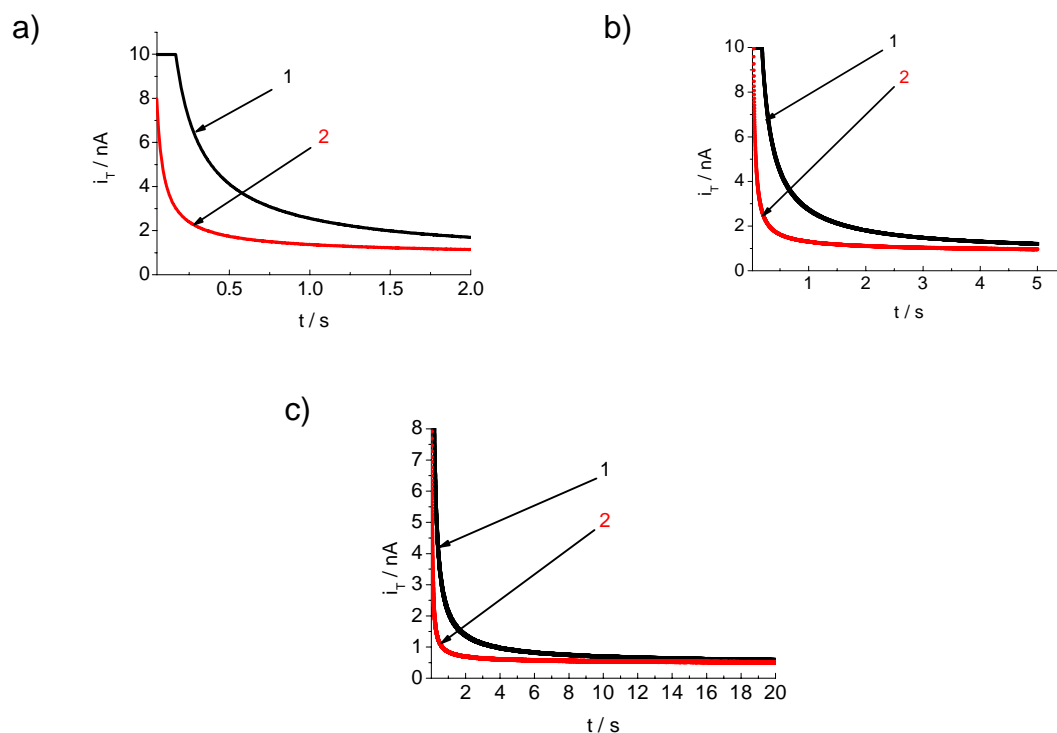


Fig. 8.5: Chronoamperometric pulse for G3 Fc-dendrimer-modified surface. a) For 2 second. b) For 5 seconds. c) For 20 seconds. Curve 1 and curve 2 represent for first pulse and second pulse respectively for each figure. Pt UME positioned at $15\mu\text{m}$ from the surface for each experiment.

8.3 Multiple pulse experiments at the same location

In order to prove the complete removal of Fc dendrimer from Fc-dendrimer βCD -modified SiO_2 , pulse experiment were performed with different time interval. Also for better surface coverage calculation a second or third pulse has to be done to obtain a background signal from the second or third pulse. A schematic for first and second pulse was shown in the Fig. 8.6a and Fig. 8.6b respectively. The feedback current measured during the first pulse corresponds to the oxidation of the Fc-dendrimers. The feedback current measured during the second pulse only corresponds to the hindered diffusion of mediator which acts as a background current for the rest of the surface concentration calculation for Fc-dendrimers at the surface. The background charge can be subtracted from the charge of the first pulse. This will give the charge corresponding to the oxidation of Fc moieties. To reach the complete removal of the Fc moieties from the surface pulse experiment were performed with different pulse time.

It was found that 20 seconds pulse experiment were long enough to remove the Fc moieties from the surface. The feedback current curve is lower at the beginning and after 20 seconds it

meets with the second curve, which is shown in Fig 8.7. The reason for high feedback current at the beginning is due to the oxidation of the Fc moieties and decrease with the time due to the removal Fc moieties after oxidation.

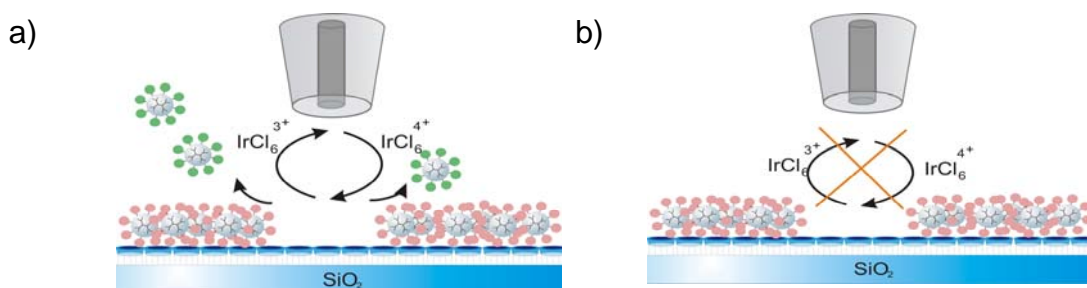


Fig. 8.6: Schematic for the local oxidation of Fc dendrimers, part (a) 1st pulse, part (b) 2nd pulse.

A third pulse experiment was done in order to check Fc dendrimers were still removed in the second pulse. The feedback current of the second and third pulse are very similar due to the complete removal of Fc dendrimer during the first pulse confirming the results shown in Chapter 8.2.

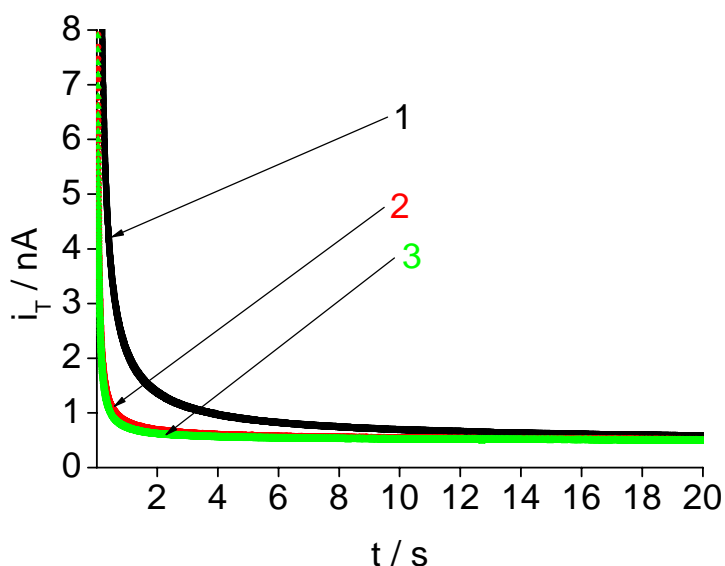


Fig. 8.7: Chronoamperometric pulse experiment performed at G3 Fc dendrimer-modified surface, (1) first pulse, (2) second pulse, (3) third pulse. All the pulses are performed at the same place. Pt UME positioned at 15 μm from the surface for each pulse experiment.

8.4 Pulse experiment comparison at SiO₂ and Fc dendrimers covered surface

In order to estimate the surface coverage of different generation of dendrimers at SiO₂, chronoamperometry pulse experiments were performed close to bare glass surfaces and close to surfaces covered with Fc dendrimers. The initial feedback current is higher over the Fc-covered surface due to the oxidation of Fc moieties which contributes to the current measured at UME (Fig. 8.8 curve 1). The feedback current decreases with the time due to the removal of Fc moieties from the current over a reference surface from glass. The current over the reference surface glass is lower for short times (Fig. 8.8, curve 2). For long time both curve converge to the same steady-state value, because after complete removal of the Fc units around the UME both surfaces are equivalent. The response over glass is almost identical to the second pulse over an Fc-covered area, when the Fc-dendrimers were completely removed in the first pulse (Fig. 8.7). This proves the interpretation put forward in sections 8.2 to 8.3.

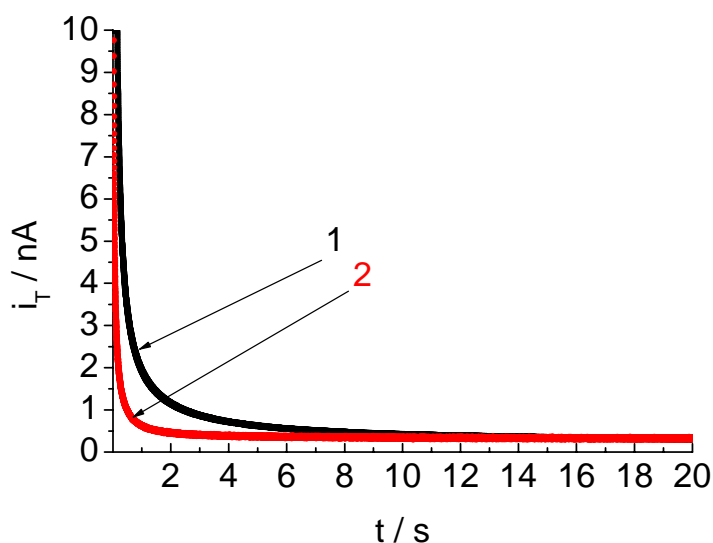


Fig. 8.8: Comparison of chronoamperometric pulse experiment, (1) G3 Fc dendrimer-modified covered surface, (2) glass surface. Pt UME positioned at 15 μ m from the surface for both experiment.

8.5 SECM imaging of spots made on SiO₂ surfaces covered with redox active dendrimers by etching

In order to find out the surface coverage of Fc dendrimers at SiO₂ for different generation of dendrimers, pulse experiment were performed at surfaces covered with different generation of

dendrimers at similar distances and pulse times. When chronoamperometric pulse experiments were carried out, it was found that G5 has a higher feedback current than the G4 and G3 respectively which is shown in Fig 8.9. This is due to the higher number of Fc end groups at higher generation of dendrimers, which contributes to the feedback current measured at the UME under the similar conditions. The charges converted can be used for the estimation of the surface concentration of the dendrimers if the modified spot area and the numbers of Fc units per dendrimers are known.

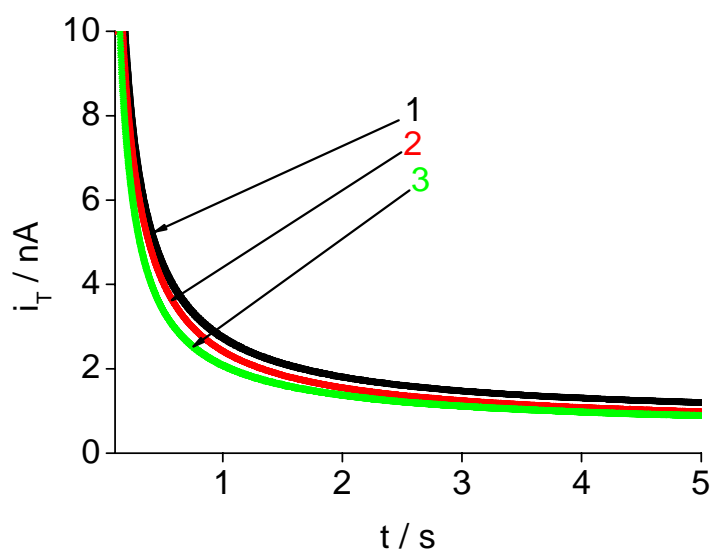


Fig. 8.9: Chronoamperometric pulse experiment comparison of different generation of dendrimers, (1) G5 Fc dendrimer-modified surface, (2) G4 Fc dendrimer-modified surface, (3) G3 Fc dendrimer-modified surface. Pt UME positioned at 15 μm from the surface for each experiment.

Patterns in the Fc-dendrimer coating on SiO_2 were obtained by locally removing the guest molecules by UME-generated $[\text{IrCl}_6]^{2-}$. The spots were obtained by etching the Fc-covered surface for 10 seconds from a distance of 15 μm with a lateral spot to spot distance of 100 μm . The modified spots were characterized by SECM in order to find out the area of the spots

The two-dimensional images were obtained by scanning the surface in aqueous solutions containing $[\text{IrCl}_6]^{3-}$ as a mediator in the positive feedback mode similar to the experiments in Chapter 7. The UME potential E_T was kept at 0.75 V well above the formal potential of $[\text{IrCl}_6]^{3-}/[\text{IrCl}_6]^{2-}$ redox mediator, such that $[\text{IrCl}_6]^{3-}$ is oxidized at the UME under diffusion-controlled conditions. The oxidized species $[\text{IrCl}_6]^{2-}$ diffuses to the surface and may accept an electron from Fc moieties of the dendrimers which have a lower E° . During this process Fc^+

dendrimers would be released and $[\text{IrCl}_6]^{3-}$ regenerated. Subsequently, $[\text{IrCl}_6]^{3-}$ may diffuse back to the UME giving rise to positive feedback current. At spots where Fc-dendrimers have already been removed $[\text{IrCl}_6]^{2-}$ can not be reduced, since no dendrimers are present, resulting in an UME current i_T that can be described by pure hindered diffusion of $[\text{IrCl}_6]^{3-}$ from the solution bulk to the UME. The redox processes that occur are outlined in Fig. 8.10.

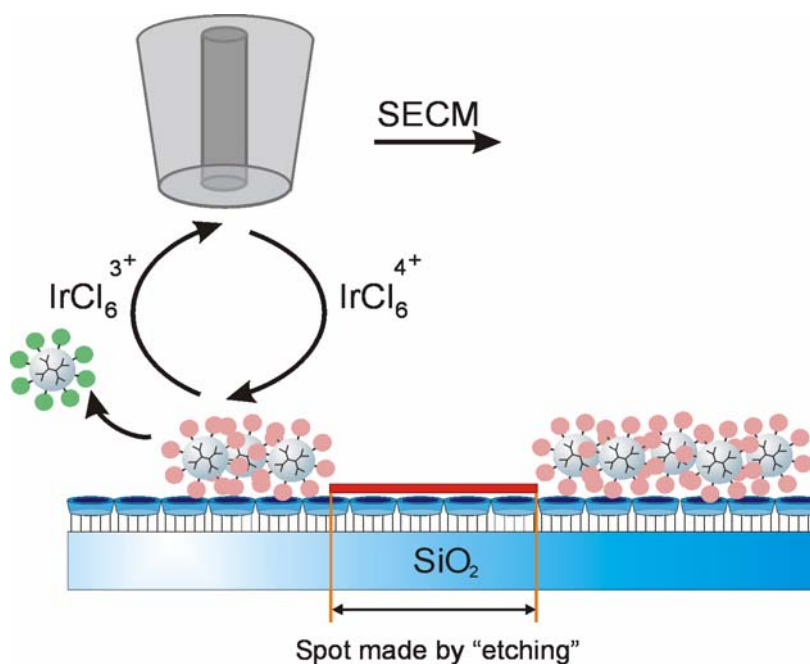


Fig. 8.10: A schematic depiction of SECM imaging, $[\text{IrCl}_6]^{3-}$ is oxidized at the UME and diffuses to the molecular printboard where it oxidizes the Fc dendrimer-covered surface. No oxidation of Fc dendrimers occurs where the spots are present giving rise to a negative feedback current at the UME.

A SECM image is shown Fig 8.11. The image clearly shows circular dots, which appear with a lower feedback current, compared to the background where the surface is covered with Fc-dendrimers. The periodicity was determined from the profile of the image indicated by the white line and the corresponding line scan is also shown in Fig 8.12. The observed periodicity of $100\ \mu\text{m}$ corresponds exactly to the spot to spot distance, with which, they were generated by etching the surface. The spots appear to be bigger than the electrode diameter ($2r_T = 25\ \mu\text{m}$). The reason for this can be explained by considering that, during the SECM imaging, the Fc dendrimers close to the spot area were also removed by making the spots bigger than the spots originally made during the etching experiment as shown in the Fig 8.13. The peak intensities of the line scan are not uniform probably due to non-uniform etching. This can be due to the slight tilt of the sample and resulting variation of distance between UME and

surface since each time the surface was approached by UME by monitoring the O_2 steady state reduction current.

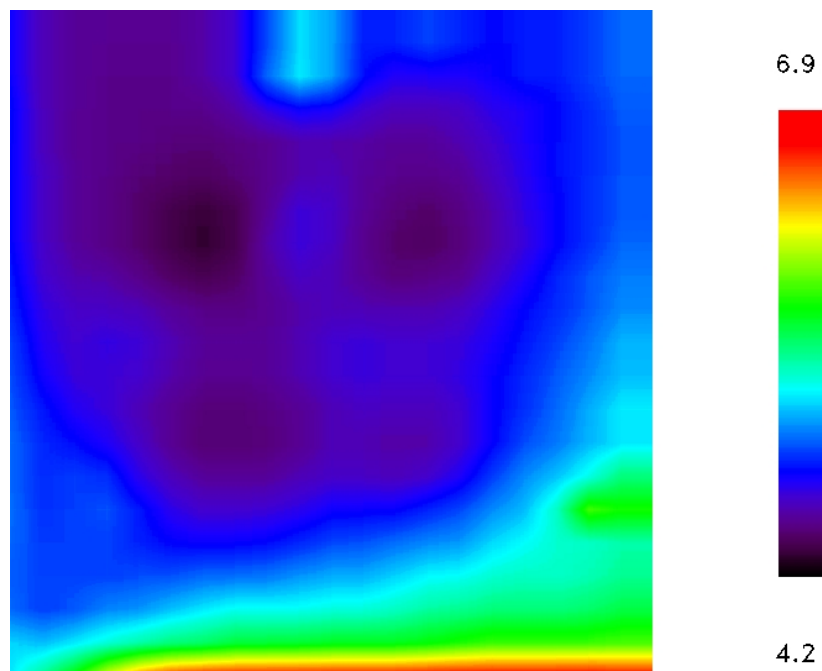


Fig. 8.11: SECM image of the etched spots made during local desorption of Fc dendrimers (pulse time 10 s) from a SiO_2 surface. SECM image was obtained over a scan area $350 \mu m \times 300 \mu m$, $E_T = 0.75 V$, $v_T = 200 \mu m s^{-1}$, $0.1 mM [IrCl_6]^{3-}$.

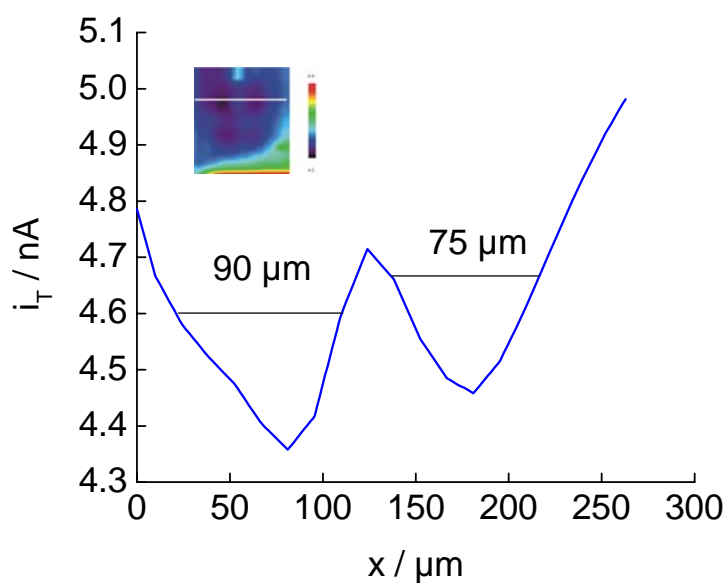


Fig. 8.12: Line scan (right) obtained from the profile of the image (left) indicated by the white line in the image showing the periodicity of the printed features. Conditions are the same as in Fig. 8.11.

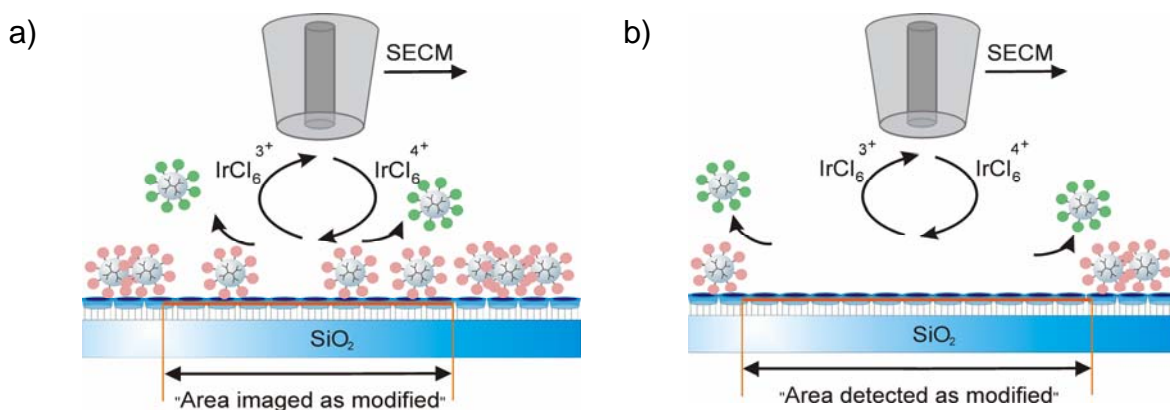


Fig. 8.13: SECM image of the etched spots made during the local desorption of Fc dendrimers from SiO₂ surface by chronoamperometric pulse, (a) area imaged as modified, (b) area detected as modified.

8.6 SECM line scans of the etching spots made by different pulse time.

After imaging the etched spots with SECM, the size of the modified spots was known. In order to find out the surface concentration of dendrimers on SiO₂ surfaces, it is important to know the area of the etched spot. The SECM line scan of the etched spots made with different pulse time is shown in Fig. 8.14. A comparison of the spot size (measured at full width at half maximum (FWHM)) shows a diameter of 150 μm (Fig. 8.14, spot A and D). This is larger than the spots for shorter pulse time (5 s, FWHM = 80 μm, spot B; 2 s, FWHM = 50 μm, spot C).

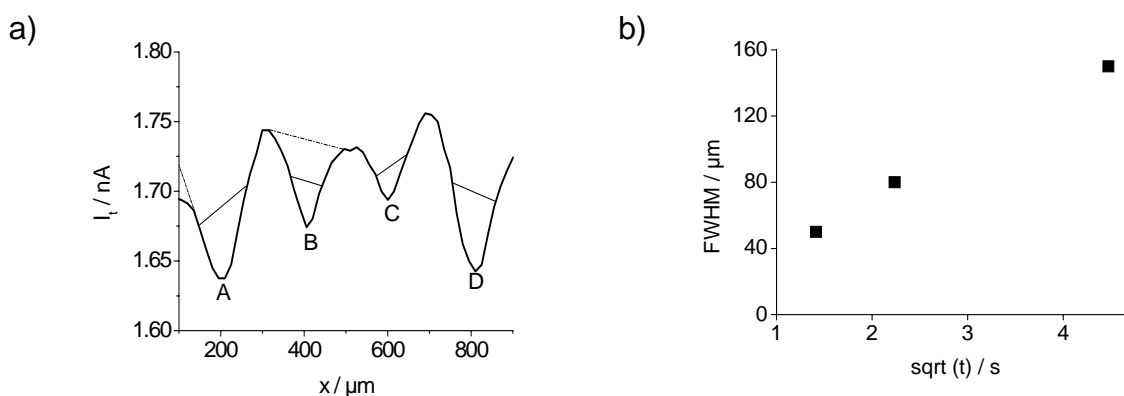


Fig. 8.14: SECM line scan of the etched spots made during pulse experiment, (a) pulse time A = 20 s, B = 5 s, C = 2 s, D = 20 s, (b) linear dependency of FWHM with square root of pulse time.

Four different factors are responsible for the shape and size of the etched spot; namely, the distance of the UME from the surface during the modification pulse, the ratio of the radii of

the insulating sheath and the UME, the diameter of the UME, and the electrolysis time. Since the same UME was used to make spots on the surface, the first three factors cannot be considered for the comparison between the spots, the last and the important factor for the consideration is the electrolysis time.

Since the oxidized mediator is generated at the UME and diffuses to the surface, it is expected that the electrolysis time, *i.e.*, the time during which a potential is applied to the UME, will determine the diffusion range and thus affect the size of the pattern formed. However, such behavior should be anticipated only when a fast electron transfers occurs between the mediator and the species at the surface. Fig. 8.13a shows the dependence of the etched spot radii on the electrolysis time. The spot grew constantly as a function of time as can be seen in the Fig 8.13a for 2 s, 5 s and 20 s pulse time. The spots are reproducible with the same size when further experiments were done at different places with the same pulse time. From Fig. 8.14b, it can be seen that even for very short time a spot size is obtained that is slightly larger than the diameter of the UME used for the pulse experiment. This is due to an almost perpendicular diffusive transport of the oxidant to the dendrimers-covered surface during the initial phases of the pulse. The concentration gradient of the oxidant is maintained as long as there are enough Fc-dendrimers at the substrate surface below the active area of UME. Once the Fc-dendrimers directly below the UME are depleted the UME-generated oxidant diffuses horizontally along the substrate surface until it is consumed by reaction with Fc-dendrimers. This leads to a growth of the spots beyond the size of the active area of the UME. During this time the spots grow with a different rate. This time window is covered by the data in Fig. 8.14b. The radii of the spots formed within the UME limits depend on the square root of time Fig 8.13b, as is expected for a diffusion-controlled process. The diffusion distance, δ , is given by Eq. 8.1, where D is the diffusion coefficient and the t represents the electrolysis time.

$$\delta \cong \sqrt{2Dt} \quad (8.1)$$

However, the radii of the spots depend on the square root of time, only if the electrode-surface distance is smaller than the spot size distance. This condition was maintained in all our experiment. If δ extends beyond the insulating sheath of the UME, the growth of the spot is expected to stop, because the oxidant dilutes quickly into the solution bulk.

8.7 Determination of surface coverage for different generation dendrimers

After finding the spot area made by SECM during pulse experiments as a function of pulse time, the pulse chronoamperograms were integrated after background subtraction to calculate the total charge associated with the oxidation of Fc dendrimers which is shown in Fig 8.15. The surface concentration Γ of Fc units for different generations of dendrimer can be determined using the formula $\Gamma_{Fc} = Q/nF\pi r_s^2$, where Q = charge associated with the oxidation of Fc moieties, n = number of electrons per mole of reaction ($n = 1$), F = Faraday constant and r_s = radius of the affected spot.

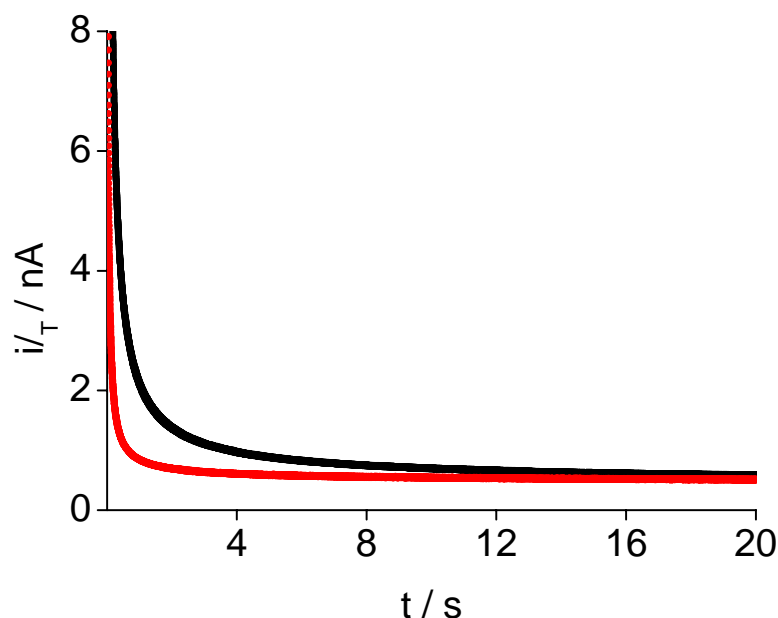


Fig. 8.15: Chronoamperometric pulse experiment at the same place, black curve first pulse, red curve second pulse. Pt UME positioned at 15 μm from the surface.

The surface concentration Γ for different generations of dendrimers from G3 to G5 was shown in the Table 8.1. with different pulse time.

Table 8.1: Calculation of surface concentration of different generation dendrimers by chronoamperometric pulse method

Fc-dendrimers	τ / s	Q / (10^{-9} As)	r_s / (10^{-4} cm) (FWHM) from SECM image	r_s / (10^{-4} cm) (diffusion length)	Γ / (10^{-10} mol cm $^{-2}$)	Γ / (10^{-10} mol cm $^{-2}$)
G3	2	5.31	60	61.44	4.87	4.64
G4	2	5.48	60	61.44	5.02	4.79
G5	2	6.19	60	61.44	5.67	5.41
G3	5	6.76	80	98.86	3.49	2.28
G4	5	7.44	80	98.86	3.84	2.51
G5	5	8.14	80	98.86	4.20	2.75
G3	20	9.95	140	199.45	1.68	0.825
G4	20	1.11	140	199.45	1.87	0.921
G5	20	1.12	140	199.45	1.89	0.929

Out of different pulse time, only the pulse for 20 s is considered for further surface coverage value and compared with values obtained for Au surface. It has been shown that in previous section for 2 s and 5 s pulse time, the complete removal of Fc moieties was not possible. Although a linear trend can be seen in surface coverage value for different generation of dendrimers for 2 s and 5 s as shown in the Table 8.1. The surface concentration for different generation of dendrimers were calculated by considering the formula $\Gamma_{Fc} = Q/nF\pi r_s^2$. The r_s represents the radii affected by the UME during the pulse experiment which is measured at full width half maximum (FWHM) from the SECM line scan and also from the diffusion length of the mediator.

The relative surface concentration $\Gamma_{\beta CD}/\Gamma_{Fc}$ provide the number P_b bound Fc molecule per dendrimers with the host surface, using $P_b = P_{tot} \Gamma_{\beta CD}/\Gamma_{Fc}$, where P_{tot} is the total number of end groups. Γ_{Fc} is linearly dependent on the end groups of the dendrimers as shown in the Fig. 8.14 for the results obtained for monolayers of dendrimers on β CD SAMs on Au. The $\Gamma_{\beta CD}$ value on SiO₂ surface is unknown, but the β CD monolayer is expected to be less ordered and might also be less densely packed compared to β CD SAMs on Au since the monolayer was prepared in a multiple covalent synthesis [266]. To compare Γ_{Fc} of both molecular

printboards, the obtained Γ_{Fc} values on SiO_2 by SECM were plotted against different generation of dendrimers and compared with the values obtained for Au surface (Fig 8.16).

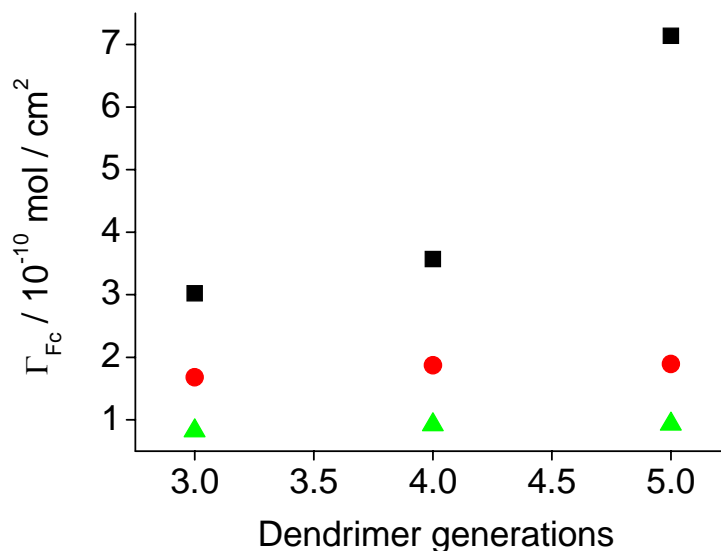


Fig. 8.16: Linear dependency of Γ_{Fc} measured at Au (■), SiO_2 (●) from FWHM and SiO_2 (▲) from diffusion length of the mediator.

Surface concentration for Fc-dendrimers at SiO_2 were calculated by considering the two different radius of the affected area during the etching process. The difference between these two measurements is not so significant. Surface concentration measured for diffusion length of the mediator affected radius is merely double from the surface concentration measured from FWHM affected area measured from SECM imaging. But when compared to Au surface, a significant difference between the Γ_{Fc} values obtained for the monolayers of dendrimers on SiO_2 and on Au can be observed. The Γ_{Fc} values for G5 dendrimers approximately four times as large on Au compared to SiO_2 for 20 s pulse time. The values for G3 and G4 dendrimers are more or less similar to each other. The greater values G5 dendrimers imply the P_b values on Au are roughly half of that on SiO_2 surfaces. Apparently, the β CDs monolayers on SiO_2 are less densely packed, thus resulting in a decrease of Γ_{Fc} values. At SiO_2 surfaces the monolayers are disordered since the β CDs are bound to the surface via covalent bonds. However, the β CDs still can react with the surface resulting the tilted conformations and thus in higher $\Gamma_{\beta\text{CD}}$ values[260]. The approach to determine Γ_{Fc} is an

qualitative treatment here, since the redox process occurs at the extreme end of the etched spot could not be mapped by UME.

The Γ_{Fc} values obtained at SiO_2 for 2 s and 5 s pulses is comparable to the Γ_{Fc} at Au surface. However, it is shown that the complete desorption of Fc-dendrimers was not obtained during 2 s and 5 s pulse time. So a clear cut conclusion would be difficult to obtain at this point.

8.8 Electrochemical reduction of cytochrome c on top of streptavidin layers at the molecular printboard

Pulse experiments were further explored to determine the surface concentration of cyt *c* on top of the streptavidin layers on molecular printboards based on the approach for Fc-dendrimers functionalised surface. The samples were obtained in collaboration with Manon et al. from University of Twente.

The general idea of the experiment is outlined in Fig. 8.17. The carbon fiber UME generates a reductant that converts oxidised bt-cyt to reduced bt-cyt. By estimation of the charge transferred to the cyt *c* units at the surface, the surface concentration of the dendrimers should be accessible similar to the approach described in Chapter 8.7. The attachment of electro-active proteins at surfaces has resulted in the characterization of several enzymes, and the development of sensing devices based on these proteins. Cytochrome *c* (cyt *c*) is a small (12.2 kDa) redox protein with one heme centre, that has been studied extensively [267, 268]. The redox potentials of the different class (I) cyt *c* vary between +200 and +350 mV (*vs.* SHE) [268-270]. Heme, which is the iron complex of protoporphyrin IX, is a rigid and planar molecule, having four pyrrole groups which are linked by methylene bridges to form a tetrapyrrole ring. The heme group in cyt *c* is covalently bound to the polypeptide chain. An important function of cyt *c* is the electron transfer between cytochrome *c* reductase and cytochrome *c* oxidase. The adsorption of cyt *c* to SAMs has been studied before [271-273]. Frago *et al.* for instance have described the surface immobilization of cyt *c* to β -cyclodextrins (β CD) SAMs on Ag via adamantyl moieties incorporated in the protein.

In order to perform this experiment carbon fiber UME were chosen over the conventional UME such as Pt and Au UME. The reason is formal potential of the redox couple $[\text{Ru}(\text{NH}_3)_6]^{3+/2+}$ were interfering with the reduction potential O_2 at a Pt or a Au UME

which contributes to the feedback current measured during the pulse experiment. The reduction process could be avoided at a carbon fiber UME since reduction potential of O_2 shifts to a negative potential. By using carbon fiber UME, the redox process of $[Ru(NH_3)_6]^{3+/2+}$ is only allowed at the UME and confirming the feedback current only due to $[Ru(NH_3)_6]^{3+/2+}$ redox couple.

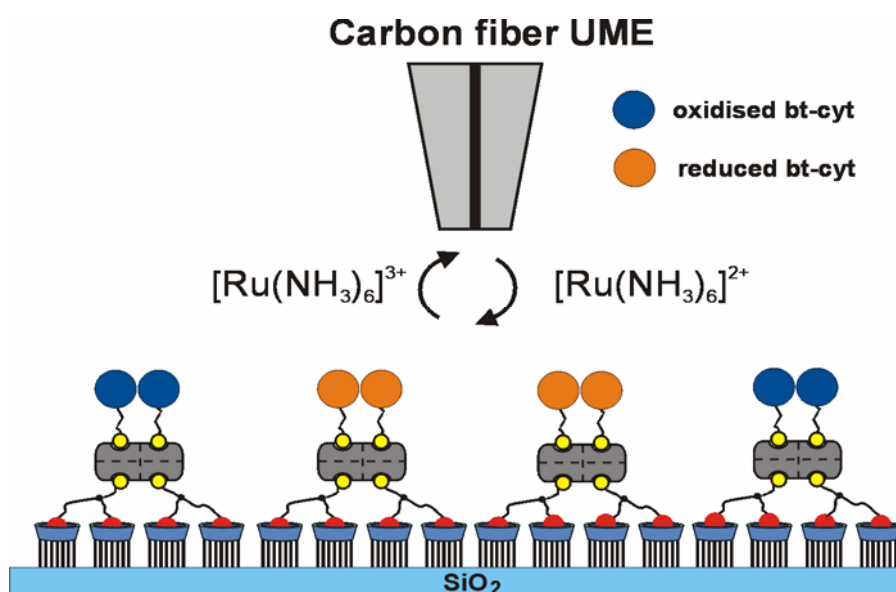


Fig. 8.17: a) Schematics of the SECM experiment. $[Ru(NH_3)_6]^{3+}$ is reduced at the UME and diffuses to the molecular printboard where it reduces (oxidized) bt-cyt c. Thereafter, $[Ru(NH_3)_6]^{2+}$ diffuses back to the UME, which results in a negative feedback current. b) Redox reactions taking place at the UME and at the surface.

In order to reduce bt-cyt at the surface, the UME was positioned in a distance d of $10\ \mu\text{m}$ from the surface and a potential pulse of $E_T = -0.35\ \text{V}$ was applied to the UME in order to reduce the mediator $[Ru(NH_3)_6]^{3+}$. Chronoamperograms of the UME current were recorded during the pulse.

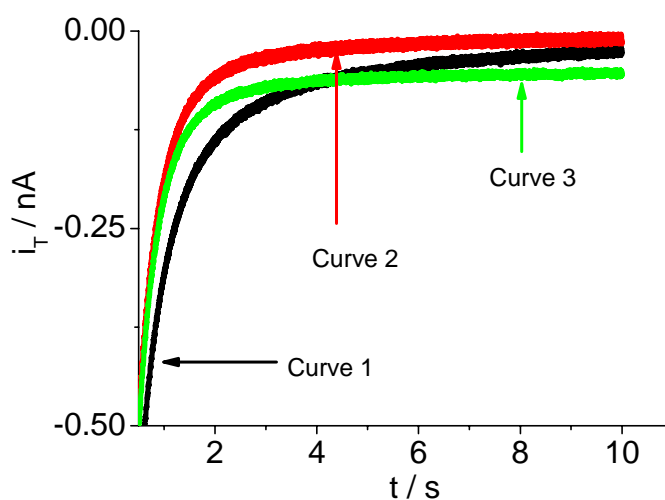


Fig. 8.18: SECM amperograms in which pulse times are in each case 10 s; (curve 1) first pulse 10 μm from the surface, (curve 2) second pulse 10 μm from the surface, (curve 3) third pulse 300 μm from the surface.

This sequence was repeated multiple times at the same location and at different distances from the surface while the horizontal position was not changed (Fig. 8.18). First, a 10 s pulse was applied to the UME positioned 10 μm above the surface (Fig. 8.18, curve 1). The pulse was repeated at the same location (Fig. 8.18, curve 2). For reference purposes, another pulse experiment was performed far away from any surface (Fig. 8.18, curve 3). Almost all cyt *c* is reduced within the first pulse of about 10 s by a bimolecular electron transfer reaction between $[\text{Ru}(\text{NH}_3)_6]^{2+}$ and oxidized cyt *c* (Fig. 8.18, curve 1). During this reaction $[\text{Ru}(\text{NH}_3)_6]^{3+}$ is regenerated. After diffusion to the UME, it enhances the UME current compared to the same pulse experiment above an inert sample at which no reaction of the mediator is possible. However, the bimolecular reaction can only be sustained as long as oxidized cyt *c* is available at the surface. Therefore, a second pulse at the same location produces much lower currents (Fig. 8.18, curve 2). This chronoamperogram is identical to one obtained at the same distance above an bare glass sample. It can be considered as a background signal. For times < 0.1 s it results from double layer charging currents and for longer times it is controlled by the hindered diffusion of $[\text{Ru}(\text{NH}_3)_6]^{3+}$ from the solution bulk through the gap between UME and sample to the active UME area. Curve 1 and curve 2 merge at around 10 s indicating the time when the oxidized cyt *c* is exhausted during the first pulse. The current resulting from hindered diffusion (Fig. 8.18, curve 2) depends on the distance between the UME and its insulating sheaths to the sample. If the working distance is

enlarged (Fig. 8.18, curve 3), the diffusion is less effectively hindered and the currents are larger than in Fig. 8.18, curve 2. However, for $t < 4$ s, the currents during the first pulse at 10 μm distance (Fig. 8.18, curve 1) are larger than the currents at large distances (Fig. 8.18, curve 3). This is a clear proof that the enhancement of the UME currents in curve 1 is a result of the chemical mediator recycling at the substrate surface. The electrical charge Q used to convert the cyt c at the surface was obtained by integrating the current difference between the first and the second pulse at $d = 10$ μm (curve 1 minus curve 2).

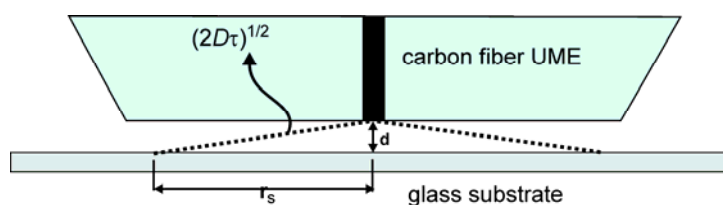


Fig.8.19: Estimation of the radius of the modified sample region by the diffusion of the UME-generated $[\text{Ru}(\text{NH}_3)_6]^{2+}$.

Table 8.2: Calculation of the surface concentration of cyt c from five independent SECM pulse experiments; for all experiment $r_T = 3.5 \times 10^{-4}$ cm, $d = 10 \times 10^{-4}$ cm, $D = 7.4 \times 10^{-6}$ cm² s⁻¹.

τ / s	$Q / (10^{-9} \text{ As})$	$r_s / (10^{-4} \text{ cm})$	$\Gamma / (10^{-11} \text{ mol cm}^{-2})$
5	0.402	85.44	1.82
10	0.707	121.2	1.59
10	1.23	121.2	2.76
10	1.05	121.2	2.36
20	2.04	171.7	2.28

The radius r_s of the sample region that is affected by the oxidation can be approximated by considering the average diffusion length of the $[\text{Ru}(\text{NH}_3)_6]^{2+}$ generated at the UME (Fig. 8.19). With the known diffusion coefficient of $D = 7.4 \times 10^{-6}$ cm² s⁻¹ [274]. The average diffusion length within the pulse time τ is $(2D\tau)^{1/2}$ and the modified radius at the sample is

$$r_s = (2D\tau - d^2)^{1/2} \quad (8.2)$$

From r_s the modified area can be estimated as $A = \pi r_s^2$. From Q , r_s and the number $n = 1$ of transferred electrons per cyt c molecule and the Faraday constant F , the surface coverage Γ is obtained.

$$\Gamma = Q / (n F \pi r_s^2) \quad (8.3)$$

The estimation according to Eq. (8.2) and (8.3) leads to a value of $\Gamma = (2.2 \pm 0.5) \times 10^{-11}$ mol cm⁻² (Table 8.2). This value compare well with the surface concentration determined by UV/Vis. This confirms that all or most all of the cyt *c* units are electrochemically functional and accessible when immobilized according to this assembly scheme.

Summary

In this thesis, monolayers of organic molecules were prepared at different substrate. The interaction of metal ions and monolayers were studied with different electrochemical and surface characterisation technique. Two experimental principles constitute a unifying concept across these systems: 1) preparation of functional surfaces from SAMs of different alkanethiols, 2) generation of defined and local flux of different redox species by an UME close to the functionalized surface. SECM DPSC has been shown to be a powerful technique for investigating the chemical kinetics of UME-generated species at solid/liquid interfaces. The technique complements earlier equilibrium perturbation transient SECM methods by allowing the study of irreversible interfacial chemical processes. The work also demonstrates the use of SECM as an imaging tool for functionalised surfaces as well as a tool for surface modification. SECM was also used to determine quantitatively the surface concentration of functional molecules at solid-liquid interfaces.

In order to study the interaction of different metal ions with organic monolayers at surfaces, different model systems were considered for this purpose. Monolayers of 1-nonanethiol and 1,9-nonanedithiol were formed at gold substrate. Further monolayer systems were explored in supramolecular system where molecular printboards were prepared from β CD. Two systems were investigated: 1) ferrocene-terminated poly (propylenimine) dendrimers, 2) biotinylated cytochrome *c* as guest molecules.

For the generation of controlled ion flux, UME of Ag and Cd were developed (Chapter 4). Electrochemical deposition of Cd has been used to fill out a etched Ag UME to produce well defined Cd microelectrode. The UMEs were characterised electrochemically where the electrode was anodically dissolved in solution. The shape and size of the electrode were characterized by optical microscope which proved the electrodes had a good shape and the metal part of the electrode was well centered. The new method of preparing Cd UMEs opens up new way to prepare metal electrodes for SECM which are difficult to produce by sealing metal wires.

The monolayers on gold substrate electrodes were characterised by CVs. The CVs revealed the blocking effect of thiols and dithiols modified electrode. The gold substrate were characterised by contact angle and PM FTIRRAS techniques (Chapter 5). The highly organisation of nonanethiol and 1,9-nonanedithiol on gold substrates were proved by PM

FTIRRAS. It also showed the presence of S-H stretching band which proved the presence of terminal SH group to be standing upward rather than laying on the surface. Although it would be difficult to comment if all the terminal groups stand upward.

The interaction of cadmium ions with thiol and dithiol monolayer surface were characterised by CV and XPS. The CV reveals the two stripping peaks indicative of some interaction of Cd with dithiol monolayers which are absent on a bare gold electrode. The monolayers of dithiols were used to sense Cd^{2+} from the solution and 2×10^{-6} M was detected by LSV. Depositions of cadmium onto the dithiol-modified surface were followed by XPS. The results from XPS measurement are at a preliminary stage. It is difficult to conclude the nature of the 1,9-nonanedithiol-modified surface during the deposition and dissolution of Cd from the surface. Further experiments need to be done in order to obtain a more detailed picture of the deposition and dissolution of Cd surface both as a bulk deposition and Cd deposition at UPD conditions. In particular the signal-noise ratio of the spectra and the spectral resolution must be enhanced to get more detailed information of the S and Cd binding states. Quantitative evaluation of the signal intensities requires a model of the surface structure (homogeneous layers, island growth).

The deposition of Ag metal was performed at bare gold and thiol-modified gold substrates (Chapter 6). The deposition of Ag on bare gold leaves a clear structure of the Ag on gold. The deposition of Ag can be controlled by applying different potential to the gold substrate. When the potential of the gold substrate was maintained at -200 mV, rapid growth of Ag by galvanic deposition on gold substrate is observed in SPSC chronoamperograms. Contrary, the growth of Ag on gold is steady and uniform when the potential of gold was maintained at 600 mV (UPD region). Only one or two monolayers of Ag could be grown at this substrate potential. The deposition of Ag is also followed in a DPSC experiment where a clear difference can be seen in chronoamperograms recorded at different substrate potentials. The higher collection efficiency from the DPSC at $E_s = 600$ mV suggests the collection of Ag^+ back to the UME. This proves that the adsorption of Ag^+ is limited to one or a few monolayers on gold although the experimental curves from DPSC and collection efficiency are only qualitative in nature at this stage. The deposition of Ag onto a modified electrode does not produce a clear pattern which suggests the insulation of the gold substrate from the monolayers of thiols and dithiols. Further work is needed to clarify the nature of the

accompanying anodic process and to understand how the structure of the surface affects the density of silver particles formed.

In addition to generating reactants from solution precursor species, as in the studies in this thesis, it should be possible to locally inject several types of metal ions, e.g., Cu^{2+} , Zn^{2+} , Pb^{2+} , etc., into the gap between the probe and the interface through the anodic dissolution of metal or mercury amalgam UMEs.

Some of the principles observed during the reaction between SAM-modified surfaces and dissolved ions can also be found in supramolecular layers on electrode surfaces. An very interesting example are "molecular printboards" based on β CDs to which redox-active guest molecules can be bind. Such electrodes were prepared at the University of Twente and characterized by SECM in this work. The systems offer even some advantages because the complexity of the surface binding of the guest is reduced. The interaction occurs by non-covalent host-guest interaction. The bound redox-active guest can be oxidized or reduced by species generated at the UME. This allows to investigate the surface redox chemistry of adsorbed guest molecules even on insulating surfaces.

In particular the electrochemical desorption of Fc-dendrimers from a microscaled patterned layer of a molecular printboards at an insulating SiO_2 surface were obtained by scanning the surface using SECM (Chapter 7). The image was obtained in feedback mode. The hexagonal patterns of Fc-dendrimers layers were successfully obtained. The periodicity of the pattern was determined to be $80\ \mu\text{m}$ which corresponds to the way the samples were prepared and it agrees well with the scanning force microscopic measurement. Repeated images at the same place reveals upon oxidation Fc-dendrimers leaves the surface and diffusion to the solution. In order to obtain the image a high scan speed was maintained ($200\ \mu\text{m}\ \text{s}^{-1}$) with higher step size ($15\ \mu\text{m}$) in both the axis. The speed was optimised over several experiments in order to obtain the image.

In order to find the surface concentration of functional molecules at molecular printboards, SPSC experiments were performed. For Fc-dendrimers, pulse experiments were performed over different pulse time for 2 s, 5 s, 20 s. It was found that for 20 s pulse time, the complete removal of Fc-dendrimers from the surface was observed. The second pulse was done at the same place in order to subtract the background current from the first pulse. The surface concentration of the Fc-dendrimers on molecular printboards was found to be less than that of

molecular printboards on Au surfaces. This is due to the inability of the UME to collect back all the generated redox mediator converted at the monolayer. The etched spot obtained due to the removal of Fc-dendrimers from the surface were successfully imaged by SECM. In another system, the surface concentration of biotinylated cytochrome *c* bound via streptavidin and a bifunctional linker on molecular printboards at SiO₂ were determined in a similar way. The surface concentration value found to be matched exactly as measured by UV/Vis spectrometry.

There is considerable scope for further applying the DPSC mode. For example, to complement the systems in this thesis, there is a option to investigate the adsorption and desorption processes of Fc-terminated dendrimers by UME-generated species using the DPSC mode. SECM can electrochemically induce the desorption of Fc dendrimers from a molecular printboard at SiO₂. The combination of supramolecular and electrochemical control of dendrimer adsorption is a promising tool in the integration of “bottom-up” (self-assembly) and “top-down” (scanning probe and microcontact printing) nanofabrication schemes. In this work local desorption has been induced by flux of redox active molecules formed at an UME. Continuation along this line using smaller conductive AFM tips may give smaller template patterns exposing the molecular printboard to which other guest molecules may bind.

Both SECM-SPSC and SECM-DPSC techniques have been shown to be a powerful techniques for monitoring the uptake of Ag⁺ by gold surface and gold surfaces modified with alkanethiols. The current–time response for the anodic oxidation of a reversible Ag/Ag⁺ electrode has been shown to be diagnostic of the nature of the uptake process, with Ag⁺ adsorption readily being distinguished from Ag nucleation and growth processes. There is a huge scope for developing this approach for examining adsorption, ion exchange and nucleation/growth processes on foreign surfaces. The approach is particular attractive for surfaces that cannot be externally contacted and therefore cannot be used as the measuring electrode by themselves.

References

- [1] D. J. Ahn, E. I. Franses, *J. Chem. Phys.* **1991**, *95*, 8486.
- [2] S. Flink, F. C. J. M. van Veggel, D. N. Reinhoudt, *Adv. Mater.* **2000**, *12*, 1315.
- [3] S. Bettarini, F. Bonosi, G. Gabrielli, G. Martini, M. Puggelli, *Thin Solid Films* **1992**, *210-211*, 42.
- [4] R. J. Nichols, D. Schroer, H. Meyer, *Scanning* **1993**, *15*, 266.
- [5] D. L. Allara, R. G. Nuzzo, *Langmuir* **1985**, *1*, 45.
- [6] H.-J. Schneider, A. K. Yatsimirsky, *Principles and Methods in Supramolecular Chemistry*, Wiley, Chichester, **2000**.
- [7] P. L. Boulas, M. Gomez-Kaifer, L. Echegoyen, *Angew. Chem. Int. Ed.* **1998**, *37*, 216.
- [8] G. Cooke, *Angew. Chem. Int. Ed.* **2003**, *42*, 4860.
- [9] M. J. W. Ludden, D. N. Reinhoudt, J. Huskens, *Chem. Soc. Rev.* **2006**, *35*, 1122.
- [10] A. W. Adamson, A. P. Gast, Editors, *Physical Chemistry of Surfaces, Sixth Edition*, Wiley, New York, **1997**.
- [11] G. E. Poirier, E. D. Pylant, *Science* **1996**, *272*, 1145.
- [12] R. G. Nuzzo, D. L. Allara, *J. Am. Chem. Soc.* **1983**, *105*, 4481.
- [13] M. D. Porter, T. B. Bright, D. L. Allara, C. E. D. Chidsey, *J. Am. Chem. Soc.* **1987**, *109*, 3559.
- [14] L. H. Dubois, R. G. Nuzzo, *Annu. Rev. Phys. Chem.* **1992**, *43*, 437.
- [15] C. D. Bain, J. Evall, G. M. Whitesides, *J. Am. Chem. Soc.* **1989**, *111*, 7155.
- [16] C. D. Bain, G. M. Whitesides, *Science* **1988**, *240*, 62.
- [17] H. A. Biebuyck, C. D. Bain, G. M. Whitesides, *Langmuir* **1994**, *10*, 1825.
- [18] P. E. Laibinis, G. M. Whitesides, D. L. Allara, Y. T. Tao, A. N. Parikh, R. G. Nuzzo, *J. Am. Chem. Soc.* **1991**, *113*, 7152.
- [19] L. H. Dubois, B. R. Zegarski, R. G. Nuzzo, *J. Chem. Phys.* **1993**, *98*, 678.
- [20] M. M. Walczak, C. Chung, S. M. Stole, C. A. Widrig, M. D. Porter, *J. Am. Chem. Soc.* **1991**, *113*, 2370.
- [21] P. Fenter, P. Eisenberger, J. Li, N. Camillone, III, S. Bernasek, G. Scoles, T. A. Ramanarayanan, K. S. Liang, *Langmuir* **1991**, *7*, 2013.
- [22] J. C. Love, D. B. Wolfe, R. Haasch, M. L. Chabinyc, K. E. Paul, G. M. Whitesides, R. G. Nuzzo, *J. Am. Chem. Soc.* **2003**, *125*, 2597.
- [23] A. Carvalho, M. Geissler, H. Schmid, B. Michel, E. Delamarche, *Langmuir* **2002**, *18*, 2406.
- [24] Z. Li, S.-C. Chang, R. S. Williams, *Langmuir* **2003**, *19*, 6744.
- [25] N. Muskal, I. Turyan, D. Mandler, *J. Electroanal. Chem.* **1996**, *409*, 131.
- [26] P. E. Laibinis, G. M. Whitesides, *J. Am. Chem. Soc.* **1992**, *114*, 1990.
- [27] T. Stora, R. Hovius, Z. Dienes, M. Pachoud, H. Vogel, *Langmuir* **1997**, *13*, 5211.
- [28] I. Rubinstein, S. Steinberg, Y. Tor, A. Shanzer, J. Sagiv, *Nature* **1988**, *332*, 426.
- [29] S. Steinberg, Y. Tor, E. Sabatani, I. Rubinstein, *J. Am. Chem. Soc.* **1991**, *113*, 5176.
- [30] D. Burshtain, D. Mandler, *J. Electroanal. Chem.* **2005**, *581*, 310.
- [31] H. Shen, J. E. Mark, C. J. Seliskar, H. B. Mark, Jr., W. R. Heineman, *J. Solid State Electrochem.* **1997**, *1*, 241.
- [32] T. Nagaoka, Z. Chen, H. Okuno, M. Nakayama, K. Ogura, *Anal. Sci.* **1999**, *15*, 857.
- [33] B. Zeng, X. Ding, F. Zhao, *Electroanalysis* **2002**, *14*, 651.
- [34] R. S. Freire, L. T. Kubota, *Electrochim. Acta* **2004**, *49*, 3795.
- [35] A.-C. Liu, D.-c. Chen, C.-C. Lin, H.-H. Chou, C.-h. Chen, *Anal. Chem.* **1999**, *71*, 1549.

- [36] W. Yang, J. J. Gooding, D. B. Hibbert, *J. Electroanal. Chem.* **2001**, 516, 10.
- [37] W. Yang, D. Jaramillo, J. J. Gooding, D. B. Hibbert, R. Zhang, G. D. Willett, K. J. Fisher, *Chem. Commun.* **2001**, 1982.
- [38] W. Yang, J. J. Gooding, D. B. Hibbert, *Analyst* **2001**, 126, 1573.
- [39] A. Profumo, D. Merli, M. Pesavento, *Anal. Chim. Acta* **2006**, 557, 45.
- [40] I. Turyan, D. Mandler, *Anal. Chem.* **1997**, 69, 894.
- [41] I. Turyan, D. Mandler, *Anal. Chem.* **1994**, 66, 58.
- [42] A. J. Moore, L. M. Goldenberg, M. R. Bryce, M. C. Petty, A. P. Monkman, C. Marengo, J. Yarwood, M. J. Joyce, S. N. Port, *Adv. Mater.* **1998**, 10, 395.
- [43] A. J. Moore, L. M. Goldenberg, M. R. Bryce, M. C. Petty, J. Moloney, J. A. K. Howard, M. J. Joyce, S. N. Port, *J. Org. Chem.* **2000**, 65, 8269.
- [44] T. K. Hansen, T. Joergensen, P. C. Stein, J. Becher, *J. Org. Chem.* **1992**, 57, 6403.
- [45] H. Liu, S. Liu, L. Echegoyen, *Chem. Commun.* **1999**, 1493.
- [46] S.-G. Liu, H. Liu, K. Bandyopadhyay, Z. Gao, L. Echegoyen, *J. Org. Chem.* **2000**, 65, 3292.
- [47] G. Trippe, M. Ocafrain, M. Besbes, V. Monroche, J. Lyskawa, F. Le Derf, M. Salle, J. Becher, B. Colonna, L. Echegoyen, *New J. Chem* **2002**, 26, 1320.
- [48] T. D. Chung, J. Park, J. Kim, H. Lim, M. J. Choi, J. R. Kim, S. K. Chang, H. Kim, *Anal. Chem.* **2001**, 73, 3975.
- [49] N. J. van der Veen, S. Flink, M. A. Deij, R. J. M. Egberink, F. C. J. M. van Veggel, D. N. Reinhoudt, *J. Am. Chem. Soc.* **2000**, 122, 6112.
- [50] M. Crego-Calama, D. N. Reinhoudt, *Adv. Mater.* **2001**, 13, 1171.
- [51] F. Lue, L. Gao, L. Ding, L. Jiang, Y. Fang, *Langmuir* **2006**, 22, 841.
- [52] E. Katz, I. Willner, *Electroanalysis* **2003**, 15, 913.
- [53] Y. Gafni, H. Weizman, J. Libman, A. Shanzer, I. Rubinstein, *Chem. Eur. J.* **1996**, 2, 759.
- [54] C. Henke, C. Steinem, A. Janshoff, G. Steffan, H. Luftmann, M. Sieber, H.-J. Galla, *Anal. Chem.* **1996**, 68, 3158.
- [55] H. O. Finklea, D. A. Snider, J. Fedyk, E. Sabatani, Y. Gafni, I. Rubinstein, *Langmuir* **1993**, 9, 3660.
- [56] S. Flink, B. A. Boukamp, A. van den Berg, F. C. J. M. van Veggel, D. N. Reinhoudt, *J. Am. Chem. Soc.* **1998**, 120, 4652.
- [57] S. Flink, F. C. J. M. Van Veggel, D. N. Reinhoudt, *J. Phys. Chem. B* **1999**, 103, 6515.
- [58] C.-Y. Chen, C.-T. Cheng, C.-W. Lai, P.-W. Wu, K.-C. Wu, P.-T. Chou, Y.-H. Chou, H.-T. Chiu, *Chem. Commun.* **2006**, 263.
- [59] K. Bandyopadhyay, H. Liu, S.-G. Liu, L. Echegoyen, *Chem. Commun.* **2000**, 141.
- [60] K. Bandyopadhyay, S.-G. Liu, H. Liu, L. Echegoyen, *Chem. Eur. J.* **2000**, 6, 4385.
- [61] R. A. Sachleben, A. Urvoas, J. C. Bryan, T. J. Haverlock, B. A. Moyer, B. P. Hay, *Chem. Commun.* **1999**, 1751.
- [62] S. Zhang, L. Echegoyen, *Tetrahedron Lett.* **2003**, 44, 9079.
- [63] S. Zhang, F. Song, L. Echegoyen, *Eur. J. Org. Chem.* **2004**, 2936.
- [64] S. Zhang, L. Echegoyen, *Org. Lett.* **2004**, 6, 791.
- [65] V. T. D'Souza, K. B. Lipkowitz, *Chem. Rev.* **1998**, 98, 1741.
- [66] R. Breslow, M. F. Czarniecki, J. Emert, H. Hamaguchi, *J. Am. Chem. Soc.* **1980**, 102, 762.
- [67] B. Siegel, R. Breslow, *J. Am. Chem. Soc.* **1975**, 97, 6869.
- [68] T. Matsue, D. H. Evans, T. Osa, N. Kobayashi, *J. Am. Chem. Soc.* **1985**, 107, 3411.

- [69] S. Shinkai, S. Mori, H. Koreishi, T. Tsubaki, O. Manabe, *J. Am. Chem. Soc.* **1986**, *108*, 2409.
- [70] R. Isnin, C. Salam, A. E. Kaifer, *J. Org. Chem.* **1991**, *56*, 35.
- [71] D. A. Tomalia, J. M. Frechet, Editors, *Special Issue: Dendrimers and Dendritic Polymers. [In: Prog. Polym. Sci.; 2005, 30(3-4)]*, **2005**.
- [72] M. W. P. L. Baars, E. W. Meijer, *Topics in Current Chemistry* **2000**, *210*, 131.
- [73] F. Vogtle, S. Gestermann, R. Hesse, H. Schwierz, B. Windisch, *Prog. Polym. Sci.* **2000**, *25*, 987.
- [74] I. Cuadrado, M. Moran, C. M. Casado, B. Alonso, J. Losada, *Coord. Chem. Rev.* **1999**, *193-195*, 395.
- [75] G. R. Newkome, E. He, C. N. Moorefield, *Chem. Rev.* **1999**, *99*, 1689.
- [76] A. Labande, D. Astruc, *Chem. Commun.* **2000**, 1007.
- [77] A. Labande, J. Ruiz, D. Astruc, *J. Am. Chem. Soc.* **2002**, *124*, 1782.
- [78] D. Astruc, J.-C. Blais, M.-C. Daniel, V. Martinez, S. Nlate, J. Ruiz, *Macromol. Symp.* **2003**, *196*, 1.
- [79] M. C. Daniel, J. Ruiz, S. Nlate, J. Palumbo, J. C. Blais, D. Astruc, *Chem. Commun.* **2001**, 2000.
- [80] D. Astruc, M.-C. Daniel, J. Ruiz, *Chem. Commun.* **2004**, 2637.
- [81] B. Alonso, M. Casado Carmen, I. Cuadrado, M. Moran, E. Kaifer Angel, *Chem. Commun.* **2002**, 1778.
- [82] I. Cuadrado, M. Moran, C. M. Casado, B. Alonso, F. Lobete, B. Garcia, M. Ibisate, J. Losada, *Organometallics* **1996**, *15*, 5278.
- [83] K. Takada, D. J. Diaz, H. D. Abruna, I. Cuadrado, C. Casado, B. Alonso, M. Moran, J. Losada, *J. Am. Chem. Soc.* **1997**, *119*, 10763.
- [84] R. Castro, I. Cuadrado, B. Alonso, C. M. Casado, M. Moran, A. E. Kaifer, *J. Am. Chem. Soc.* **1997**, *119*, 5760.
- [85] G. Binnig, H. Rohrer, *Helv. Phys. Acta* **1982**, *55*, 726.
- [86] G. Binnig, C. F. Quate, *Phys. Rev. Lett.* **1986**, *56*, 930.
- [87] E. H. Syngé, *Philos. Mag.* **1928**, *6*, 356.
- [88] A. J. Bard, F. R. F. Fan, D. T. Pierce, P. R. Unwin, D. O. Wipf, F. Zhou, *Science* **1991**, *254*, 68.
- [89] D. O. Wipf, A. J. Bard, *J. Electrochem. Soc.* **1991**, *138*, 4.
- [90] D. B. Murphy, *Fundamentals of Light Microscopy and Electronic Imaging*, Wiley, Chichester, **2001**.
- [91] R. Young, J. Ward, F. Scire, *Phys. Rev. Lett.* **1971**, *27*, 922.
- [92] S. H. Cohen, M. L. Lightbody, Editors, *Atomic Force Microscopy/Scanning Tunneling Microscopy 2. (Proceedings of the Second Symposium held 7-9 June 1994, at U.S. Army Soldier Systems Command, Natick Research, Development and Engineering Center, in Natick, Massachusetts.)*, **1997**.
- [93] P. A. Christensen, *Chem. Soc. Rev.* **1992**, *21*, 197.
- [94] O. M. Magnussen, W. Polewska, L. Zitzler, R. J. Behm, *Faraday Discuss.* **2002**, 43.
- [95] L. Zitzler, B. Gleich, O. M. Magnussen, R. J. Behm, *Proc. - Electrochem. Soc.* **2002**, *2000-30*, 49.
- [96] P. K. Hansma, J. P. Cleveland, M. Radmacher, D. A. Walters, P. E. Hillner, M. Bezanilla, M. Fritz, D. Vie, H. G. Hansma, et al., *Appl. Phys. Lett.* **1994**, *64*, 1738.
- [97] C. A. J. Putman, K. O. van der Werf, B. G. De Groot, N. F. Van Hulst, J. Greve, *Appl. Phys. Lett.* **1994**, *64*, 2454.
- [98] E. A. Ash, G. Nicholls, *Nature* **1972**, *237*, 510.

- [99] W. Denk, D. W. Pohl, *J. Vac. Sci. Technol., B* **1991**, 9, 510.
- [100] H. Aoki, S. Tanaka, S. Ito, M. Yamamoto, *Macromolecules* **2000**, 33, 9650.
- [101] H. Aoki, S. Ito, *J. Phys. Chem. B* **2001**, 105, 4558.
- [102] H. Aoki, Y. Kunai, S. Ito, H. Yamada, K. Matsushige, *Appl. Surf. Sci.* **2002**, 188, 534.
- [103] H. Aoki, S. Ito, *Thin Solid Films* **2004**, 449, 226.
- [104] A. J. Bard, F.-R. F. Fan, D. T. Pierce, P. R. Unwin, D. O. Wipf, F. Zhou, *Science* **1991**, 254, 68.
- [105] J. Kwak, A. J. Bard, *Anal. Chem.* **1989**, 61, 1794.
- [106] P. James, L. F. Garfias-Mesias, P. J. Moyer, W. H. Smyrl, *J. Electrochem. Soc.* **1998**, 145, 64.
- [107] M. Ludwig, C. Kranz, W. Schuhmann, H. E. Gaub, *Rev. Sci. Instrum.* **1995**, 66, 2857.
- [108] A. Hengstenberg, C. Kranz, W. Schuhmann, *Chem. Eur. J.* **2000**, 6, 1547.
- [109] A. J. Bard, M. V. Mirkin, Editors, *Scanning Electrochemical Microscopy*, Marcel Dekker, Basel, **2001**.
- [110] D. Mandler, S. Meltzer, I. Shohat, *Isr. J. Chem.* **1996**, 36, 73.
- [111] M. V. Mirkin, *Anal. Chem.* **1996**, 68, 177.
- [112] M. V. Mirkin, F.-R. F. Fan, A. J. Bard, *J. Electroanal. Chem.* **1992**, 328, 47.
- [113] J. V. Macpherson, P. R. Unwin, *J. Phys. Chem.* **1994**, 98, 1704.
- [114] J. V. Macpherson, P. R. Unwin, *J. Phys. Chem.* **1995**, 99, 3338.
- [115] J. V. Macpherson, P. R. Unwin, *J. Phys. Chem.* **1995**, 99, 14824.
- [116] J. V. Macpherson, P. R. Unwin, *J. Phys. Chem.* **1996**, 100, 19475.
- [117] J. V. Macpherson, P. R. Unwin, A. C. Hillier, A. J. Bard, *J. Am. Chem. Soc.* **1996**, 118, 6445.
- [118] J. V. Macpherson, P. R. Unwin, *J. Phys. Chem.* **1994**, 98, 11764.
- [119] P. R. Unwin, A. J. Bard, *J. Phys. Chem.* **1992**, 96, 5035.
- [120] C. J. Slevin, J. A. Umbers, J. H. Atherton, P. R. Unwin, *J. Chem. Soc. Faraday Trans.* **1996**, 92, 5177.
- [121] C. Demaille, P. R. Unwin, A. J. Bard, *J. Phys. Chem.* **1996**, 100, 14137.
- [122] C. J. Slevin, J. V. Macpherson, P. R. Unwin, *J. Phys. Chem. B* **1997**, 101, 10851.
- [123] A. L. Barker, J. V. Macpherson, C. J. Slevin, P. R. Unwin, *J. Phys. Chem. B* **1998**, 102, 1586.
- [124] R. D. Martin, P. R. Unwin, *Anal. Chem.* **1998**, 70, 276.
- [125] R. D. Martin, P. R. Unwin, *J. Chem. Soc. Faraday Trans.* **1998**, 94, 753.
- [126] A. L. Barker, P. R. Unwin, S. Amemiya, J. Zhou, A. J. Bard, *J. Phys. Chem. B* **1999**, 103, 7260.
- [127] R. L. Birke, Q. Huang, T. Spataru, D. K. Gosser, Jr., *J. Am. Chem. Soc.* **2006**, 128, 1922.
- [128] E. Ahlberg, O. Hammerich, V. D. Parker, *J. Am. Chem. Soc.* **1981**, 103, 844.
- [129] M. G. Kanatzidis, D. Coucouvanis, A. Simopoulos, A. Kostikas, V. Papaefthymiou, *J. Am. Chem. Soc.* **1985**, 107, 4925.
- [130] C. P. Andrieux, P. Hapiot, J. M. Saveant, *J. Am. Chem. Soc.* **1987**, 109, 3768.
- [131] J.-B. Raoof, R. Ojani, H. Beitollahi, R. Hosseinzadeh, *Anal. Sci.* **2006**, 22, 1213.
- [132] Y. Hishida, M. Nishi, Y. Baba, H. Ikeuchi, *Anal. Sci.* **2006**, 22, 931.
- [133] J. Galvez, *J. Electroanal. Chem.* **1996**, 413, 15.
- [134] J. Galvez, M. L. Alcaraz, Y. B. Shim, S. M. Park, *J. Electroanal. Chem.* **1992**, 341, 209.
- [135] J. Galvez, M. L. Alcaraz, Y. B. Shim, S. M. Park, *J. Electroanal. Chem.* **1992**, 341, 15.

- [136] W. Hyk, Z. Stojek, *Anal. Chem.* **1998**, *70*, 5237.
- [137] C.-Y. Li, L.-M. Huang, T.-C. Wen, A. Gopalan, *Solid State Ionics* **2006**, *177*, 795.
- [138] K. Kikuchi, Y. Tanaka, Y. Saihara, Z. Ogumi, *Electrochim. Acta* **2006**, *52*, 904.
- [139] K.-i. Kamei, T. Haruyama, M. Mie, Y. Yanagida, M. Aizawa, E. Kobatake, *Anal. Biochem.* **2003**, *320*, 75.
- [140] C. P. Andrieux, P. Hapiot, J. M. Saveant, *J. Phys. Chem.* **1988**, *92*, 5992.
- [141] G. Kissel, S. W. Feldberg, *J. Phys. Chem.* **1969**, *73*, 3082.
- [142] J. Edwin, W. E. Geiger, *J. Am. Chem. Soc.* **1990**, *112*, 7104.
- [143] J. P. Collman, J. E. Hutchison, P. S. Wagenknecht, N. S. Lewis, M. A. Lopez, R. Guilard, *J. Am. Chem. Soc.* **1990**, *112*, 8206.
- [144] D. H. Evans, M. J. Kelly, *Anal. Chem.* **1982**, *54*, 1727.
- [145] W. Hyk, A. Nowicka, Z. Stojek, *Anal. Chem.* **2002**, *74*, 149.
- [146] R. G. Evans, O. V. Klymenko, P. D. Price, S. G. Davies, C. Hardacre, R. G. Compton, *ChemPhysChem* **2005**, *6*, 526.
- [147] R. J. Forster, *Phys. Chem. Chem. Phys.* **1999**, *1*, 1543.
- [148] J. J. Fei, S. S. Hu, *Russ. J. Electrochem.* **2005**, *41*, 1296.
- [149] J. V. Macpherson, P. R. Unwin, *Anal. Chem.* **1997**, *69*, 2063.
- [150] A. J. Bard, G. Denuault, R. A. Friesner, B. C. Dornblaser, L. S. Tuckerman, *Anal. Chem.* **1991**, *63*, 1282.
- [151] P. R. Unwin, A. J. Bard, *J. Phys. Chem.* **1991**, *95*, 7814.
- [152] A. J. Bard, F.-R. F. Fan, *Faraday Discuss.* **1992**, *94*, 1.
- [153] M. Arca, A. J. Bard, B. R. Horrocks, T. C. Richards, D. A. Treichel, *Analyst* **1994**, *119*, 719.
- [154] J. Kwak, A. J. Bard, *Anal. Chem.* **1989**, *61*, 1221.
- [155] F. Zhou, P. R. Unwin, A. J. Bard, *J. Phys. Chem.* **1992**, *96*, 4917.
- [156] Y. Saito, *Rev. Polarogr.* **1968**, *15*, 177.
- [157] J. Heinze, *Angew. Chem.* **1993**, *105*, 1327.
- [158] M. Fleischmann, S. Pons, D. R. Rolison, P. P. Schmidt, *Ultramicroelectrodes*, Datatech Systems, Inc., Morganton, NC, **1987**.
- [159] A. Baranski, A. Kryska, Z. Galus, *J. Electroanal. Chem.* **1993**, *349*, 341.
- [160] A. Baranski, W. Lu, *J. Electroanal. Chem.* **1993**, *355*, 205.
- [161] K. Winkler, A. Baranski, *J. Electroanal. Chem.* **1993**, *346*, 197.
- [162] R. A. Clark, S. E. Zerby, A. G. Ewing, *Electroanal. Chem.* **1998**, *20*, 227.
- [163] K. Stulik, *Pure Appl. Chem.* **1987**, *59*, 521.
- [164] A. J. Bard, F. R. F. Fan, M. V. Mirkin, *Electroanal. Chem.* **1994**, *18*, 243.
- [165] C. E. D. Chidsey, R. W. Murray, *Science* **1986**, *231*, 25.
- [166] A. J. Bard, M. V. Mirkin, *Scanning Electrochemical Microscopy*, Marcel Dekker, Inc., New York, Basel, **2001**.
- [167] B. de Boer, M. M. Frank, Y. J. Chabal, W. Jiang, E. Garfunkel, Z. Bao, *Langmuir* **2004**, *20*, 1539.
- [168] T. Ohgi, D. Fujita, W. Deng, Z. C. Dong, H. Nejoh, *Surf. Sci.* **2001**, *493*, 453.
- [169] T. Ohgi, H. Y. Sheng, Z. C. Dong, H. Nejoh, *Surf. Sci.* **1999**, *442*, 277.
- [170] T. Ohgi, H. Y. Sheng, Z. C. Dong, H. Nejoh, D. Fujita, *Appl. Phys. Lett.* **2001**, *79*, 2453.
- [171] T. Ohgi, H. Y. Sheng, H. Nejoh, *Appl. Surf. Sci.* **1998**, *130-132*, 919.
- [172] M. J. Esplandiu, P. L. M. Noeske, *Appl. Surf. Sci.* **2002**, *199*, 166.
- [173] M. J. Tarlov, *Langmuir* **1992**, *8*, 80.

- [174] R. P. Andres, T. Bein, M. Dorogi, S. Feng, J. I. Henderson, C. P. Kubiak, W. Mahoney, R. G. Osifchin, R. Reifenger, *Science* **1996**, *272*, 1323.
- [175] E. A. Speets, B. Dordi, B. J. Ravoo, N. Oncel, A.-S. Hallbaeck, H. J. W. Zandvliet, B. Poelsema, G. Rijnders, D. H. A. Blank, D. N. Reinhoudt, *Small* **2005**, *1*, 395.
- [176] E. A. Speets, B. J. Ravoo, F. J. G. Roesthuis, F. Vroegindeweij, D. H. A. Blank, D. N. Reinhoudt, *Nano Lett.* **2004**, *4*, 841.
- [177] X. D. Cui, A. Primak, X. Zarate, J. Tomfohr, O. F. Sankey, A. L. Moore, T. A. Moore, D. Gust, G. Harris, S. M. Lindsay, *Science* **2001**, *294*, 571.
- [178] Y. Xiao, F. Patolsky, E. Katz, J. F. Hainfeld, I. Willner, *Science* **2003**, *299*, 1877.
- [179] K. Ramachandran Ganesh, J. Hopson Theresa, M. Rawlett Adam, A. Nagahara Larry, A. Primak, M. Lindsay Stuart, *Science* **2003**, *300*, 1413.
- [180] J. A. M. Sondag-Huethorst, L. G. J. Fokkink, *Langmuir* **1995**, *11*, 4823.
- [181] H. Hagenstroem, M. A. Schneeweiss, D. M. Kolb, *Langmuir* **1999**, *15*, 7802.
- [182] T. Baunach, D. M. Kolb, *Anal. Bioanal. Chem.* **2002**, *373*, 743.
- [183] Y. Ren, K.-i. Iimura, T. Kato, *Langmuir* **2001**, *17*, 2688.
- [184] L. Dziri, B. Desbat, R. M. Leblanc, *J. Am. Chem. Soc.* **1999**, *121*, 9618.
- [185] Q. Huo, L. Dziri, B. Desbat, K. C. Russell, R. M. Leblanc, *J. Phys. Chem. B* **1999**, *103*, 2929.
- [186] E. Le Calvez, D. Blaudez, T. Buffeteau, B. Desbat, *Langmuir* **2001**, *17*, 670.
- [187] H. Bourque, I. Laurin, M. Pezolet, J. M. Klass, R. B. Lennox, G. R. Brown, *Langmuir* **2001**, *17*, 5842.
- [188] S. H. Brewer, S. J. Anthireya, S. E. Lappi, D. L. Drapcho, S. Franzen, *Langmuir* **2002**, *18*, 4460.
- [189] R. G. Nuzzo, L. H. Dubois, D. L. Allara, *J. Am. Chem. Soc.* **1990**, *112*, 558.
- [190] B. J. Hinch, L. H. Dubois, *J. Electron. Spectrosc. Relat. Phenom.* **1990**, *54-55*, 759.
- [191] X. Ding, K. Moumanis, J. J. Dubowski, L. Tay, N. L. Rowell, *J. Appl. Phys.* **2006**, *99*, 054701/1.
- [192] R. A. Meyers, Editor, *Encyclopedia of Analytical Chemistry*, Wiley, Chichester, **2000**.
- [193] D. S. Karpovich, G. J. Blanchard, *Langmuir* **1994**, *10*, 3315.
- [194] M. E. Schrader, G. I. Loeb, Editors, *Modern Approaches to Wettability: Theory and Applications*, **1992**.
- [195] V. L. Colvin, A. N. Goldstein, A. P. Alivisatos, *J. Am. Chem. Soc.* **1992**, *114*, 5221.
- [196] A. Ulman, *An Introduction to Ultrathin Organic Films: From Langmuir-Blodgett to Self-Assembly*, Academic Press, San Diego, **1991**.
- [197] A. J. Bard, L. R. Faulkner, *Electrochemical Methods: Fundamentals and Applications*, Wiley, New York, **1980**.
- [198] J. G. Nikelly, W. D. Cooke, *Anal. Chem.* **1957**, *29*, 933.
- [199] R. D. MeMars, I. Shain, *Anal. Chem.* **1957**, *29*, 1825.
- [200] M. M. Nicholson, *J. Am. Chem. Soc.* **1957**, *79*, 7.
- [201] L. B. Rogers, D. P. Krause, J. C. Griess, Jr., D. B. Ehrlinger, *J. Electrochem. Soc.* **1949**, *95*, 33.
- [202] D. M. Kolb, *Angew. Chem. Int. Ed.* **2001**, *40*, 1162.
- [203] H. Wolter, M. Schmidt, M. Nohlen, K. Wandelt, *Surf. Sci.* **1996**, 232.
- [204] B. M. Ocko, O. M. Magnussen, J. X. Wang, R. R. Adzic, T. Wandlowski, *Physica B: Condensed Matter (Amsterdam)* **1996**, *221*, 238.
- [205] T. Wandlowski, *Encyclopedia of Electrochemistry* **2003**, *1*, 383.
- [206] T. Nakanishi, B. Ohtani, K. Shimazu, K. Uosaki, *Chem. Phys. Lett.* **1997**, *278*, 233.
- [207] T. Nakanishi, B. Ohtani, K. Uosaki, *J. Phys. Chem. B* **1998**, *102*, 1571.

- [208] U. Weckenmann, S. Mittler, K. Naumann, R. A. Fischer, *Langmuir* **2002**, *18*, 5479.
- [209] B. M. Hutton, D. E. Williams, *Anal. Commun.* **1999**, *36*, 17.
- [210] M. Subirade, A. Lebugle, *Thin Solid Films* **1994**, *243*, 442.
- [211] A. Schaufuss, P. Rossbach, I. Uhlig, R. Szargan, *Fresenius J. Anal. Chem.* **1997**, *358*, 262.
- [212] A. G. Schaufuss, H. W. Nesbitt, I. Kartio, K. Laajalehto, G. M. Bancroft, R. Szargan, *J. Electron. Spectrosc. Relat. Phenom.* **1998**, *96*, 69.
- [213] A. G. Schaufuss, H. W. Nesbitt, I. Kartio, K. Laajalehto, G. M. Bancroft, R. Szargan, *Surf. Sci.* **1998**, *411*, 321.
- [214] R. Szargan, A. Schaufuss, P. Rossbach, *J. Electron. Spectrosc. Relat. Phenom.* **1999**, *100*, 357.
- [215] D. Briggs, M. P. Seah, *Practical Surface Analysis*, John Wiley & Sons Ltd, West Sussex, **1990**.
- [216] E. Budevski, G. Staikov, W. J. Lorenz, Editors, *Electrochemical Phase Formation and Growth: An Introduction to the Initial Stages of Metal Deposition*, VCH, Weinheim, **1996**.
- [217] A. J. Bard, M. V. Mirkin, P. R. Unwin, D. O. Wipf, *J. Phys. Chem.* **1992**, *96*, 1861.
- [218] S. B. Basame, H. S. White, *Langmuir* **1999**, *15*, 819.
- [219] N. Casillas, S. J. Charlebois, W. H. Smyrl, H. S. White, *J. Electrochem. Soc.* **1994**, *141*, 636.
- [220] A. J. Bard, F.-R. F. Fan, J. Kwak, O. Lev, *Anal. Chem.* **1989**, *61*, 132.
- [221] J. V. Macpherson, P. R. Unwin, *J. Chem. Soc. Faraday Trans. 1* **1993**, *89*, 1883.
- [222] M. Riskin, E. Katz, V. Gutkin, I. Willner, *Langmuir* **2006**, *22*, 10483.
- [223] D. Borissov, R. Tsekov, W. Freyland, *J. Phys. Chem. B* **2006**, *110*, 15905.
- [224] B. Bozzini, G. Pietro De Gaudenzi, C. Mele, *J. Electroanal. Chem.* **2004**, *563*, 133.
- [225] N. Ikemiya, K. Yamada, S. Hara, *Surf. Sci.* **1996**, *348*, 253.
- [226] O. E. Hüusser, D. H. Craston, A. J. Bard, *J. Electrochem. Soc.* **1989**, *136*, 3222.
- [227] A. J. Bard, G. Denuault, C. Lee, D. Mandler, D. O. Wipf, *Acc. Chem. Res.* **1990**, *23*, 357.
- [228] K. Borgwarth, C. Ricken, D. G. Ebling, J. Heinze, *Ber. Bunsenges. Phys. Chem.* **1995**, *99*, 1421.
- [229] E. Ammann, D. Mandler, *J. Electrochem. Soc.* **2001**, *148*, C533.
- [230] O. de Abril, D. Mandler, P. R. Unwin, *Electrochem. Solid-State Lett.* **2004**, *7*, C71.
- [231] S. Sauter, G. Wittstock, *J. Solid State Electrochem.* **2001**, *5*, 205.
- [232] D. Hofmann, W. Schindler, J. Kirschner, *Appl. Phys. Lett.* **1998**, *73*, 3279.
- [233] Y. Yatziv, I. Turyan, D. Mandler, *J. Am. Chem. Soc.* **2002**, *124*, 5618.
- [234] W. Deng, L. Yang, D. Fujita, H. Nejoh, C. Bai, *Appl. Phys. A: Mater. Sci. Process.* **2000**, *71*, 639.
- [235] P. R. Unwin, J. V. Macpherson, R. D. Martin, C. F. McConville, *Proc. - Electrochem. Soc.* **2000**, *99-28*, 104.
- [236] H. Flood Amar, J. F. Stoddart, W. Steuerman David, R. Heath James, *Science* **2004**, *306*, 2055.
- [237] R. F. Service, *Science* **2001**, *294*, 2442.
- [238] C. Joachim, J. K. Gimzewski, A. Aviram, *Nature* **2000**, *408*, 541.
- [239] J. M. Tour, *Acc. Chem. Res.* **2000**, *33*, 791.
- [240] D. I. Gittins, D. Bethell, D. J. Schiffrin, R. J. Nichols, *Nature* **2000**, *408*, 67.
- [241] C. P. Collier, G. Matterstei, E. W. Wong, Y. Luo, K. Beverly, J. Sampaio, F. M. Raymo, J. F. Stoddart, J. R. Heath, *Science* **2000**, *289*, 1172.

- [242] A. D. Mehta, M. Rief, J. A. Spudich, D. A. Smith, R. M. Simmons, *Science* **1999**, 283, 1689.
- [243] S. Weiss, *Science* **1999**, 283, 1676.
- [244] H. Nakamura, I. Karube, *Anal. Bioanal. Chem.* **2003**, 377, 446.
- [245] M. C. Pirrung, *Angew. Chem. Int. Ed.* **2002**, 41, 1276.
- [246] D. S. Wilson, S. Nock, *Angew. Chem. Int. Ed.* **2003**, 42, 494.
- [247] D. A. Tomalia, *Prog. Polym. Sci.* **2005**, 30, 294.
- [248] P. A. Chase, R. J. M. K. Gebbink, G. van Koten, *J. Organomet. Chem.* **2004**, 689, 4016.
- [249] A. W. Bosman, H. M. Janssen, E. W. Meijer, *Chem. Rev.* **1999**, 99, 1665.
- [250] U. Boas, P. M. H. Heegaard, *Chem. Soc. Rev.* **2004**, 33, 43.
- [251] V. Balzani, P. Ceroni, M. Maestri, C. Saudan, V. Vicinelli, *Topics in Current Chemistry* **2003**, 228, 159.
- [252] J. Twyman Lance, S. H. King Amy, K. Martin Ian, *Chem. Soc. Rev.* **2002**, 31, 69.
- [253] M.-C. Daniel, J. Ruiz, S. Nlate, J.-C. Blais, D. Astruc, *J. Am. Chem. Soc.* **2003**, 125, 2617.
- [254] W. Ong, M. Gomez-Kaifer, A. E. Kaifer, *Chem. Commun.* **2004**, 1677.
- [255] J. J. Michels, J. Huskens, D. N. Reinhoudt, *J. Chem. Soc. Perkin Trans 2.* **2002**, 102.
- [256] R. M. Crooks, B. I. Lemon, III, L. Sun, L. K. Yeung, M. Zhao, *Topics in Current Chemistry* **2001**, 212, 81.
- [257] C. A. Nijhuis, J. Huskens, D. N. Reinhoudt, *J. Am. Chem. Soc.* **2004**, 126, 12266.
- [258] G. Wittstock, W. Schuhmann, *Anal. Chem.* **1997**, 69, 5059.
- [259] C. A. Nijhuis, J. K. Sinha, G. Wittstock, J. Huskens, B. J. Ravoo, D. N. Reinhoudt, *Langmuir* **2006**, 22, 9770.
- [260] S. Onclin, A. Mulder, J. Huskens, B. J. Ravoo, D. N. Reinhoudt, *Langmuir* **2004**, 20, 5460.
- [261] D. Mandler, A. J. Bard, *Langmuir* **1990**, 6, 1489.
- [262] D. Mandler, A. J. Bard, *J. Electrochem. Soc.* **1990**, 137, 1079.
- [263] D. Mandler, A. J. Bard, *J. Electrochem. Soc.* **1990**, 137, 2468.
- [264] D. Mandler, A. J. Bard, *J. Electrochem. Soc.* **1989**, 136, 3143.
- [265] P. R. Unwin, A. J. Bard, *Anal. Chem.* **1992**, 64, 113.
- [266] C. M. Bruinink, C. A. Nijhuis, M. Peter, B. Dordi, O. Crespo-Biel, T. Auletta, A. Mulder, H. Schoenherr, G. J. Vancso, J. Huskens, D. N. Reinhoudt, *Chem. Eur. J.* **2005**, 11, 3988.
- [267] R. A. Scott, A. G. Mauk, Editors, *Cytochrome c: A Multidisciplinary Approach*, University Science Books, Sausalito, California, **1996**.
- [268] G. Battistuzzi, M. Borsari, M. Sola, *Antioxid Redox Signal* **2001**, 3, 279.
- [269] G. Battistuzzi, M. Borsari, M. Sola, *Eur. J. Inorg. Chem.* **2001**, 2989.
- [270] G. Battistuzzi, M. Borsari, M. Sola, F. Francia, *Biochemistry* **1997**, 36, 16247.
- [271] J. Deere, M. Serantoni, K. J. Edler, B. K. Hodnett, J. G. Wall, E. Magner, *Langmuir* **2004**, 20, 532.
- [272] A. S. Haas, D. L. Pilloud, K. S. Reddy, G. T. Babcock, C. C. Moser, J. K. Blasie, P. L. Dutton, *J. Phys. Chem. B* **2001**, 105, 11351.
- [273] A. Fantuzzi, M. Fairhead, G. Gilardi, *J. Am. Chem. Soc.* **2004**, 126, 5040.
- [274] S. E. Pust, D. Scharnweber, S. Baunack, G. Wittstock, *J. Electrochem. Soc.* **2007**, 154, C508.

Own Publications

- [A1] C. Zhao, J. K. Sinha, C. A. Wijayawardhana, G. Wittstock, *J. Electroanal. Chem.* **2004**, *561*, 83.
- [A2] C. A. Nijhuis, J. K. Sinha, G. Wittstock, J. Huskens, B. J. Ravoo, D. N. Reinhoudt, *Langmuir* **2006**, *22*, 9770
- [A3] M. J. W. Ludden, J. K. Sinha, G. Wittstock, J. Huskens, B. J. Ravoo, D. N. Reinhoudt, *Small* (submitted, **2007**)
- [A4] J. K. Sinha, C. A. Nijhuis, G. Wittstock, J. Huskens, B. J. Ravoo, D. N. Reinhoudt, *Phys.. Chem. Chem. Phys.* (to be submitted, **2007**)

Symbols and Abbreviations

Symbols

<u>Symbol</u>	<u>unit</u>	<u>quantity</u>
A	cm^{-2}	area
c	M cm^{-3}	local concentration
c^*	M cm^{-3}	bulk concentration
D	$\text{cm}^2 \text{s}^{-1}$	diffusion coefficient
d	cm	UME-sample distance
E_T, E°	V	electrode potential, formal potential
E_S	V	substrate potential
e^-	-	electron
F	C M^{-1}	the Faradic constant
G1, G2, G3, G4	-	generations of dendrimers
I_C	A	charging current
i_T	A	electrode current
n	-	number of transferred electrons
$i_{T,\infty}$	A	electrode current in absence of a sample
P_b		bound interactions per dendrimer molecule
Q	C	charged passed in electrolysis
r	cm	2D radial coordinates
RG	-	insulation sheath to electrode ratio
r_S	cm^{-1}	radius of the affected spot
r_T	cm	radius of an axisymmetric electrode
t	s	time
v_T	cm s^{-1}	translation speed
x, y, z	cm	Cartesian coordinates
Γ	mol cm^{-2}	surface concentration
δ	cm	diffusion distance of mediator
∞	-	infinity

Abbreviations

AFM	atomic force microscope(y)
BE	binding energy
CDs	cyclodextrins
CV	cyclic voltammetry
DPSC	double potential step chronoamperometry
EIS	electrochemical impedance spectroscopy
Fc^+	oxidised ferrocene
MPA	mercaptopropionic acid
OSWV	osteryoung square wave voltammetry
PLAA	polymeric aspartic acid

PMIRRAS	polarisation modulation infrared reflection absorption spectroscopy
PPI	polypropylene imine
SAM	self-assembled monolayers
SECM	scanning electrochemical microscope(y)
SNOM	scanning near-field optical microscopy
SPM	scanning probe techniques
SPSC	single potential step chronoamperometry
STM	scanning tunneling microscope(y)
TBEA	thio-bis(ethylacetoacetate)
TTF	tetrathiafulvalene
UHV	ultra high vacuum
UME	ultramicroelectrode
UPD	under-potential deposition
XPS	X-ray photoelectron spectroscopy
Fc	ferrocene
β CD	β -cyclodextrin
O	oxidized form of mediator
R	reduced form of mediator

Lebenslauf

Jatin Kumar Sinha

Geboren: 07.07.1978 in Puri, Orissa, India

Familienstand: verheiratet seit 08.12.2004

Schulischer und beruflicher Werdegang

07/1988-07/1993: High School Certificate Examination, Orissa, India

07/1993-07/1995: Higher Secondary Examination Certificate, Bhubaneswar, India

07/1995-06/1998: B.Sc., Utkal University, Bhubaneswar, India

07/1998-07/2000: M.Sc., Utkal University, Bhubaneswar, India

07/2000-01/2002: M.Tech, IIT Bombay, India

Promotion

03/2003-08/2007: Arbeitsgruppe Prof. Dr. Gunther Wittstock, Carl-von-Ossietzky Universität Oldenburg

Sprachen

English, German (scientific and technical terms), Sanskrit

Hiermit versichere ich, dass ich diese
Arbeit selbstständig verfasst und keine anderen
als die angegebenen Quellen und Hilfsmittel benutzt habe.
Oldenburg 18.09.2007